In-situ detection of strontium 90 in groundwater boreholes with a novel detector at nuclear decommissioning sites

Graeme Turkington

School of Engineering
College of Science and Engineering
University of Glasgow

November 2021

Contents

List of Figures

List of Tables

Acknowledgements

I would like to thank my academic supervisor, Kelum Gamage, for the opportunity to undertake this PhD. I have enjoyed his patience, approach to supervision and his advice has always pushed me in the right direction.

I must thank my industrial supervisor from the National Nuclear Laboratory, James Graham, and the Nuclear Decommissioning Authority for their funding support and supervision. James has provided invaluable insight into the industry, excellent feedback on journal papers, and expertise on environmental science.

I'd like to extend gratitude to all the other PhD students who have helped me out along the way, the Nuclear and Hadron Physics Group for their lab space and support to complete experiments and all the staff at the University who help to make things possible.

I'm extremely grateful to my parents for their love and support.

Author's Declaration

I declare that, except where explicit reference is made to the contribution of others, this dissertation is the result of my own work and has not been submitted for any other degree at the University of Glasgow or any other institution. All experimental work was carried out within the Nuclear and Hadron Physics Group at the University of Glasgow.

Abstract

Strontium-90 is one of the primary beta-emitting radionuclides found at nuclear decommissioning sites. Monitoring its activity in the environment is of utmost importance given its radiotoxicity. Current procedures for the beta detection of strontium-90 are time consuming, produce secondary waste and expensive. Therefore there is a demand for more cost-effective detectors which can mitigate the downsides of existing techniques.

This thesis discusses the design and development of a proof-of-concept detector which can meet the nuclear decommissioning industry's demand for in-situ detection of ^{90}Sr . Semiconductors were identified as an appropriate detector technology to use in a compact and water deployable detector. The current state of semiconductor detector technologies was evaluated and relevant semiconductor materials were compared using Monte Carlo simulations. Suitable detector components were researched and identified to fit a small scale form factor. Other practicalities were implemented such as rudimentary waterproofing.

The basic operation of the detector and its sensitivity to radiation was demonstrated experimentally and its response to environmental conditions was assessed by changing the temperature of the water it was submerged in. The sensitivity of the detector to various radionuclides found in groundwater was evaluated using Monte Carlo simulations and the limit of detection for ^{90}Sr was determined. The ability of such a detector to identify individual beta emitting radionuclides from a mixed spectrum obtained in a simulated groundwater borehole was demonstrated by using a linear regression technique.

1. Introduction

1.1 Introduction to the UK's nuclear industry and waste

The UK's first nuclear reactors were built in 1947 at the Atomic Energy Research Establishment (AERE) located in Oxfordshire. Sellafield became the location of the world's first commercially viable nuclear power station, Calder Hall, in 1957. After 47 years of operation Calder Hall was closed and today Sellafield is responsible for nuclear fuel recycling, storage and treatment. Over the years, Sellafield has been a site for nuclear fuel fabrication, reprocessing, radioactive waste management and storage. The site is projected to be fully decommissioned by the year 2120. The Calder Hall station featured 4 Magnox reactors and after its opening in the 1950s a further 10 Magnox stations were built in the following 15 years. Nuclear power capacity peaked in the UK during the 1990s supplying 26.9% of power to the national grid. Now, the UK currently operates eight nuclear power reactors which supply a 18.7% share of the grid but this is set to reduce further as 5 stations will cease operations within the next decade. However, there are plans to build a new generation of reactors with an advanced gas-cooled reactor (AGR) set to open at Hinkley Point C in 2026.

Nuclear power exploits a reaction called nuclear fission. This is a process in which the nucleus of an atom is split by an incident neutron into smaller nuclei. This releases further neutrons and energy in the form of radiation and heat. The resulting heat is captured and, depending on the type of reactor, directly or indirectly used to turn water into steam which powers a turbine to generate electricity. A nuclear reactor contains approximately 100 tonnes

of uranium-235 (^{235}U) fuel. After the fuel has been used to the limit of its commercial viability, the spent fuel is retrieved from the detector and stored in cooling ponds for minimum of 90 days. Uranium can be recovered from spent fuel however this procedure, known as reprocessing, can produce additional radioactive waste. Many of the smaller nuclei which result from fission interactions are radioactive and classified as waste. Due to the dangerous nature of ionising radiation the waste produced from the nuclear fuel cycle must be managed and securely stored so that it does not harm the environment and the public.

1.2 Nuclear decommissioning

Nuclear power stations which have ceased operations are put into a state of decommissioning. The goal of nuclear decommissioning is to deconstruct a nuclear facility and manage its removal until the point at which radiation protection is no longer necessary. Given the long half-life of many nuclear waste products this is a process which can take decades to complete. Decommissioning involves many different stages, outlined in Fig. 1.1.

After the reactor has been shut down the facility enters a transitory phase which involves the removal of fuel from the facility and preparations for future decommissioning. At this stage further decommissioning may be deferred. The reactor is sealed and the process is delayed. This allows for the core to cool, radiation to dissipate, and can help to manage logistical challenges. The facility is then decontaminated and dismantled. Radioactive materials and equipment are removed and surfaces are cleaned. Finally, the site is demolished and the grounds are remediated. This can involve monitoring radiation activity in groundwaters and removing contaminated soil to protect the environment from any lingering contamination.

Current estimates put the cost of nuclear decommissioning in the UK at £124 billion and it is expected to take at least 120 years to complete. Given the long term nature of decommissioning the industry must constantly evolve to incorporate developments in technology and public policy. One of the primary motivations for new research is to develop new ways to reduce costs to the public and reduce risks to workers.

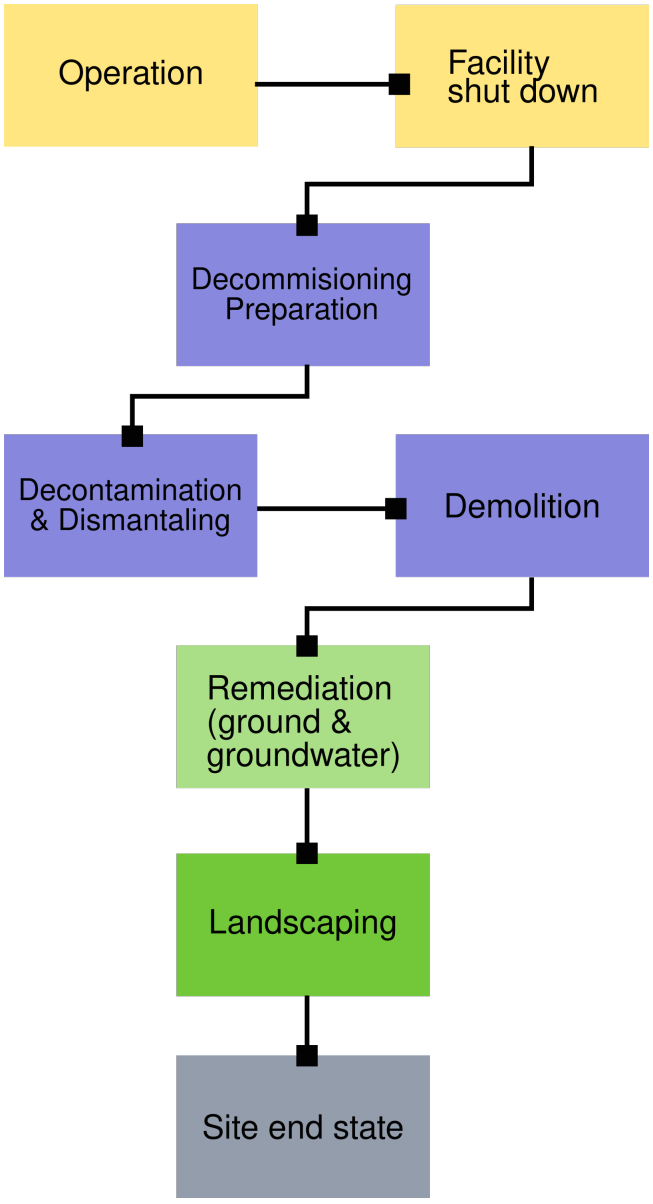

Figure 1.1: Decommissioning a nuclear facility is a multi-stage process, outlined in the above figure. [1]

1.3 Nuclear waste

Some radioactive elements are naturally occurring in the Earth's crust such as uranium-238 (^{238}U), thorium-232 (^{232}Th), and potassium-40 (^{40}Th) while others, like ^{90}Sr are introduced as a consequence of human actions. ^{90}Sr is produced when ^{235}U is broken down during the fission process in nuclear reactors. Radioactive waste is any substance which is radioactive or has been contaminated by radioactivity and has been determined to have no further use. Radioactive waste can take many forms including liquid waste, solid waste, medical waste and aqueous waste. There are six classes of radioactive waste [16]:

- Exempt waste (EW) is waste that meets the criteria for clearance, essentially is designated as not requiring radiation protection.

- Very short lived waste (VSLW) usually includes waste which decays rapidly over a short time frame of a few years. Radionuclides used for medical purposes are usually placed in this category.

- Very low level waste (VVLW) that does not meet the standard of exempt waste but can be disposed of, without significant containment, in landfill-like facilities.

- Low level waste (LLW) contains fewer long lived radionuclides but is still above clearance levels for disposal. This waste can be stored on surface level facilities, albeit for hundreds of years.

- Intermediate level waste (ILW) is waste which still contains long lived radionuclides but requires fewer accommodations made for heat dissipation. Must be stored under ground, although generally not as deeply as HLW.

- High level waste (HLW) consists of long lived radionuclides which generate significant quantities of heat and is typically disposed of hundreds of meters underground.

Depending on whether the waste is solid or liquid, it goes through a stage of characterisation and segregation into different categories. The waste is then treated in order to achieve volume reduction, radionuclide removal and a change of physical or chemical composition [17]. This can include removing radionuclides with ion exchange resins, neutralising chemicals, or incinerating solid waste.

1.4 Strontium 90 monitoring and motivation for the project

During the process of processing or storing radioactive wastes, leaks and spills into the environment can occur. Once nuclear material enters the ground it may reach the groundwater table, contaminating water resources and posing a potential threat to human health and the wider environment. For this reason nuclear licensed sites must routinely monitor groundwater to determine the level of contamination and take steps to ensure the safety of the surrounding environment. As the nuclear decommissioning process can take hundreds of years to complete, the task of monitoring this contamination is on-going and requires forward planning to achieve a high standard of results while also managing budgetary concerns in a long term project.

^{90}Sr is a product of the nuclear fuel cycle and one of the primary beta emitting radionuclides found at nuclear decommissioning sites. ^{90}Sr is chemically similar to calcium and if ingested it can accumulate around skeletal features and induce cancerous disease. As a pure beta emitter it is difficult to identify its presence due to the limited range of beta particles in matter and the continuous spectrum over which they are emitted. ^{90}Sr is currently monitored by taking groundwater samples from the site to a lab and chemically isolating the radionuclide before counting its activity with a liquid scintillation counter. There is an interest in developing new techniques and methods for monitoring radionuclide contamination in the

environment which can reduce risk and minimise costs. Therefore this research proposes a novel approach to ^{90}Sr monitoring with in-situ detection.

1.5 Outline of the thesis

This thesis will introduce the reader to the practice of monitoring strontium-90 in a groundwater monitoring context and attempt to explain the creative process behind designing a novel detector to improve this practice. Ultimately this will be done by establishing the potential of the device with proof-of-concept experiments and simulations. The thesis is broadly made up of three sections:

- Introduction, background and motivation
- Detector design, implementation and experiments
- Detector sensitivity and radionuclide identification

1.6 Aim, scope and novelty

This research aims to conceive, design and evaluate a novel method for monitoring ^{90}Sr contamination to meet the demand of the nuclear industry. The two challenges which must be overcome are the short range of beta particles in water and the difficulty in identifying beta emitting radionuclides from their spectra.

There are three aspects to this. Firstly, conceiving and designing a detector type which is small enough to be deployed inside a groundwater borehole and water tight without attenuating a significant fraction of radiation. Secondly, demonstrating the practical use of such a detector in terms of its deployment in water and sensitivity to the radionuclides encountered in a borehole. Finally, the thesis presents a solution to the historic problem for beta detectors for radionuclide identification.

This was done by first conducting a review of existing groundwater monitoring techniques, and establishing the difficulties faced by in-situ techniques. This highlighted the need for a new approach using an in-situ detector. Semiconductors were identified as an appropriate detector technology to use in a compact and water deployable detector. The current state of semiconductor detector technologies was evaluated and relevant semiconductor materials were compared using Monte Carlo simulations. Suitable detector components were researched and identified to fit a small scale form factor. Other practicalities were considered such as rudimentary waterproofing. The operation of the detector and its sensitivity to radiation was demonstrated experimentally and its response to environmental conditions was considered. The sensitivity of the detector to various radionuclides was evaluated using Monte Carlo simulations. The ability of such a detector to identify individual radionuclides in a mixed spectrum was demonstrated by using a linear regression technique.

1.7 Publications

1.7.1 Journal papers

G. Turkington, K. A. A. Gamage, J. Graham, Beta detection of strontium-90 and the potential for direct in situ beta detection for nuclear decommissioning applications, Nuclear Instruments and Methods in Physics Research Section A: Accelerators, Spectrometers, Detectors and Associated Equipment 911 (2018) 55–65. doi:10.1016/j.nima.2018.09.101. [18]

G. Turkington, K. A. A. Gamage, J. Graham, Direct measurement of strontium 90 in groundwater: Geometry optimisation of a photodiode based detector, Journal of Instrumentation 14 (10) (2019) P10018–P10018. doi:10.1088/1748- 0221/14/10/P10018. [19]

G. Turkington, K. A. A. Gamage, J. Graham, The Simulated Characterization and Suitability of Semiconductor Detectors for Strontium 90 Assay in Groundwater, Sensors 21 (3) (2021) 984. doi:10.3390/s21030984. [20]

G. Turkington, K. A. A. Gamage, J. Graham, Characterisation and suitability of a CdTe detector for strontium 90 assay in groundwater, Nuclear Instruments and Methods in Physics Research Section A: Accelerators, Spectrometers, Detectors and Associated Equipment 997 (2021) 165155. doi:10.1016/j.nima.2021.165155. [21]

G. Turkington, K. A. A. Gamage, J. Graham, The Simulation of In-Situ Groundwater Detector Response as a Means of Identifying Beta Emitting Radionuclides by Linear Regression Analysis, Sensors 21 (17) (2021) 5732. 10.3390/s21175732. [22]

1.7.2 Conferences

G. Turkington, K. A. A. Gamage, J. Graham, Detection of Strontium-90, a Review and the Potential for Direct In Situ Detection. In: IEEE Nuclear Science Symposium, Sydney, Australia, 10-17 Nov 2018.

G. Turkington, K. A. A. Gamage, J. Graham, A Proof-of-concept CdTe Detector for In-situ Measurement of Strontium-90 in Groundwater. 2019 IEEE Nuclear Science Symposium and Medical Imaging Conference (NSS/MIC 2019), Manchester, UK, 26 Oct - 02 Nov 2019.

G. Turkington, K. A. A. Gamage, J. Graham, Optimising sensor geometry of a photodiode based detector for the direct detection of strontium 90 in groundwater Published under licence by IOP Publishing Ltd Journal of Physics: Conference Series, Volume 1643, 27th International Nuclear Physics Conference (INPC2019) 29 July - 2 August 2019, Glasgow, UK

G. Turkington, K. A. A. Gamage, J. Graham, Experimental Investigation of Impact on Submerged Detector with Changing Temperature 2020 IEEE Nuclear Science Symposium and Medical Imaging Conference (NSS/MIC 2020), Boston, USA, 31 Oct - 07 Nov 2020.

G. Turkington, K. A. A. Gamage, J. Graham, Modelling the sensitivity of semiconductor detectors for in-situ monitoring of strontium-90 contamination at nuclear decommissioning sites 7th Advancements in Nuclear Instrumentation Measurement Methods and their Applications, Herceg Novi, Montenegro 14 June - 18 June 2021.

G. Turkington, K. A. A. Gamage, J. Graham, Modelling the response of an in-situ CdTe detector to radionuclides in groundwater. 7th Advancements in Nuclear Instrumentation Measurement Methods and their Applications, Prague, Czech Republic, 21 June - 25 June 2021.

2. Background

2.1 Fundamental science of radiation and its interaction with matter

Radiation is emitted as a result of either radioactivity or nuclear reactions. Radioactive decay is a process through which unstable nuclei find stability by spontaneously converting excess energy into emitted radiation. These unstable nuclei are known as radionuclei and there are two varieties, naturally occurring and artificially produced radionuclides. The significant naturally occurring radionuclides which relate to nuclear power are ^{238}U, ^{235}U, and ^{232}Th. These radionuclides have long decay chains and are mined from the earth's surface. Artificially made radionuclides are typically short lived and often the result of nuclear reactions inside reactors. Nuclear reactions are interactions between nuclear particles, or nuclei, which result in the emission of radiation and transformation of the reactants into different products [23]. In nuclear reactors, the nucleus is split upon bombardment with neutrons which exceed the binding energy of the nucleus. The amount of released energy is called the Q-value - the difference between the binding energy of the reactants and products of the reaction. The fission products (fission fragments) can receive approximately 85% of this energy as kinetic energy.

The emitted radiation takes one of two forms, electromagnetic radiation or particle radiation. The radiation is considered ionising when it can leave an atom positively charged by the removal of an electron. This includes energetic charged particles or high energy photons such as gamma-rays or x-rays. Many particles with sufficient energy can be ionising and frequently these are helium nuclei (alpha particles) or electrons and positrons (beta par-

ticles). Charged particles continuously lose their energy through ionisation as they pass through matter, and this gives them a limited range in matter compared to photons which can travel long distances before they interact with a nucleus or electron and are absorbed. Alpha particles have a range of a few centimetres in air but can be stopped by a sheet of paper. Beta particles can travel up to a metre in air but can be stopped by skin, clothing or layers of plastic. Gamma rays can travel much further in air and require a thick layer of lead to absorb the majority of incident rays. These different properties mean that each type of radiation presents different risks to humans which must be carefully considered when designing radiation protection methods and different techniques must be used to detect each type of radiation. Gamma photons can be more easily detected from a distance while alpha and beta particles must be captured at very close range. This has presented difficulties when designing detectors.

2.1.1 Beta particles

A beta particle is a fast and energetic electron or positron which is emitted during radioactive decay.

$$ {}^{A}_{Z}X \rightarrow {}^{A}_{Z+1}Y + \beta^{-} + \overline{\nu} \tag{2.1} $$

Beta decay is represented by the above equation, where X is the parent nuclei, Y is the daughter nuclei, $\overline{\nu}$ is an anti-neutrino, and β^{-} is the beta particle. When ^{90}Sr decays it is a result of an excess of neutrons in the nucleus, one of which will convert into a proton, a beta particle and an anti-neutrino. The emission of the anti-neutrino during beta decay is significant and explains why beta particles are emitted over a continuous energy spectrum as opposed to the narrow energetic distributions of gamma and alpha radiation. The resulting nucleus has little recoil energy and the decay energy is shared between the beta particle and the neutrino. The maximum endpoint of the spectrum is the difference in mass between the

parent nucleus and its products - the Q-value. Sometimes beta decay can leave nuclei in an excited state which is resolved by the emission of a gamma-ray. This is the source for gamma emission in ^{137}Cs and ^{60}Co.

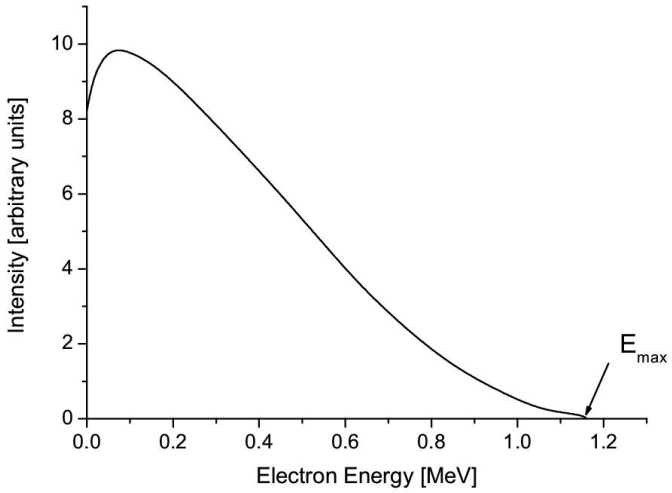

Figure 2.1: An example of a generic continuous beta spectrum which terminates at an end-point energy, E_{Max}. [2]

When beta particles travel through matter their path is erratic with large deviations in direction. This is a result of the interactions beta particles have with either the nuclei of atoms or the orbital electrons of atoms. These interactions can either be elastic, where none of the beta particle's energy is lost, or inelastic where the energy of the beta particle changes. Elastic interactions are of limited importance to radiation detection as no energy exchange occurs. When a beta particle collides inelastically with an orbital electron, some energy is passed from the incident beta particle to the electron. The orbital electron may transfer to a higher energy shell corresponding with the emission of a x-ray photon as the gap in the orbital shell is filled by an electron, or if the orbital electron is sufficiently energised it can escape the atom. The freed electron may cause further ionisations and this is the basis for radiation detection in semiconductor detectors. The emitted gamma photons are mono-energetic and this is determined by the energy levels of the daughter nucleus, this characteristic feature allows for the identification of radionuclides based on their gamma emission. Alpha particles can interact similarly with matter, but because they are thousands of times more massive the

likelihood of interactions is increased and their range is significantly reduced. When a beta particle interacts inelastically with a nucleus, its velocity can change and the lost energy is released as an x-ray photon. This is known as Bremsstrahlung radiation and this phenomenon can be manipulated to produce x-ray beams for practical purposes.

Electromagnetic radiation such as gamma rays do not lose their energy continuously but instead interact with matter through three processes: photo-electric absorption, the Compton effect and pair production. In the photo-electric effect a photon is absorbed by an outer orbital electron which is ejected from the atom, in turn ionising nearby atoms. Compton scattering is when the energy of an incident photon is only partially absorbed, resulting in a recoiling electron and the emission of a lower energy photon scattering at a different angle. Pair production is a phenomenon for gammas with energy in excess of 1.022 MeV which annihilates in the Coulomb field of a charged particle resulting in the production of an electron-positron pair. The positron typically annihilates resulting in the further emission of two 0.511 MeV photons.

2.1.2 Gamma radiation

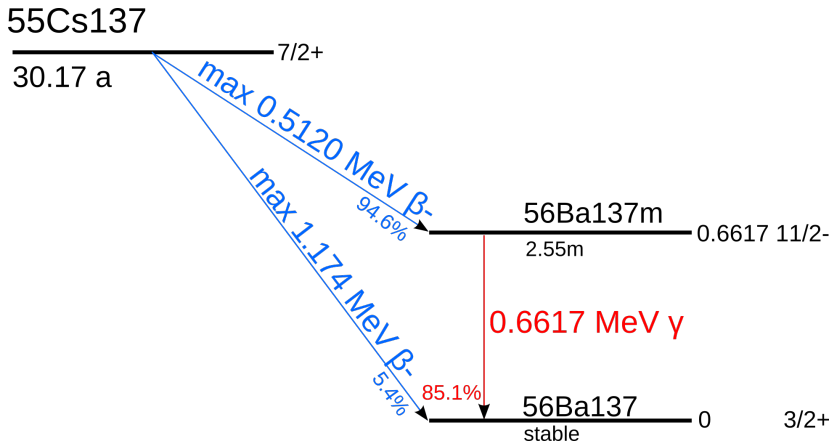

Figure 2.2: Unstable ^{137}Cs transitions to the meta-stable ^{137m}Ba, via beta emission, which in turn decays via gamma emission to its stable state, ^{137}Ba. [3]

Gamma emission is the result of nuclei transitioning from an excited energy state to another. Nuclei can be left unstable or energised after a nuclear reaction or decay and the energy states are considered to be discretised. As the nucleus moves to the ground state, the excess en-

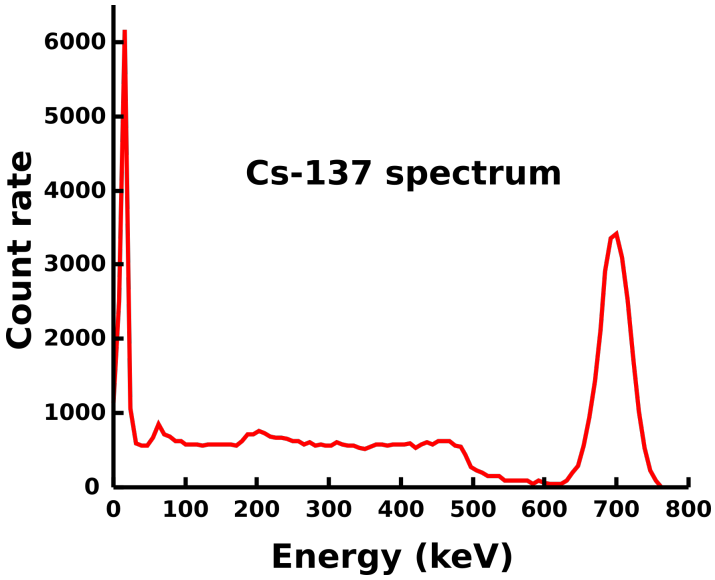

Figure 2.3: An example of the ^{137}Cs gamma spectrum. There is an x-ray photopeak at the beginning and the spectrum culminates in the 662 keV gamma photopeak. [4]

ergy is released as a gamma photon equivalent to the discrete energy difference between the energy states. This is illustrated in Fig. 2.2. Gamma emission can also result after positron decay, the emitted positron annihilates and this results in the emission of two oppositely directed 0.511 MeV gamma photons. As gamma photons are emitted for discrete energies, gamma spectra are characterised by peaks corresponding to these energy transitions. This allows for gamma emitting radionuclides to be easily identified by their spectra.

2.1.3 Alpha radiation

Alpha particles are made up of two protons and two neutrons bound together in a form identical to a ^{4}He nucleus. Alpha particles are only emitted by heavy nuclei, seen in Fig. 2.4. Alpha particles are emitted over discrete energies in the range from 4 to 10 MeV [23]. As alpha particles carry a +2 charge and are relatively massive, they are highly ionising and have a very short range in matter, only a few centimetres in air. An alpha particle's energy dissipation is characterised by the Bragg curve, which features a sharp peak in energy loss as the particle declines in speed. This property has presented difficulty when designing alpha detectors because it's very difficult to design a detection medium which can capture

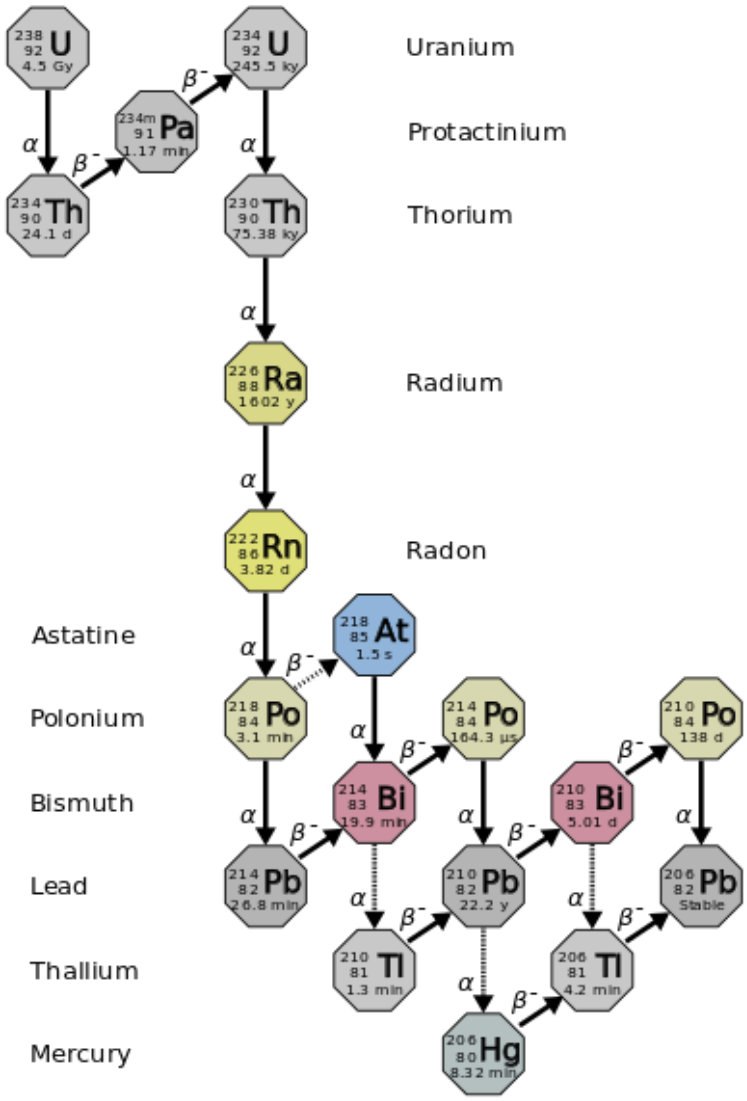

Figure 2.4: The ^{238}U decay chain which ultimately terminates in ^{206}Pb. Alpha emission is the predominant decay process for the heavy nuclides in the chain. [5]

the particles before they are completely absorbed. Despite the fact that alpha particles are unable to penetrate human skin, if alpha emitters are ingested they are highly destructive due to the amount of energy which is released in a short distance.

2.2 *The fundamentals of radiation detectors*

2.2.1 Detector history

Radiation detection is a technique in which radiation interacts with a material in a controlled system such that changes in the system can be observed. The changes generated in the detection material are used to infer information about the nature of the radiation incident on it. One of the earliest forms of radiation detection was the use of photographic plates to detect X-rays, discovered by Rontgen in 1895. The X-rays striking the plate darkened it, leaving a 2-D image of objects between the radiation and the plate. This simple technology still has a legacy today in the form of film badges which are used as dosimeters for workers in environments at risk of radiation. However this technology can only be applied to measure the dose of radiation and its position relative to the plate. Electronic detectors which produce a measurable current pulse in response to ionising radiation were developed, and these are now used to detect the energy of radiation and its activity. Broadly speaking there are two ways to detect radiation: indirectly with scintillation or directly with ionisation.

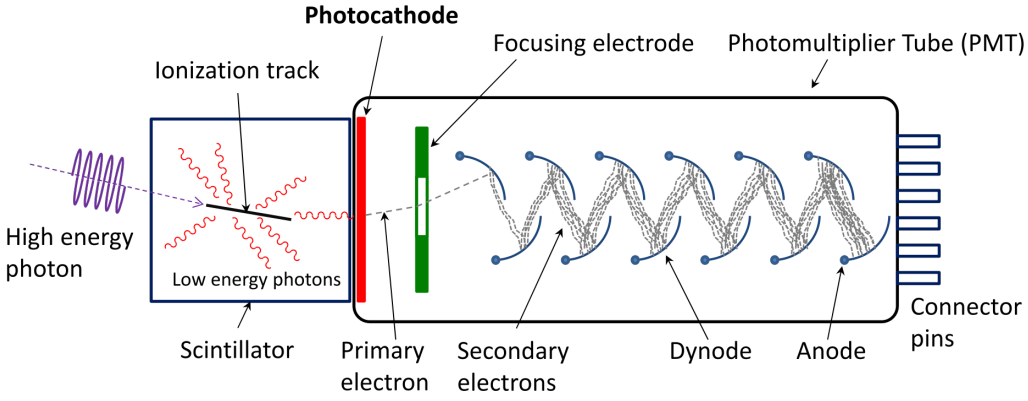

Figure 2.5: A schematic of a scintillation detector and PMT. Ionising radiation generates photons in the scintillator which are converted into an electron avalanche in the PMT. These electrons are processed by the electronics onboard the detector. [6]

Scintillation detectors have long been used to indirectly detect ionising radiation. Incident radiation on a scintillator does not ionise it, but instead transfers energy to atoms. This causes the atoms to ascend to higher energy states and emit a photon as they relax back to

the ground state. This was initially discovered when alpha particles were observed to induce luminescence in zinc sulphide screens. Each scintillation could be attributed to one alpha particle, leading scientists to manually count each flash of light. To the relief of eye-strained scientists, the invention of the photomultiplier tube (PMT) in the 1940s allowed the counting to be done electronically. A PMT converts incident photons into an avalanche of electrons, which produce a current pulse in proportion to the energy of the photon. In recent years photodiode detectors have been used to count the photons, as they are more efficient, can be made much smaller and require less voltage to operate. A scintillator detector is illustrated in Fig. 2.5. Scintillators can be made out of organic material such as plastic, and organic liquids. Liquid scintillators are a mainstay in decommissioning applications as it allows for radionuclides to be mixed into the scintillation medium itself, thereby reducing inefficiency. Inorganic material in the form of crystalline structures like doped sodium iodide are also commonly used.

2.2.2 Detector properties

The sensitivity of a detector describes its ability to generate a signal in response to ionising radiation. There are four factors which contribute to detector sensitivity: the likelihood of radiation ionising the detection medium, the volume of the detection medium, the noise in the detector system, and the attenuation of radiation as it travels through the detector casing [24]. It's desirable to achieve high sensitivity in the detector because it means that the signal produced by the detector is large and subsequently reduces statistical uncertainty in the final estimation of activity. However, it is not possible to design a detector which is sensitive to all types of radiation and energy.

If the detector is sufficiently sensitive, then the energy deposited by the radiation can correlate with the magnitude of the output signal. This relationship is described by the detector response. This function can be linear or non-linear depending on the type of detector and the type of radiation. In an ideal situation, the incident radiation is completely absorbed

within the sensitive medium of the detector and is correlated linearly with the output signal. The detector response can be characterised by measuring the detector output to radiation of known energy. A linear detector response is desirable as it is relatively simple to then design the detector's electronic systems [25].

$$(\Delta E)^2 = (\Delta E_{Statistical})^2 + (\Delta E_{Noise})^2 + ... \tag{2.2}$$

When the detector's output signal correlates with the input radiation energy then it follows that the detector will have an ability to resolve between different energies. An ideal detector would produce an infinitely narrow peak in response to mono-energetic radiation. In reality, detectors produce a Gaussian shaped peak and the full width at half maximum (FWHM) of the peak describes the energy resolution of the detector - its ability to distinguish between two energy peaks. The number of charge carriers generated by radiation of a given energy fluctuates according to Poisson-like statistics. Furthermore, the total energy resolution of the detector contains a contribution from electronic noise and other sources of noise as summarised in Equation 2.2. ΔE is the full-width half-maximum of the energy resolution of the detector.

The summation of detector responses to a mono-energetic beam of radiation is defined as the response function of the detector. The detector response to a mono-energetic beam deviates from a sharp peak because the radiation can become attenuated as it travels through the environment and detector casing which means only a fraction of the initial energy of the particle is deposited in the detector. This combines with the previously described statistical fluctuations in the detector to radiation to generate the response function. The response function can be calibrated by measuring the energy resolution of the detector in response to particle beams of known energy.

Another characteristic to consider is the efficiency of the detector. There are two types of detector efficiency, absolute and intrinsic. The absolute efficiency is a ratio of the total hits in the detector to the total number of particles emitted by the source. As most radiation is emitted isotropically, the physical design of the detector plays an important role in the absolute efficiency. A detector which encompasses the source of radiation will be able to capture radiation emitted at all angles, while a planar detector will only subtend a fraction of the emitted radiation. The intrinsic efficiency is the ratio of particles which strike the detector to the number of hits detected by the detector. It may be the case that some particles are absorbed by the detector geometry or scattered upon contact with the detector surface.

2.3 Semiconductor detectors

Semiconductor detectors essentially work on the same principle as gas ionisation chambers. Ionising radiation creates electron-hole pairs in the semiconductor material and by applying a reverse bias voltage to the semiconductor the number of electron-hole pairs can be counted electronically. This section will explain some of the underlying properties of semiconductors and their suitability as radiation detectors.

2.3.1 The fundamentals of semiconductors

A semiconductor is simply a material with conductive properties that fall between an insulator, like glass, and a conductor, like metal. Unlike metals, a semiconductor's conductivity rises with its temperature. In practice this is an undesirable property for a radiation detector, but it arises from the physical structure of the semiconductor material. Semiconductors have a lattice crystal structure and the outer shell of electrons is considered to have an energy band structure, Fig. 2.6. Electrons bound in the lattice structure occupy the lower valence band, and electrons which occupy the upper valence band are free to navigate the lattice structure

thereby giving rise to conductivity. These bands are separated by forbidden energy levels, which arise as a result of the Pauli exclusion principle, and their difference in energy is called the band gap, E_g. The magnitude of the band gap is related to the physical lattice spacing between atoms, and electrons gain sufficient energy to traverse the gap when they are thermally excited. In a semiconductor the bandgap is sufficiently wide such that only a few electrons are able to traverse the bandgap and therefore the material is "semi-conducting".

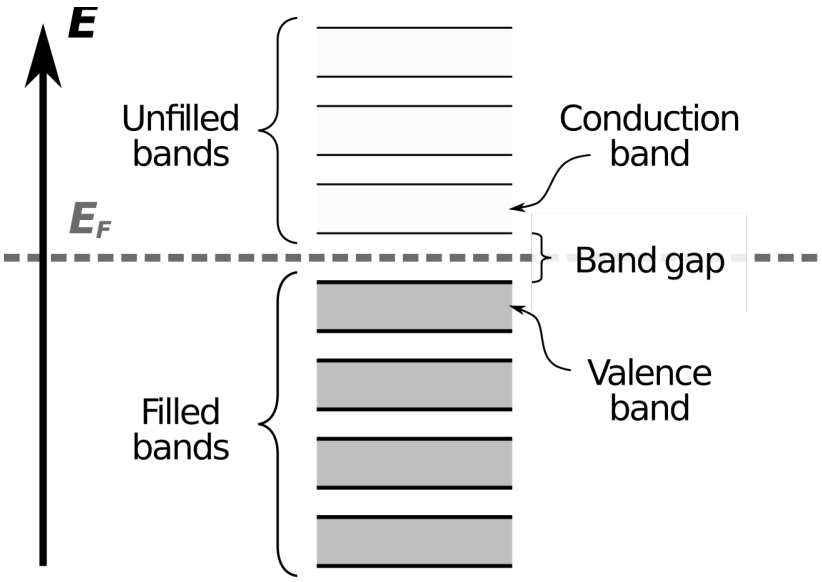

Figure 2.6: The electrical bands in a semiconductor are discrete. [7]

In a semiconductor the charge carriers are electrons in the conduction band and the holes they leave behind in the valence band. When the material is sufficiently cooled, no electron-hole pairs are generated and the material is not conductive. In a pure semiconductor material the number of electrons and holes are equal. This can be changed to altered the properties of the semiconductor by introducing another element to the lattice structure, known as a dopant. When the dopant results in an excess of negative charge carriers, the compound material is called an n-type semiconductor. The excess of negative charge carriers are loosely bound, and are energetic enough to sit near the top of the band gap. Very little energy is required for these electrons to move to the conduction band and at room temperature the conduction band becomes heavily concentrated with donor electrons. When an excess of holes is introduced, the material is known as a p-type semiconductor. The excess of holes creates a new energy

state close to the valence band which gets occupied by electrons, reducing the concentration of free electron charge carriers in the material. Both types are electrically neutral as a result of donor impurities.

The foundation of modern semiconductor detectors is the junction which forms when n-type and p-type semiconductor materials are brought together. These junctions can be a p-n or p-i-n type, with an intrinsic layer sandwiched between. When a p and n type semiconductor are fused together, the excess of electrons and holes seeks to redistribute such that the free electrons fill holes in the p-type material, creating a negative charge density, and the lack of electrons in the n-type material leaves behind a region of positive charge on the other side of the junction. This results in a region at the junction which is filled with recombined charge carriers as the electric field across the gradient prevents any further diffusion of charge. This is known as the depleted region and it is this region which is sensitive to ionising radiation. The charge carries ionised by radiation in this field are swept away by the electric field and can generate a current pulse in proportion to the energy of the radiation. The width of the depleted region should be enhanced in order to improve charge collection and make the detector more sensitive to radiation. This is principally achieved by applying a reverse biased voltage to the semiconductor, by supplying a negative voltage to the p-side of the junction. This widens the depleted region and makes charge collection more efficient as charge carriers are more strongly pulled towards the metal contacts on the detector. Additionally, some undoped, or intrinsic, semiconductor material can be placed between the p and n material to form a p-i-n junction. This can significantly widen the sensitive region of the detector.

2.3.2 Semiconductor materials

Two of the most commonly used semiconductor materials are silicon (Si) and germanium (Ge), in this thesis two compound semiconductors cadmium-telluride (CdTe) and gallium-arsenide (GaAs) are discussed in depth . Some of the properties which are used to compare semiconductor materials are electron mobility, hole mobility, the energy required to create an

electron-hole pair, atomic number (Z). Other things like impurities can lead to material specific characteristics which affect detector performance, like charge trapping and polarisation. The energy required to create an electron-hole pair is material dependent, and in general it is much lower for semiconductors than other detection mediums like gases and scintillators. As a result, many more charge carriers are created by ionising radiation and it is possible for semiconductor detectors to achieve a much higher energy resolution. If it is assumed that the radiation is fully absorbed in the detector body, then the relationship between charge carriers and energy should be linear [25]. When the particles are not stopped by the detector, there is a non-linear relationship between energy loss and charge carriers. However, it is observed that there are fluctuations in these numbers and they do not necessarily follow Poisson statistics. The variance in the number of charge carriers is described by the Fano factor, a term which describes all the mechanisms by which radiation can lose energy in a material. This factor is difficult to calculate and therefore is determined empirically for each material. In a detector it's desirable that there is as little signal as possible when ionising radiation is not incident on the detector. Therefore if the band gap is narrow, at room temperature more electrons will have sufficient thermal energy to leap the gap. Si and Ge have a bandgap of 1.12 and 0.75 eV respectively. This is considered to be a narrow bandgap, and in particular Ge detectors must be cooled below 100k in order to reduce the leakage current in the detector[26]. This has practical implications for Ge detectors, they require sophisticated cooling systems with vacuums which are impractical for in-situ use. CdTe and GaAs have band gaps of 1.5 and 1.44 eV and this has made them practical for room temperature operation [27, 28, 29]. In ideal conditions a reverse biased semiconductor would be non-conducting however in reality this is not the case. There is always a small current present which prevents the smallest signal pulses from being recognised and ultimately damages detector performance. The leakage current arises from two principal factors, thermal excitation of charge carriers and predominantly current which channels through the surface of the detector as a result of manufacturing techniques, imperfections, contaminants and mounting materials. This is difficult to generalise and should be determined experimentally for each detector.

2.3.3 The application of semiconductors as radiation detectors

Most semiconductor detectors operate on the same principles. A reverse bias voltage is applied to the semiconductor material, ionising radiation generates a current pulse, and this current pulse is amplified by electronics and then counted to determine the activity of the radiation. The voltage used in a semiconductor detector can range from 30V to 800V or greater. In principle a higher voltage will widen the depletion region but may introduce some instability in the long run.

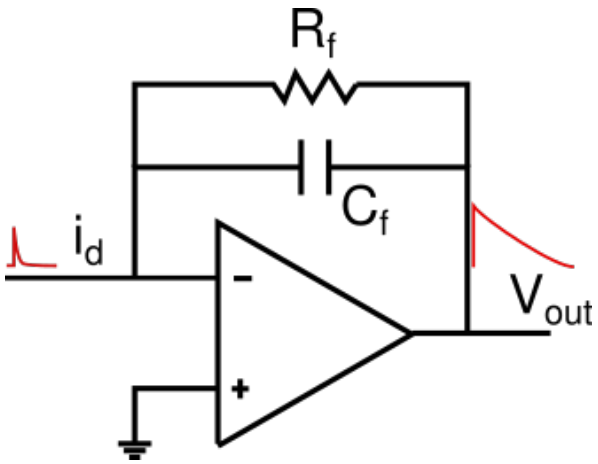

Figure 2.7: A charge sensitive pre-amplifier, the feedback capacitor C_f collects charge from the detector and the feedback resistor R_f tails off the output signal.

The signals produced by semiconductor detectors are small and it is advantageous to amplify them so that they can counted more easily. The amplification of the signal is done in two stages, first a charge sensitive pre-amplifier (CSP) is used to boost the magnitude of the signal and second the signal is shaped to a more suitable waveform using a shaping amplifier. Fig. 2.7 shows the typical components in a CSP. The feedback capacitor C_f collects charge from the detector and performs an integrating function. The feedback resistor R_f is used to shape the output so that it tails off and approximates a pulse. The amplifier steps up the output signal in relation to the charge collected by the amplifier. The long tailed pulse is unsuited to counting and the shaping amplifier is used to generate a Gaussian like pulse shape. The shaping amplifier further modifies the pulse shape, producing a Gaussian pulse. The purpose

of this is to make the pulse easily detected by an analog-to-digital converter and to improve the signal to noise ratio in the detector [26].

2.3.4 Digitisation

A field programmable gate array (FPGA) is a type of microcontroller which consists of a series of logic gates that can be reprogrammed ad hoc. FPGAs are used to compile programs from a series of logic blocks, and as they are reprogrammable allow for quick iteration in program development and prototyping. Essentially this allows for large scale physical circuits to be modelled digitally on a small scale device. This flexibility means that FPGAs have become common place as a tool for instrument design. FPGAs typically have low power consumption and can be manufactured in small scale form factors. These qualities make FPGAs ideal for use in compact detectors.

FPGAs consist of reprogrammable logic blocks, and input/output (I/O) blocks which are reprogrammable. This hardware is interfaced with by software, or specifically a hardware description language (HDL). The two dominant HDLs are VHDL and Verilog, and these are packaged by the major manufacturers of FPGA chips, Intel and Xilinx, into user friendly graphical user interfaces (GUI). The HDLs are used to define the role of various logic blocks, which include addition, multiplication and accumulation, within the FPGA. Newer FPGA devices have incorporated memory storage, and use histograms to compile data. In this case, the FPGA was programmed off the shelf to function as a digital pulse processor to create a lightweight solution for a portable multichannel analyser. This was done with the software RayPanel, based on VHDL, which programs the device to function as a spectroscope.

In the past pulse processing has been done with analog components, for example an oscilloscope. FPGA technology allows this to be done digitally, eliminating the need for bulky analog electronics, reducing the sensitivity to thermal noise, and allows for the detection algorithm to easily be tuned to fit the purpose. In this case, digital processing consists of an initial analog conditioning stage for the signal acquired from the detector, the conditioned

signal is then digitised by a fast ADC and a FPGA where the pulse is further processed and sorted into a histogram in accordance with its amplitude. The ADC samples at 100 MHz and the digital processing consists employs a trapezoidal filter

This programming used in this project based on open source code for a digital spectroscope, and is developed with the ISE WebPack (Xilinx Inc).

3. Literature review

Reprinted from: *G. Turkington, K. A. A. Gamage, J. Graham, Beta detection of strontium-90 and the potential for direct in situ beta detection for nuclear decommissioning applications*, Nuclear Instruments and Methods in Physics Research Section A: Accelerators, Spectrometers, Detectors and Associated Equipment 911 (2018) 55–65. doi:10.1016/j.nima.2018.09.101. [18]

3.1 Abstract

Strontium-90 is one of the primary beta-emitting radionuclides found at nuclear decommissioning sites. Monitoring its activity in the environment is of utmost importance given its radiotoxicity. Current procedures for the beta detection of strontium-90 are time consuming, produce secondary waste and expensive. There is a demand for real-time in situ radiostrontium monitoring in groundwater at nuclear decommissioning sites. This paper presents a review of existing techniques for strontium-90 monitoring and examines a novel approach through direct beta detection with a gallium arsenide photodiode based detector. A proof of concept detector was modelled in the physics simulation software, Geant4, and evaluated as candidate for in situ detection of beta emitting radionuclides. The simulation results indicate that the detector is physically capable of counting 89.86% of incident 0.546 MeV electrons from a 1 mm range in water. This validation will provide the basis for further development of an in situ beta detector.

3.2 Introduction

Strontium-90, ^{90}Sr , is a beta emitting radioisotope produced during nuclear fission and has been dispersed into the environment as a result of accidents at nuclear power plants, leaks from nuclear waste storage and as fallout from nuclear weapons testing. Commonly known as a "bone seeker", ^{90}Sr is chemically similar to fellow alkaline metal calcium, and when it is ingested into the body it has the propensity to accumulate in bone structure [30, 31]. Given the long half-life of ^{90}Sr , 28.8 years [32], its presence in the body can lead to prolonged irradiation of skeletal bone structure, increasing the risk of damage to bone marrow, leukaemia and other bone cancers [33, 34]. As a consequence, it is of great importance to monitor its activity in the environment, particularly in groundwater surrounding nuclear facilities.

^{90}Sr is one of the major beta emitting radionuclides found at the Sellafield site in Cumbria, UK. Leaks and spills from corroded Magnox fuel cladding silos and neutralised nitrate containing wastes [33, 35] have introduced radiostrontium into the environment, where it has mixed with groundwater. Currently, counting beta emitting radionuclides is a long and arduous process. Samples must be collected from groundwater boreholes, transported to a laboratory, and processed with hazardous chemicals before the activity can be measured. With nuclear decommissioning set to continue at sites like Sellafield for the next 100 years and more, these procedures present logistical and financial challenges for the nuclear industry. The recent disaster at the Fukushima Daiichi nuclear power plant (FDNPP) has brought increased scrutiny on the proliferation of ^{90}Sr in the environment and highlighted the need for rapid and agile measurement procedures [36, 37].

Traditionally, contaminated groundwater is collected for analysis from monitoring boreholes installed into the groundwater table. Within an aquifer comprised of unconsolidated deposits, a filter pack and slotted PVC screen are typically installed into a borehole at a target depth. These features prevent the influx of aquifer material while allowing water to flow into the borehole. Water samples may then be pumped to the surface and transported to the laboratory

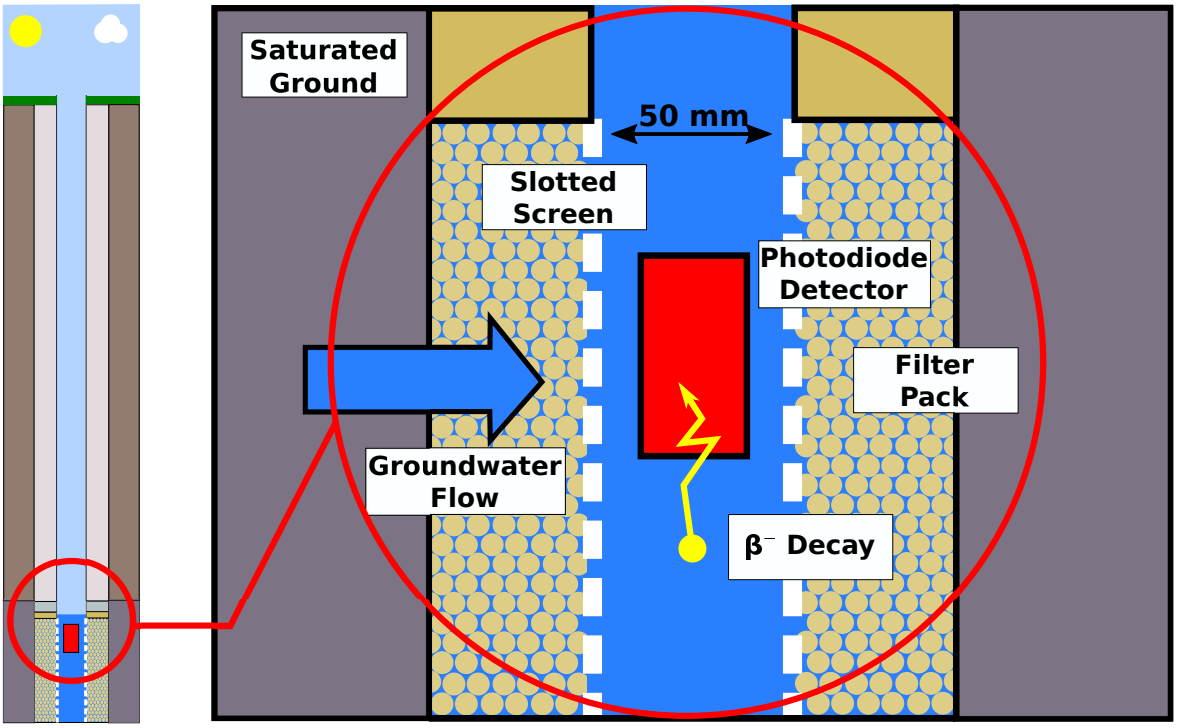

Figure 3.1: A simplified diagram of a typical groundwater borehole scenario, and the prospective deployment of an in situ photodiode detector.

where ^{90}Sr activity is determined by radiochemical analysis. This paper presents a review of the current techniques used in beta detection and explores the potential for in situ beta-counting by direct detection with gallium arsenide photodiode based detectors. This scenario is illustrated in Figure 3.1, where a detector is placed directly into contaminated groundwater in the screened interval of a borehole.

3.3 Beta radiation

Beta particles are electrons (e^-) or positrons (e^+) which are emitted during nuclear decay processes. When an unstable nucleus decays via beta emission, a neutron transforms into a proton and excess energy is shared between the emitted beta particle (e^-) and an antineutrino ($\overline{\nu}$). Equation 3.1 illustrates this through the beta-decay of ^{90}Sr . ^{90}Sr is a pure beta-emitter with a maximum energy of 0.546 MeV [32]. Its daughter nuclei Yttrium-90, ^{90}Y has a shorter

half-life of 64 hours and decays itself, via 2.28 MeV beta emission, into stable Zirconium-90, ^{90}Zr. The short half-life of ^{90}Y means that it is often found in secular equilibrium with ^{90}Sr , a property which can be exploited in radiochemical analysis.

$$^{90}_{38}Sr \longrightarrow ^{90}_{39}Y + e^{-} + \overline{\nu} \tag{3.1}$$

Beta particles are emitted over a continuous energy spectrum, from zero to their maximum end-point energy, see Figure 3.2. Depending on their initial energy, beta particles may have a range of a few metres in air, centimetres in water and millimetres in aluminium [38]. Fast moving electrons typically ionise matter as a result of inelastic coulomb collisions. When a fast-moving electron is decelerated, usually by the electric field of an atomic nucleus, excess energy may be released in the form of electromagnetic radiation, known as Bremsstrahlung radiation [25].

As a beta particle travels through matter, coulombic interactions cause it to lose energy, eventually to the point at which it is no longer detectable. This limited range in matter has presented difficulties when designing beta detectors. In an ideal scenario a direct detector would be small, lightweight and immersible in the detection medium. The detector must operate at very close range in order to capture particles before they have lost a significant fraction of their energy. In addition, an ideal device would be compatible with existing borehole dimensions, be low maintenance and produce no waste. Wireless communications and solar power could remove the need for obstructive headworks, thereby reducing infrastructure requirements. However, in the past these technologies have not been sufficiently developed or readily available. In light of this, many existing techniques have adopted an indirect approach to detection. Indirect radiation detection sees the source stimulate a scintillator, which produces flashes of light which are in turn detected by a photomultiplier tube (PMT) or photodiode. These techniques see water pumped to the surface for sample collection, necessitating surface infrastructure and regular maintenance.

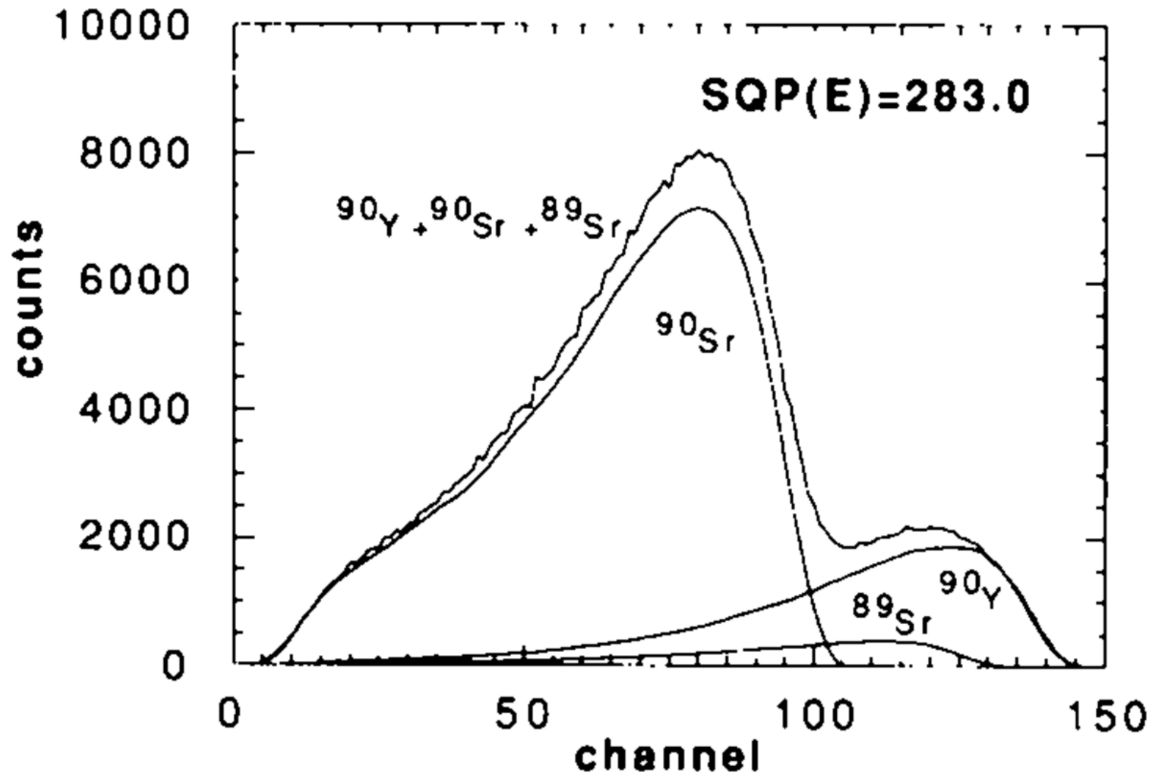

Figure 3.2: The gross beta spectrum observed, with a liquid scintillation spectrometer, from a sample containing ^{90}Sr , ^{90}Y and ^{89}Sr, where the constituent spectra have been deconvolved. SQP(E) refers to the quenching parameter attributed to the sample [8].

3.4 Existing methods for ^{90}Sr monitoring

When a sample of unknown radionuclear composition is collected from the environment, the overlapping of their energy spectra makes it difficult to identify individual beta emitters by spectroscopy. For many beta monitoring techniques, it is essential to isolate the target radionuclide from the sample matrix, thereby removing any other source of radiation entering the detector. There are a number of different methods which can be employed to achieve this, including precipitation [39], liquid-liquid extraction [40], solid-phase extraction [41] and chromatography [42]. When multiple radionuclides are present in the sample, which is inevitable as ^{90}Sr decays to ^{90}Y , it is possible to resolve radionuclides by their spectra provided their beta energies differ significantly [43]. This is achieved by measuring activity over multiple energy windows, and using the resulting information to mathematically resolve

the individual energy spectra of the radionuclides present. C.K. Kim et al. demonstrated a variation on this technique designed for rapid response to emergency scenarios. Their two window approach generated results with minimum detectable limits compliant with IAEA safety standards, with a counting time of just 1.5 hours [44].

Once a radionuclide has been isolated, it can be measured using existing beta counting devices, such as gas ionisation chambers and liquid scintillation counters (LSC). Gas ionisation counting is one of the oldest radiation counting techniques, and measures the avalanche of charge induced as ionising radiation traverses a gas. Despite no longer being at the cutting edge of technology, proportional gas counters have remained popular over the years due to their simplicity, cheap construction and low operational costs. They are still used in the standard procedure for ^{90}Sr monitoring in seawater by the Japanese Government [45]. Liquid scintillation counting (LSC) sees a cocktail of organic fluorescence compounds stimulated by ionising radiation into the emission of light which can be detected and used to determine the activity of a radioactive source. Given the low energy of some beta-emitters and the relatively short penetration depth, LSC has become the most widely used technique for measuring pure beta emitters [46]. However, beta counting by Cherenkov radiation and gas proportional counters are the primary groundwater counting procedure used at Sellafield. Provided the composition of the groundwater sample is known, gross beta counting may offer a cheaper and quicker alternative. However, naturally occurring ^{40}K and ^{90}Sr may conceal ^{90}Sr contamination from nuclear waste, meaning results are not suitable. This section shall review the Cherenkov counting procedure, from sample preparation to activity counting, and highlight the short-comings of this technique for nuclear decommissioning applications.

3.4.1 Groundwater sample collection and pre-treatment

In a traditional groundwater monitoring programme, samples of groundwater are obtained from installed monitoring boreholes, typically through either a dedicated or portable pump

[47]. Samples for gross beta analysis are then filtered, if a dissolved concentration measurement is required, before collection in a pre-acidified plastic container [48], which gives a maximum recommended holding time of 1 month or 2 months for ^{90}Sr .

3.4.2 Radiochemical separation

Many beta counting procedures cannot resolve the spectra of different beta emitting particles, therefore in order to accurately determine the activity of ^{90}Sr in an environmental groundwater sample, it must be separated from contaminants and other radionuclides which may interfere with the counting process. A number of techniques have been developed over the years, each with its own advantages and disadvantages. This section shall investigate the three most commonly used procedures, precipitation, liquid-liquid extraction and extraction chromatography.

The oldest method for radiostrontium separation is by precipitation. In this procedure, strontium is separated from calcium by exploiting the different solubilities of Ca and Sr nitrates in concentrated fuming nitric acid [49, 39]. Radium, lead and barium are collected with barium chromate and the remaining fission products are eliminated with iron hydroxide. ^{90}Y can be separated with hydroxide precipitation and prepared as an oxalate, ready for counting [39]. This procedure, and ones similar to it, have been developed, popularised and standardised since the 1960s. The precipitation technique was popularised because it is robust, efficient and can be applied to large volumes of samples. However it is also laborious, precipitations must be repeated several times to sufficiently extract strontium from the sample [50, 51]. In addition, the health and safety risks, posed through the use of extremely hazardous chemicals, has motivated the development of more rapid and safe techniques.

The liquid-liquid extraction technique selectively isolates radionuclides with the use of two immiscible chemical solvents, typically water and an organic solvent. When the analyte is favourably soluble in the solvent, it will distribute itself from one phase to another, almost completely [40]. This concept can be used to either separate ^{90}Y from the sample, for indi-

rect measurement of ^{90}Sr activity, or for selective extraction of ^{90}Sr using crown ethers. ^{90}Y stripping from the sample is achieved with the use of tri-n-butyl phosphate (TBP), an organic extractant compound [52]. The organic solvent must then be discarded by washing the sample with water, leaving the remaining ^{90}Y to be precipitated to oxalate form and counted by Cherenkov methods.

Extraction chromatography with crown ethers was investigated by Horowitz et. al. in 1990. A crown ether, 4,4,(5')-bis(tert-butyl cyclohexano)-18-crown-6 in 1-octanol, was sorbed onto an inert substrate and used to selectively capture the strontium ions of interest [42]. Given the simplicity of preparation of the ether, and its strong performance in removing strontium from a nitric acid sample, the ether was commercialised and is now sold as Sr Resin, produced by EiChrom Industries, Inc [51]. Sr Resin has been widely adopted in the nuclear industry because it is simple, can be completed in a few hours and is attractive economically since the resin can be reused. However, as the properties of Sr Resin were further investigated, some downsides were revealed. The process of acidifying large volumes of water samples requires precipitation which is time-consuming and may be completed at the expense of some strontium [53], particularly relevant when considering low activity samples. Other extraction chromatography products have been manufactured, including 3M Empore^{TM} Strontium Rad Disks and AnaLig®(R) gels. Empore^{TM} Rad Disks consist of a mesh of PTFE (teflon) fibres hosting AnaLig Sr-01^{TM} selective adsorption chromatographic ligands [41, 54]. Essentially these filters consist of specifically crafted polymers, templated on the desired molecule for extraction. The result is a very selective procedure which is capable of separation ^{90}Sr from even its daughter nuclei, ^{90}Y [55].

Table 3.1: A comparison of radiochemical separation procedures for ^{90}Sr in groundwater.

Method	Avg. radiochemical yield ^{85}Sr %	Avg. Activity $\pm$ 2U (Bq dm^{-3})
3M Empore^{TM} Sr Rad Disk	96	377.6 $\pm$ 43.2
AnaLig® Sr-01(60–100 mesh)	99	328.8 $\pm$ 36.9
AnaLig® Sr-01(230–425 mesh)	97	383.9 $\pm$ 43.3
Sr®(R) Resin	89	319.8 $\pm$ 34.4
Liquid extraction —TBP	86	377.9 $\pm$ 25.0
Carbonate precipitation	54	375.5 $\pm$ 45.5

A comparative investigation of five different radiochemical separation techniques for ^{90}Sr in water was undertaken by J. Ometakova et al. in a 2011 study [56]. The traditional techniques of strontium separation, carbonate co-precipitation and TBP liquid-liquid extraction, were compared along side commercial Solid Phase Extraction (SPE) techniques using 3M Empore^{TM} Strontium Rad Disks and AnaLig(R) Sr-01 resin at two different mesh levels. The results, summarised in table 6.2, compare modern SPE extraction with older techniques. SPE achieved higher radiochemical yields while also being substantially quicker and easier to complete compared to liquid-liquid extraction and precipitation. Separation using 3M Empore^{TM} Strontium Rad Disks was possible in 20 minutes. The authors also found that the traditional methods incurred large volumes of liquid waste as well as the use of hazardous concentrated acids. This is of significance to the nuclear decommissioning industry where thousands of samples must be prepared each year, it is highly desirable to reduce the production of secondary waste as much as possible.

3.4.3 Cherenkov radiation counting

When a charged particle moves through a medium with a velocity greater than the phase velocity of light in that medium, energy is released in the form of light known as Cherenkov radiation. Typically the photons released as Cherenkov radiation are from the UV and visible portion of the electromagnetic spectrum, hence the characteristic blue glow which can be observed in images from the interior of nuclear reactors. This phenomenon has been utilised in the detection of beta particles released from ^{90}Sr and its daughter nuclei. To produce Cherenkov radiation in a medium, such as water, beta-particles must exceed a threshold energy which is dependent on the refractive index of the medium [57, 58]. As such, the refractive index of the selected medium can be used to discriminate between different sources of radiation as the maximum energy of emitted energy from the radioisotope must greatly surpass the threshold energy, given the spectrum of energised beta-particles released [59]. The light produced by Cherenkov radiation can be measured with existing commercial liquid scintillators [60, 61, 62].

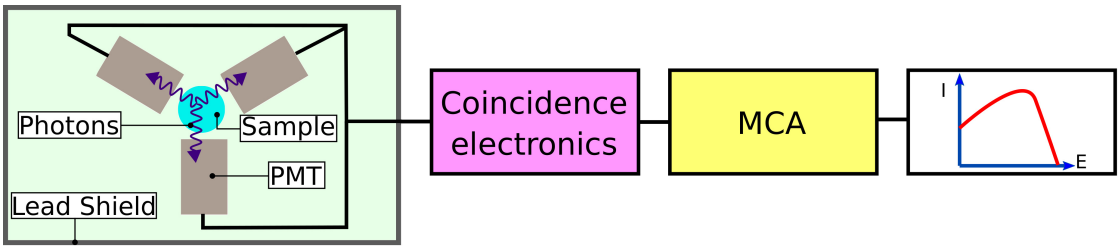

Figure 3.3: A schematic view of the primary components in a typical TDCR LSC device.

Cherenkov radiation counting has a few advantages over similar liquid scintillation techniques. The sample used in Cherenkov counting does not need to be incorporated into a scintillation cocktail, resulting in more efficient sample preparation, disposal and the ability to reuse samples [61]. One of the primary performance limiting factors in Cherenkov counting is known as quenching. This is any process which reduces the intensity of light available for detection by the PMTs. The primary quenching effect in Chernekov counting is colour quenching, simply a consequence of discolouration of the sample, which contributes to the absorption of light emitted during the Cherenkov process. However, this can be compensated by calibration with a colour quench correction curve [62, 63].

An alternative is to use the Triple to Double Coincidence Ratio (TDCR) technique. TDCR has recently become popular with many national metrology institutes as a method of determining primary activity standards. It is an absolute method of determining radioactivity in a source and requires no reference to internal or external sources. TDCR requires a liquid scintillation detector with three photomultiplier tubes (PMT) uniformly arranged around a sample, Figure 3.3, with an electronics package capable of recording triple and double coincidence events [64]. The activity of the source is calculated with a free-parameter statistical model, which considers assumptions about the number of electrons generated during a decay event in the detector [65, 66].

J. M. Olfert et. al. investigated a method for the rapid determination of ^{90}Sr and ^{90}Y in water samples by liquid scintillation and Cherenkov counting [9]. Groundwater samples were collected from the discharge of a groundwater plume, filtered and acidified in preparation

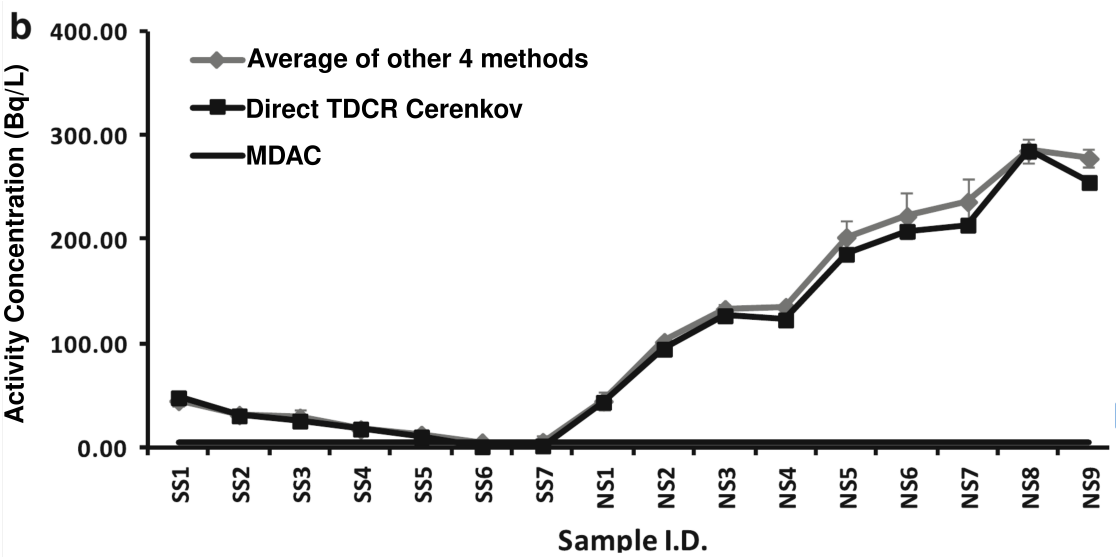

Figure 3.4: A comparison of radiochemical separation procedures for ^{90}Sr in groundwater [9]. MDAC refers to the minimum detectable activity concentration.

for counting. This study compared five different techniques for ^{90}Sr analysis: direct TDCR counting of ^{90}Y , LS counting for ^{90}Sr and ^{90}Y after radiochemical separation, Cherenkov counting for ^{90}Y after radiochemical separation and LS counting of the ^{90}Sr sample for ^{90}Y in growth. After direct Cherenkov counting of ^{90}Y , the samples were radiochemically separated, using Sr and DGA-N resins, into ^{90}Sr and ^{90}Y . The ^{90}Sr sample was counted via LSC, and recounted after 8 days to allow for ^{90}Y in growth. Meanwhile, the ^{90}Y sample was measured by Chernkov and LSC. Each sample was counted with a Hidex 300SL TDCR Liquid Scintillation counter [67]. The results produced by each technique were consistent with each other, validating the TDCR technique against the standard radiochemical procedure as a method for detecting beta-emitting radionuclides (see Fig. 3.3). This affirmation highlights TDCR as a technique with a number of advantages over radiochemical separation. The procedure is fast, requires no sample preparation and does not suffer from chemical quenching. However, radiochemical separation assures that no interfering radionuclides are present in the sample and results were produced within 1 day.

Initially, with a lack of suitable detectors commercially available, many TDCR systems were purpose-built in laboratories. In the last few years, commercially produced detectors have

become available such as the Hidex 300SL. However, these detectors are large and immobile, rendering them ill-suited for in situ detection purposes. The European Metrology Research Programme (EMRP) and the Joint Research Project MetroFission launched an initiative to design and develop a portable TDCR device for use in situ at next generation power plants. Four different national metrology institutes, NPL (UK), ENEA (Italy), LNHB (France), and PTB (Germany) were tasked with producing a device. Each design had to be distinct yet conform with a number of fundamental design principles. Chiefly that the device must fit into a standard car and be light enough to be comfortably handled by one person [68].

The PTB design featured three channel photomultipliers packed into a compact optical chamber itself ensconced in a foam carrying case, a portable mini NIM bin to house the electronics and a portable PC for data acquisition and processing [64, 69]. Initial validations of the device found that it could measure the activity of some high energy nuclides, such as ^{90}Sr , with uncertainties under 1% and a similar percentage deviation from reference TDCR measurements. However, the performance of the device suffered when measuring lower energy emitters as uncertainty contributions from low count statistics and background radiation took on increased significance in the model. It was concluded that while the device was not of the standard required for metrology applications, the device could be sufficient for other field-based research. Indeed each of the devices produced in the design initiative showed promising results in their initial validation measurements and offer promising potential for further development.

Many procedures for Cherenkov counting of ^{90}Sr have been developed over the years [70, 71] and the technique has become the primary method for ^{90}Sr analysis at the Sellafield decommissioning site. Currently, groundwater samples are pumped from boreholes and transported to laboratories for analysis. Strontium is separated using ion exchange resins, and counted in a two window approach[72]. The activity of the ^{90}Sr source is counted immediately after separation and again, after 20 to 30 days, once it has achieved secular equilibrium with its daughter nuclei ^{90}Y. The activity of the original ^{90}Sr source is determined by the ingrowth

of ^{90}Y. Across the Nuclear Decommissioning Authority, thousands of groundwater and solid samples require analysis each year, and there is demand for ever more data to provide a greater understanding of groundwater systems [72]. As this demand increases, the financial and temporal costs associated with Cherenkov counting will mount. This puts financial and organisational strain on decommissioning sites and is the motivation for an alternative approach.

3.4.4 Demand for next generation beta detectors

Sellafield, and other nuclear decommissioning sites, must plan their operation for the next 100+ years and there is an increasing demand for data to be collected more frequently and in real-time while decreasing lifetime monitoring costs. This functionality will allow sites to immediately respond to unexpected spikes in groundwater mobility, which may have gone undetected with existing monitoring routines. In addition, more frequent data acquisition would allow decommissioning sites to enhance their understanding of groundwater systems and the daily factors which influence contaminant mobility. This would provide evidence in the development of conceptual models for radionuclide transport in groundwater, and enhance safety assessments which indicate whether groundwater strontium is being managed correctly. Although more rapid and streamlined versions of existing techniques have been developed [45, 55] , these are reserved for use in emergency scenarios and still suffer from the same drawbacks in terms of chemical waste, sample collection and expenses.

Beta detection by gas ionisation chambers, liquid scintillation counting and Cherenkov counting is very sensitive and precise, with minimum detectable limits of activity well below the standards required to meet World Health Organisation (WHO) guidelines, 10 BqL^{-1} [73]. Indeed, LSC has been adopted by many metrology institutions across the world, such is the calibre of results it can provide. However, the practicalities of these procedures present hazards for workers through manual handling of samples and the risk of exposure to radiation. Samples must be collected from remote locations, delivered to laboratories, treated

with chemicals, counted and finally disposed of. As these procedures must be completed hundreds of times per year for the duration of the facility's lifetime, there will be significant operating costs and production of secondary wastes.

This paper seeks to propose an alternative approach to beta spectroscopy, through direct in situ detection of beta radiation. Attempts have been made to produce in situ versions of the weighty lab-based detectors required for existing techniques, but this does little to satisfactorily address the demands for real-time radiostrontium monitoring in groundwater. This paper considers a novel approach where the detector is deployed within groundwater boreholes, directly at the source of radiation. This would require a radiation detector that is sensitive to beta radiation, offers real-time detection, while also being highly portable. Such a device would be unburdened by time-consuming sample collection and chemical treatment procedures. One potential solution comes in the form of photodiodes, adapted for use as direct radiation detectors. Photodiodes are devices designed to convert light into electrical current, recognisably used in solar panels. The same mechanisms that allow for the conversion of visible light to current also apply to ionising radiation.

3.5 PIN photodiodes

This research aims to develop a highly mobile, fast and efficient beta-radiation detector, free from the lengthy chemical separation and counting procedures outlined in the previous section. To this end, PIN photodiodes are being investigated as candidate for a light weight radiation detector. Initially developed to detect photons and used as an alternative to PMTs, photodiodes have been increasingly investigated in recent years as a tool for direct radiation detection. In comparison with gas-filled or scintillation detectors, semiconductors have a lower energy requirement for charged particle detection resulting in superior energy resolu-

tion [74]. They now have a number of applications in medical imaging, dosimetry, power generation and high-energy radiation experiments[75, 76, 11, 77].

In contrast to PN-junction semiconductors, PIN photodiodes have a large intrinsic layer separating the p and n-type layers. Figure 3.5 illustrates a simplified configuration of a PIN photodiode and its interaction with ionising radiation. As radiation enters the intrinsic layer, it disrupts electron-hole pairs which are swept up by a reverse-biased voltage and the resulting current is measured. The more energy is deposited, the greater the current pulse produced. By extending the size of the depleted region, a larger volume is presented for ionising radiation to fully deposit its energy within the sensitive region of the detector.

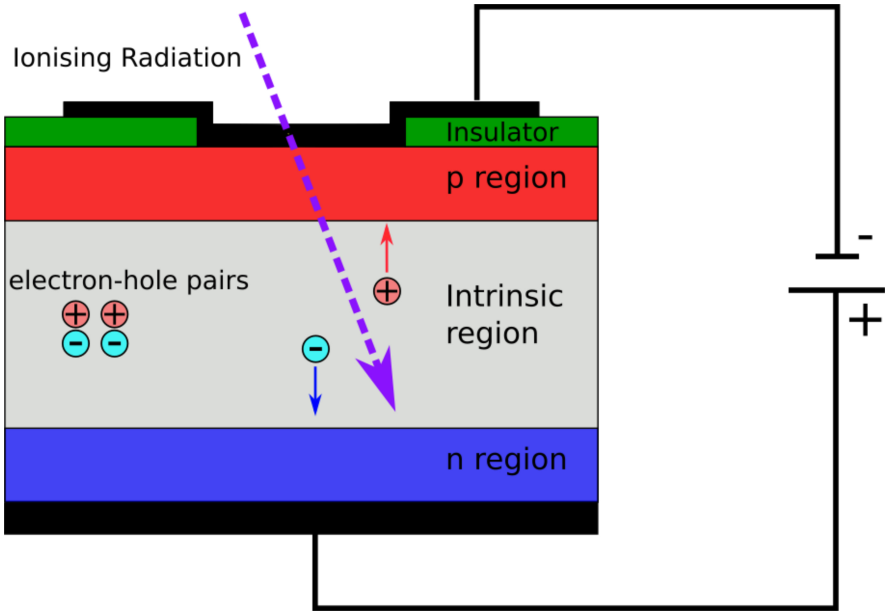

Figure 3.5: A simplified view of ionising radiation generating a current pulse in a PIN photodiode operating under reverse biased voltage.

A number of materials are used to construct semiconductor photodiodes, each with their own strengths and weaknesses. Silicon and germanium rapidly emerged as widely used semiconductors, largely due to early advances in manufacturing allowing for high quality devices to be made cheaply and quickly. However, these materials have properties which make them less than ideal candidates for in situ beta detection. Germanium detectors offer excellent energy resolution but, due to a very narrow bandgap of 0.66 eV, require cooling

to liquid nitrogen temperatures to reduce thermally induced noise [25]. This clearly makes germanium ill-suited for mobile applications. While silicon has a wider bandgap, 1.1 eV, it still requires cooling and its low atomic number, 14, means it has relatively poor stopping power for ionising radiation.

3.5.1 Gallium arsenide

Gallium arsenide has a number of properties which make it an attractive alternative to silicon and other semiconductor materials. Gallium and arsenic have atomic numbers of 31 and 33, respectively, resulting in the material having greater stopping power for ionising radiation, like X-rays, in comparison with silicon devices [78, 79]. The bandgap of the compound material, 1.42 eV, is wide enough that devices can be operated at room temperature [13, 78, 79] without overwhelming thermal noise. Table 3.2 compares some of the fundamental properties of GaAs and Si. As the electron mobility of the GaAs is approximately 6 times greater than Si, this should allow for a device which functions over a shorter time scale.

Table 3.2: A comparison between the semiconductor properties of Si and GaAs [14].

Property	Silicon	Gallium-arsenide
z	14	32
ρ (gcm^{-3})	2.33	5.31
Radiation Length (cm)	9.36	2.3
Pair Production Energy (eV)	3.55	4.27
Electron Mobility (cm^2/Vs)	1500	7000-8500

Radiation detectors, unsurprisingly, are bombarded with ionising radiation and it is important that the device is not degraded or significantly damaged over time. The ability of a material to withstand the damage is known as its radiation hardness. There are two principal ways in which radiation can negatively affect a semiconductor, displacement damage and ionisation damage. Displacement damage refers to the permanent physical dislocation of atoms from their lattice positions by incoming radiation. This produces defects in the material resulting in intermediate energy states, facilitating easier separation of electron-hole pairs, thus generating current and contributing to noise in the detector. Additionally, charges can become trapped on intermediate levels, which will negatively affect counting statistics. Ionisation

damage occurs after energy deposition in the detector frees electron-hole pairs which drift to other locations and become trapped. When sufficient concentrations of charge are trapped, localised parasitic electric fields can develop [80].

A. Sagatova et al investigated the radiation hardness of GaAs devices against gamma radiation, high energy electrons and fast neutrons [15]. The detectors, beams and doses used in their experimentation is summarised in Table 4.1. An Am^{241} gamma spectrum was captured at each dosage and the results of electron damage on the spectra acquired, photopeak area, charge collection efficiency (CCE) and full width half maximum (FWHM), indicative of the energy resolution, were documented. Curiously, the results reported indicated that low doses, 1 kGy, of electron damage may even improve the performance of the detector, and this was attributed to the radiation damage compensating for pre-existing defects in the device. The study found that the damaging induced by electrons was up to 10 times worse than that of gamma photons, and up to 1000 time worse for neutrons. Indeed, the device was no longer functional after a dose of 0.576 kGy of fast neutrons, and was still functional, albeit in a limited capacity, after the full course of electrons and gamma.

Table 3.3: Experiments carried out by A. Sagatova et al [15] determining the radiation hardness of GaAs.

Radiation	Detector Thickness (μm)	Energy (MeV)	Max Dose (kGy)
Gamma	250	1.33	1140
Electrons	230	5	104
Neutrons	300	2-30	3.215

The radiation damage in GaAs sensors has been investigated by numerous studies [14, 81, 82] and has been compared favourably with silicon [82]. The strong radiation hardness of GaAs, has seen the material used radiation harsh environments like high energy particle accelerators and satellites, and suggests that GaAs is a viable candidate for use at nuclear waste disposal facilities.

In recent years, GaAs photodiodes garnered increasing interest for their potential as X-ray imaging devices. One of the hurdles in this has developing detectors with intrinsic layers

thick enough to stop energetic radiation such as X-rays, with as few defects as possible to maintain strong energy resolution. Detectors designed for beta detection will likely require similarly thick intrinsic layers.

The major imperfection associated with GaAs crystals is known as the EL2 defect. This defect is present in many fabrications techniques, including Metal Organic Chemical Vapour Deposition (MOCVD) and Liquid Encapsulated Czochralski (LEC), however is notably absent in Molecular Beam Epitaxy (MBE) [83]. The exact nature of this defect is the subject of much debate, but it is known to produce a midgap deep level, essentially a trap for electrons. The presence of the EL2 defect restricts the sensitive volume of the device, which is crucial for radiation detection. The ionised form of the defect meanwhile reduces electron lifetime, dampening charge collection efficiency and therefore energy resolution [11]. This defect has presented a stumbling block in the use of GaAs photodiodes in sensitive applications, such as medical imaging and radiation detection.

3.5.2 Applications in radiation detection

One of the limiting factors in the adoption of GaAs devices as radiation detectors has been the presence of defects, such as EL2, in the bulk material. This induces a small sensitive layer thickness, low values of electron charge collection efficiency, current oscillations in the detector and non-uniform field distribution. A. V. Tyazhev et al [10] noted these flaws in the LEC process. As an alternative, they proposed using chromium compensated GaAs layers. Their study validated the composition through I-V characterisation, electric field distribution tests and CCE assessment. It was found that chromium doped GaAs offers high resistivity, thickness approaching 1 mm, more uniform electric field distribution and functional levels of CCE for use in X-ray pixel detectors. Figure 3.6 offers a point of comparison between a LEC GaAs device, operating at 250 V, and a chromium compensated device, on the right. The function plotted is $F = 1-T$, where T is the spatial distribution of light transmission through the detector thickness. This demonstrates that chromium compensated GaAs structures offer

a more uniform electric field distribution, which is stable over a range of operating voltages. This uniformity of electric field is significant, because it allows for detectors with very thick intrinsic layers to be operational.

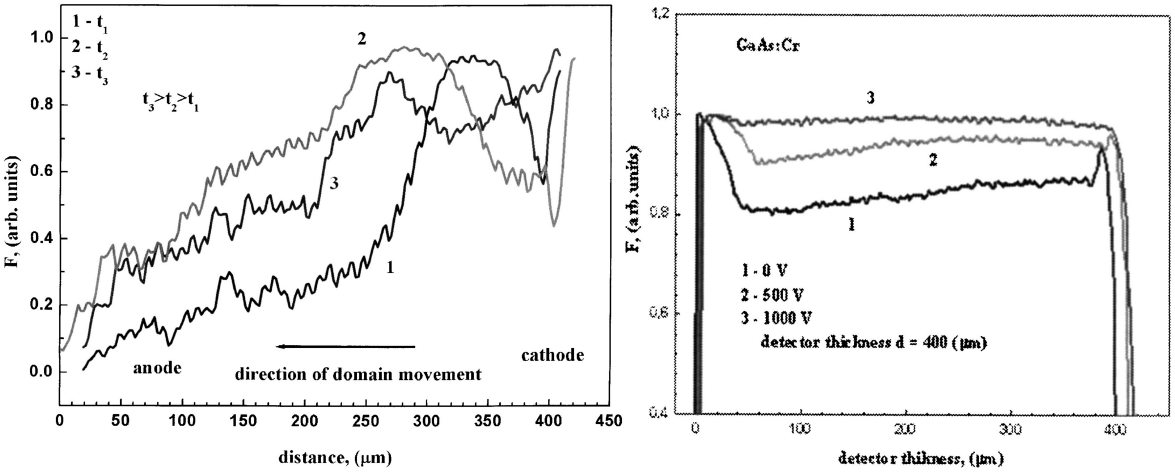

Figure 3.6: These graphs plot the function F, a cypher for electric field distribution, through a LEC frabricated detector, left, and a chromium compensated detector, right [10].

Building on A. V. Tyazhev's research, M.C. Veale et al [11] produced 500 μm thick chromium compensated GaAs devices and tested their potential for X-ray and γ-ray spectroscopy and imaging. The GaAs wafer was affixed to Schottky electrodes, etched with an 80x80 array of 200 μm anode pixels and bonded to a HEXITEC ASIC readout chip. I-V characteristics for the device were measured at 280 K and 298 K, with the room temperature resistivity measured as 2.5×10^{9} Ωcm. To investigate the spectroscopic ability of the detector, an ^{241}Am γ spectrum was collected at 280 K. The FWHM of the 60 keV photopeak in this figure is 2.9 keV. As a proof of concept for X-ray imaging a test object, fitted with different materials, and imaged by 5-80 keV X-rays. This is illustrated in Figure 3.7. The materials, from clockwise, are adhesive putty, indium, lead, tin, and indium. The image produced, right, indicates the ability of the detector to distinguish between different materials thereby functioning as an imaging device.

Elsewhere, C. Erd et al [84] developed a spectroscopic X-ray imaging device based on epitaxially grown GaAs. The prototype array was fabricated by growing a 325 μm epitaxial intrinsic GaAs layer onto a 200 μm n+ substrate, topped with a 6 μm p+ layer, completing

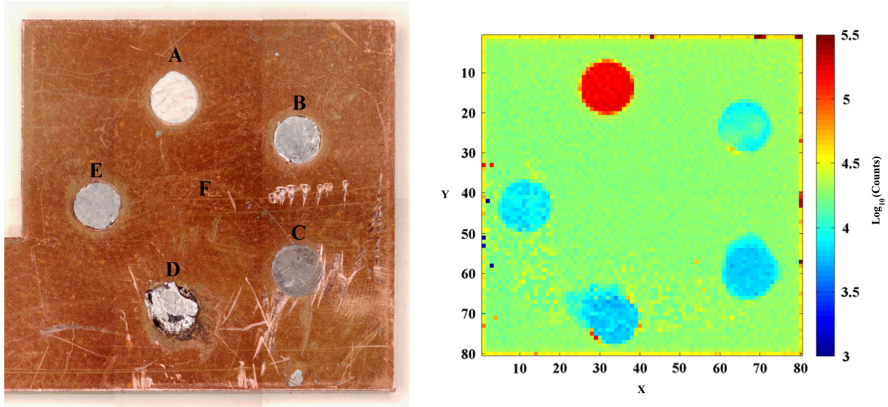

Figure 3.7: A proof of concept demonstration of X-ray imaging with a GaAs sensor [11].

the PIN structure. The 1.1 cm^2 surface area was etched into a grid of 32x32 pixels. Optimal operating conditions for the reverse bias, 60 V, were established and the energy resolution of individual pixels were found to range from approximately 290 eV for a 5.9 keV beam and 780 eV for a 100 keV beam. These results were obtained at room temperature, and the investigations into variation of resolution with temperature found a 10% gain in resolution as the device was cooled to 5 °C with negligible improvements at cooler temperatures.

The results found here can be contrasted with the previously cited study into chromium compensated GaAs. C. Erd et al's device was anticipated to achieve a resolution of 0.5 keV for the 60 keV photopeak on an ^{241}Am source at room temperature. The same photopeak has a resolution of 2.9 keV for the GaAs:Cr detector. The GaAs:Cr detector has a thicker intrinsic layer, which should contribute to better energy resolution in principle, however this device was not based on epitaxially grown GaAs, as was the case with C. Erd's device. Veale et al selected the LEC growth technique in order to grow a thick material bulk whereas the MBE technique allows for the precise and orderly growth of crystal layers, at lower temperatures than LEC, reducing the risk of defect inducing effects like interdiffusion [85]. Deficiencies in material quality can give rise to charge collection inefficiencies which introduce noise to the detriment of energy resolution. Furthermore, C. Erd et al developed and tested low noise pre-amplifier designs which may have played an additional role in the superior energy resolution of their device. C. Erd, et al also found the FWHM of a 5.9 keV photopeak, 0.26 keV,

which can be contrasted with a more recent study by G. Lioliou et al [79]. They conducted a comprehensive characterisation of MOVCD GaAs photodiodes, fabricating 200 μm and 400 μm diameter device with 10 μm thick intrinsic layers. The detectors have energy resolutions of 0.69 keV and 0.73 keV respectively. The authors suggest their relatively thin device suffers primarily from the effects dielectric noise in addition to white series noise and Fano noise. These factors are all correlated with the capacitance of the device, which is reduced in thicker devices. This can give rise to a number of benefits including increased quantum efficiency and lower pulse shaping times [25]. Future work will see the authors reconsider the design of the pre-amplifier by combining the photodiode and the junction gate field-effect transistor (JFET) into the same substrate with the aim of reducing dielectric noise. Additionally, further refinements in device passivation may reduce surface leakage current and bring the energy resolution performance closer to the previously discussed devices.

There are many other studies investigating the burgeoning field of X-ray spectroscopy by GaAs photodioes and it can be concluded that these devices have potential in this field [86, 87]. These studies have validated some of the advantages of using GaAs including radiation hardness, energy resolution and room temperature operation. In addition to giving insight into suitable fabrication techniques, I-V characteristics and potential readout electronics. However, there have been few documentations of their application to beta radiation.

Barnett, Lees, and Bassford attempted direct detection of ^{3}H and ^{14}C beta particles with GaAs photodiodes [12]. Their detectors were grown by MBE and photolithographically etched into 200 μm diameter diodes with 2 μm thick intrinsic layers. Beta propagation through the device was simulated with the Monte Carlo software, CASINO [88]. Particles ranging in energy from 1 keV to 156.48 keV were simulated, investigating their penetration depth and deposition of energy within the detector. Figure 3.8 shows the results of the simulation of 156.48 keV electrons. It can be observed that the thin intrinsic layer of this detector is not sufficient to stop incoming radiation of this energy, and the electrons penetrate into the substrate layer of the diode. This indicates that a much thicker intrinsic layer would be

required for beta particles approaching the energy of those released by ^{90}Sr and ^{90}Y . Other results from this study indicate that the limiting factor on the detection of low energy beta particles, less than 5 keV, is the p-type layer on the surface of the detector. This region attenuates the particles sufficiently such that the maximum proportion of their energy deposited in the intrinsic layer is only 50%. The detector was used to capture ^{3}H and ^{14}C spectra which, after calibration, showed accordance with accepted spectra for these nuclides. The results presented here are promising for the potential of GaAs detectors, although evidently the intrinsic layer is likely much too thin for efficient ^{90}Sr detection.

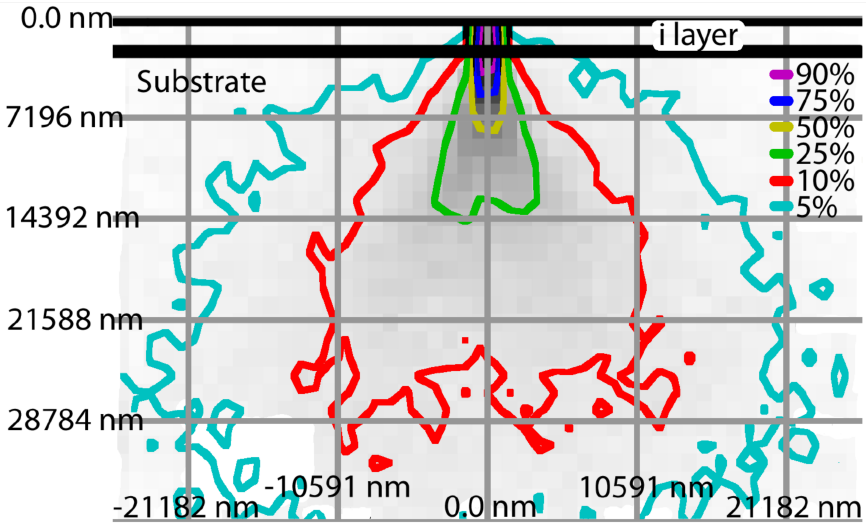

Figure 3.8: The percentage of initial energy, 156.48 keV, of beta particles deposited in a GaAs detector [12]

Lioliou and Barnett [89] characterised GaAs p^+-i-n^+ mesa photodiodes to assess their potential as low energy beta spectrometers with a view to using them in applications for space plasma physics. GaAs photodiodes were fabricated for this study at the EPSRC National Centre for III-V Technologies, Sheffield, with a 10 μm undoped GaAs intrinsic layer sandwiched between a 0.50 μm thick GaAs p^+ layer and a 1 μm n^+ layer. Reportedly the thickest X-ray mesa photodiodes produced to date, the wafers used for beta spectroscopy had a 200 μm diameter. Initially, the detectors were simulated with the Monte Carlo simulation software, CASINO. A point source of 4,000 electrons, varying from 1 keV to 66 keV, were fired at the detector surface and the depth of their penetration is summarised in Figure 3.9. Simu-

lations were run with and without the presence of the Ohmic contact required on the detector, which covered 45% of the detector's surface. The simulation predicted a maximum external quantum efficiency of 49% from a 66 keV source, with the major limiting factors being the absorption of electrons in the top layers of the diode and the Ohmic contacts.

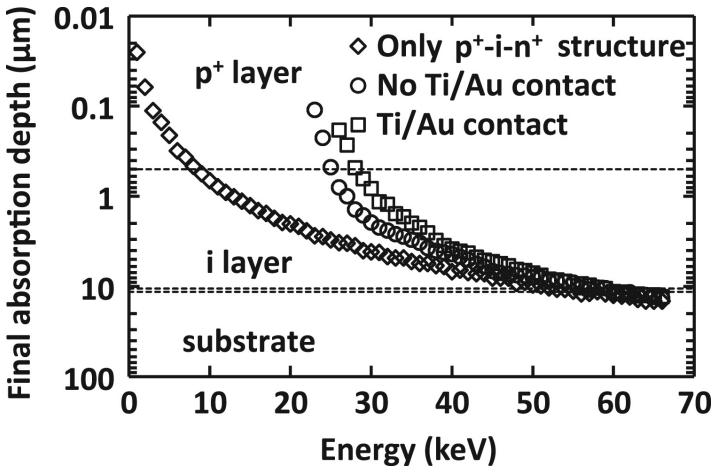

Figure 3.9: The simulated absorption depth of electrons in a GaAs p^+-i-n^+ detector as a function of their energy [13]

Following on from the simulation, a real-world validation was carried out. A ^{63}Ni source was placed 5 mm above the surface of the GaAs photodiode, which was operating under a 10 V reverse bias. After a counting time of 400 s the collected beta spectrum was compared with the accepted spectrum of a ^{63}Ni beta source, normalised to reflect experimental conditions. The maximum energy observed in the intrinsic region was approximately 50 keV, suggesting that maximum energy particles were losing 16 keV. This was a 9 keV difference from the maximum energy predicted in the simulation. This discrepancy was attributed to the absorption of energy in insensitive sections of the detector, including the p^+ layer in the device, the nickel protective layer around the source and the air gap between source and detector. While these results were promising for the potential of GaAs photodiodes as electron spectrometers, they were conducted with a device designed for X-ray rather than beta-spectrometry in mind. The response of the device to much higher energy electrons remains to be seen, whether they are stopped by the intrinsic layer in sufficient numbers to produce a clear signal. It is likely that detection of ^{90}Sr with GaAs photodiodes will require devices thicker

than the 10 μm devices which have been tested in these studies. The photodiodes fabricated for X-ray detection have demonstrated that it is possible to produce thicker detectors and by producing a chromium doped or epitaxially grown device can address the defects which have previously hindered the development of GaAs devices.

3.6 Monte-Carlo simulations

Reviewing the literature has highlighted some tentative studies applying GaAs photodiodes as beta radiation detectors, however, these have only been applied to low energy beta emitters. The devices used have relatively thin intrinsic layers, particularly in comparison with some of the detectors being developed for X-ray detection. A proof of concept simulation was developed to investigate the potential for GaAs as a beta detector in a groundwater borehole scenario, for energies on the scale of ^{90}Sr and ^{90}Y decay. The physics simulation package, Geant4, was used to construct a basic model of a GaAs detector and simulate its interaction with beta-particles. Geant4 is a Monte Carlo simulation based software and is written in the object-oriented programming language C++ [90]. Step by step the software tracks the path of radiation as it travels through matter. At each step the probability of interaction and random number generation predict the next step along the particle's track. The exact nature of the physics processes invoked in the simulation and their cross-sections are defined by the "Physics List" selected for the simulation. Geant4 includes a number of reference Physics Lists and this simulation used the FTFP_BERT list, the Geant4 default which is valid for electrons up to 100 TeV.

The proof of concept detector was based on a device created by C. Erd et al [84]. This design was selected due to the relatively thick intrinsic layer, especially in comparison with previous detectors applied to beta radiation. Matching the thickness of the intrinsic layer, 0.325 mm, and surface area, 1.1 cm^2, a GaAs detector was created in Geant4 code and placed in

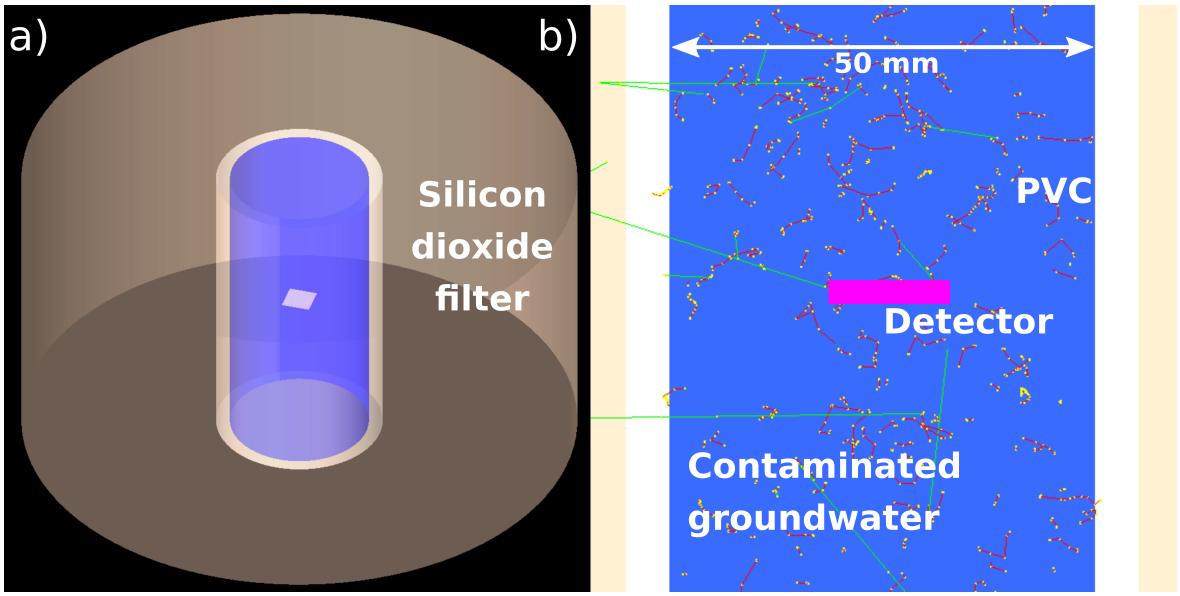

Figure 3.10: An overall visualisation of the Geant4 simulation can be seen in image a). Image b) is a cross section of the well, filled with ^{90}Sr contaminated groundwater. As nuclei decay beta particles are released and traverse the water in erratic paths. They are either fully absorbed, deflected, or release bremsstrahlung radiation, the long straight lines. Bright dots mark steps in the particle's path.

a modelled groundwater borehole. Figure 3.10a visualises the borehole with the detector submerged in groundwater. A cross section of the scenario is seen in Figure 3.10b. Here, decaying ^{90}Sr particles are randomly dispersed throughout the groundwater. As ^{90}Sr decays, electrons, the short erratic trajectories, are released and tracked as they travel through space. Bright dots mark steps along the particle's trajectory before it is fully absorbed by the environment or the detector. As the particles interact the detector they are either backscattered, pass through the detector while only depositing a fraction of their energy, or fully absorbed within the intrinsic layer of the detector. Their energy and path are recorded, along with the number of counts in the detector for the entire run. The long and straight particle lines shown in this image represent photons, likely the result of the Bremsstrahlung effect. The anti-neutrinos released during beta decay are hidden for visual clarity.

The initial simulation examined whether the detector had sufficient stopping power to detect electrons emitted during ^{90}Sr and ^{90}Y decay. A particle gun was positioned 0.1 mm from the surface of the detector and the energy of the beam was increased from 0.1 MeV to 2.2 MeV.

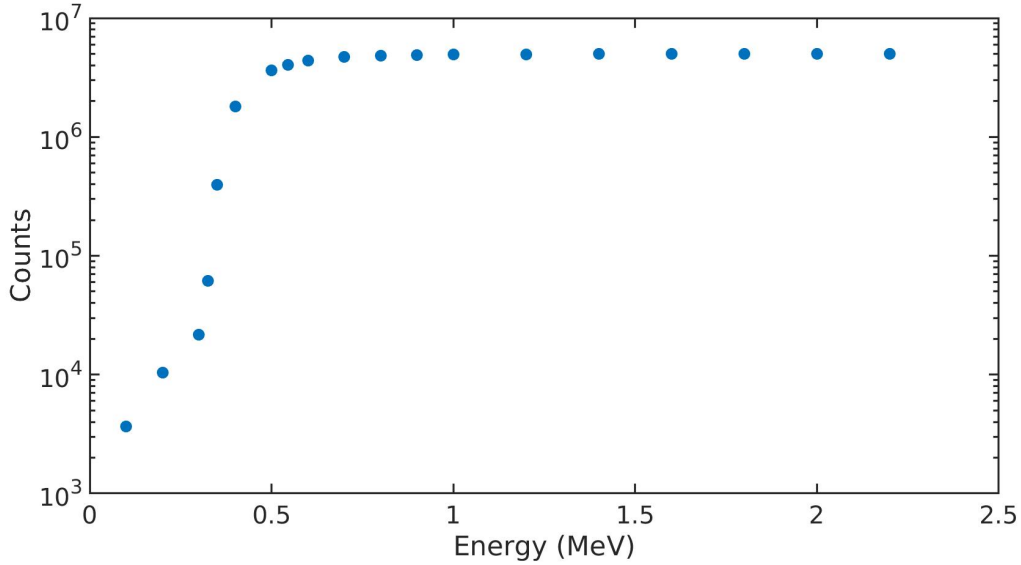

Figure 3.11: The number of counts recorded in the detector for increasing beams of electron energy. Errors range from ± 35 to $\pm 1.290 \times 10^3$ and as such are not clearly visible on the graph.

Each run consisted of 5×10^6 electrons and the results can be seen in Figure 3.11. Fewer counts are observed at lower energies, attributed to the increased likelihood of low energy electrons to be absorbed before detection and to backscatter on the surface of the detector. As the energy increases to 1.2 MeV, nearly the entire run of electrons, 99% on average, deposit energy in the detector and are counted. However, this does not account for how much energy is being deposited by each particle. Some electrons are backscattered, leaving only a fraction of their energy, or simply pass through the detector. When designing the photodiode, it will be of utmost importance to ensure the intrinsic layer is thick enough to fully capture the energy of particles released by the radionuclides of interest, thereby being capable of fully recording their beta spectra.

The second simulation investigated how the intensity of the radiation detected varied with increasing distance from the source. A 0.546 MeV beam of electrons was fired at the detector from 0.1 cm away increasing to 8.5 cm. Figure 3.12 displays the results. The number of counts observed by the detector decays exponentially with increasing distance. Particles released within few millimetres from the detector's surface, dropping to tens of counts at a

range of 8 cm. This detector aims to be used in situ, and will have to operate at some distance from the source, so the detectable range of the detector is a key characterisation.

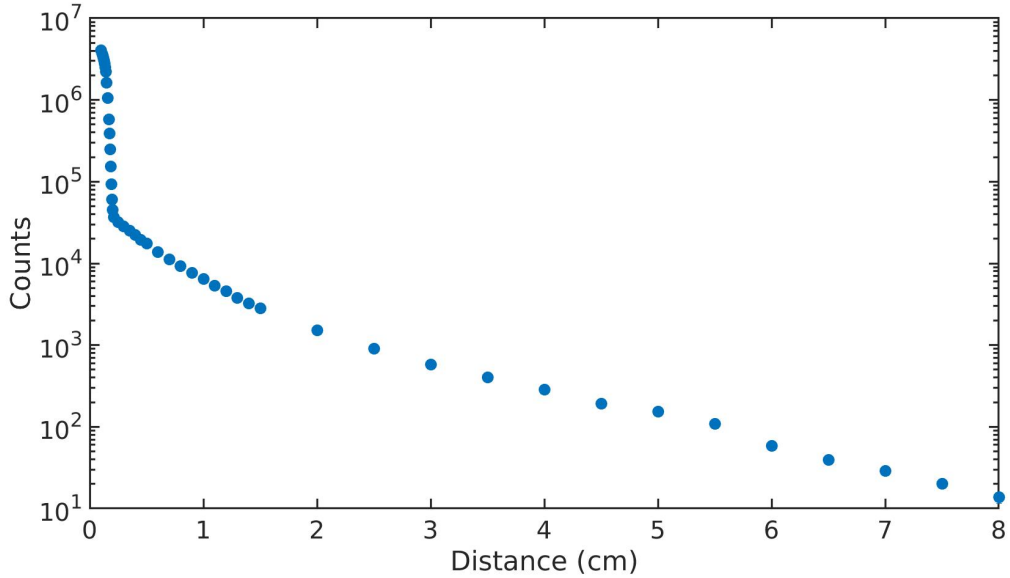

Figure 3.12: The number of counts detected as the detector is moved further away from a 0.546 MeV electron beam source.

As an exhibition of the potential application of the detector, the device was used to collect a spectrum of radiation from a contaminated groundwater source. A 5 cm deep cylinder of water was randomly filled with decaying ^{90}Sr particles. A full decay chain was realised for each ^{90}Sr particle, resulting in ^{90}Y production and decay to stable Zr. The simulation ran for 1×10^7 decay events. The spectrum of beta radiation captured in the detector is seen in Figure 3.13. The first peak is largely comprised of beta particles released during ^{90}Sr decay, and the lower second peak is indicative of ^{90}Y decay, which tails off at a much higher energy, approximately 1.8 MeV. It should be noted that the particles generated during this simulation must travel some distance before reaching the detector, and as such will have already lost some of their kinetic energy to the surrounding environment.

The simulation results presented here are encouraging for the potential of GaAs photodiodes as in situ detectors for the radiometric assay of ^{90}Sr . It has been demonstrated that a detector of real-world proportions can be successfully detect beta particles of the energy scale

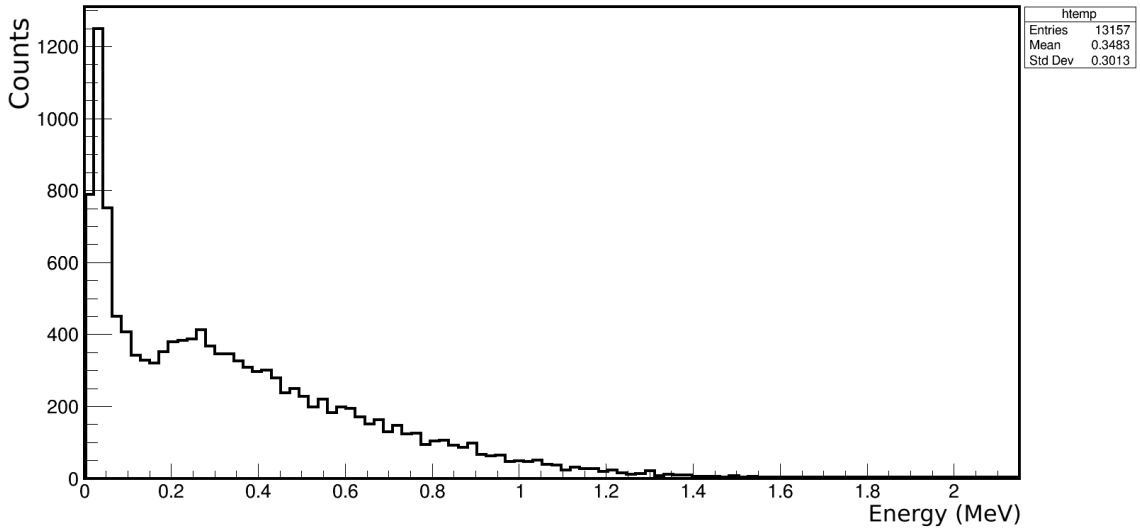

Figure 3.13: The spectra of beta particle energy recorded in the detector after 1×10^7 ^{90}Sr decay events were simulated. The large peak at the start of the spectrum is a result of partially absorbed beta particles. The peak visible at the start of the spectrum is due to to the backscatter and partial absorption of beta particles in the detector. The second peak, at 0.3 MeV, is due to the emission of ^{90}Y.

required in a situation modelled on a real world scenario. This suggests there is potential to use GaAs photodiodes in the development of an in situ beta detector.

3.7 Conclusions

This paper has presented a review of existing methods for the radiometric analysis of ^{90}Sr in the environment and their suitability, or lack thereof, for in situ detection has been examined. Nuclear decommissioning sites have a demand for real-time, in situ, monitoring of radionuclides in groundwater to improve their response to fluctuations in groundwater activity and to further evaluate waste management. Current techniques are lab-based, time consuming and expensive. While there have been attempts to reduce the time-scales involved in these procedures, and create more mobile detectors, these only go part way to addressing the practical difficulties associated with these techniques. A novel approach based on the direct detection of beta radiation has been proposed. GaAs photodiodes were examined for their ability to directly detect ionising radiation, and their suitability for beta radiation was validated through simulation.

The research presented here has suggested that GaAs is indeed a strong candidate for an in situ beta detector. The wide bandgap of the material means it can eschew the cooling requirements of other semiconductors, reducing the size and weight of the detector. Meanwhile its radiation hardness suggests GaAs devices are well suited for operation at sites of nuclear waste and spillage. Development of such a device will enable real-time counting of beta radiation in difficult to reach areas, such as groundwater boreholes, reducing risk of exposure to workers.

Initial Geant4 simulations have demonstrated that GaAs has right physical properties to detect beta radiation. The fabrication technique selected can have an influence on the defects present in the device and its operating characteristics, energy resolution and efficiency. Photodiode junction layers and electronics readout systems will also influence the energy deposition of radiation in the detector.

4. Detector Design

Reprinted from: *G. Turkington, K. A. A. Gamage, J. Graham, Direct measurement of strontium 90 in groundwater: Geometry optimisation of a photodiode based detector*, Journal of Instrumentation 14 (10) (2019) P10018–P10018. doi:10.1088/1748- 0221/14/10/P10018. [19]

4.1 Abstract

This paper examines the feasibility of detecting strontium 90 in groundwater directly with photodiodes and considers the physical parameters which maximise radiation absorption within the detector. Geant4 simulations were used to draw comparisons between silicon, gallium arsenide and cadmium telluride detectors of varying surface area and thickness. Detectors were compared in their ability to absorb point and scattered sources of radiation. The results indicate that a large surface area detector, up to 10 mm^2, and 1 mm thick offered the highest detection efficiency in a contaminated groundwater simulation. 1 mm thick and 100 mm^2 detectors cadmium telluride and gallium arsenide detectors were modelled in a groundwater borehole scenario. Each material offered similar detection efficiency, but the greater backscattering effect in cadmium telluride resulted in a greater peak at lower energies compared to that observed in gallium arsenide.

4.2 Introduction

Leaks and spills of waste at nuclear decommissioning sites have introduced radionuclides, such as ^{90}Sr, into environment resulting in contamination of the groundwater table. ^{90}Sr has a half-life of 28.8 years and decays with an end-point energy at 0.546 MeV. Its daughter, Yttrium 90, decays with an end-point energy of 2.278 MeV with a significantly shorter half-life of 64 hours [32]. Due to its half life and radiotoxicity Sr-90 will need routinely monitoring for many decades on some sites. Current techniques necessitate the manual sampling of groundwater from boreholes and analysis is performed in off-site laboratories. Samples are radiochemically treated and activity is measured by liquid scintillation, Cherenkov or proportional gas counting methods [49]. These processes are time consuming, produce secondary waste and are expensive. By detecting radiation directly and in situ, the need for sample collection can be eliminated which may reduce the worker dose and lifetime monitoring costs [18]. This paper proposes the optimal physical characteristics for a photodiode detector for in situ ^{90}Sr measurement in groundwater.

4.2.1 Semiconductor diodes

Photodiodes are semiconductor materials which produce a current pulse in response to ionising radiation when operating under a reverse bias voltage. Incident radiation separates electron-hole pairs within the intrinsic region, producing a current pulse in proportion to the energy deposited by the incident particle. Photodiodes may be formed by placing a layer of undoped semiconductor between positively, p, and negatively, n, doped layers, forming a p-i-n junction, or the deposition of metal contacts onto the semiconductor material, forming an ohmic or Schottky diode. The undoped intrinsic layer is the sensitive region and responsible for charge generation as ionising radiation is absorbed within the detector. Originally developed as photon detectors, in recent years photodiodes have been used to detect ionising radiation [91, 92].

Photodiodes are fabricated from numerous materials, each with unique properties. Silicon is the most commonly used, mature and widely available semiconductor. It has a low atomic number, 14, and a narrow bandgap, 1.17 eV. The narrow bandgap means that silicon detectors must often be cooled to reduce thermal noise [25]. GaAs has a higher effective atomic number, 32, and a bandgap of 1.42 eV which makes it viable at room temperature [78] and has superior resistance to radiation damage [15]. In recent years GaAs detectors been developed as gamma and X-ray detectors with applications in medical physics and astronomy [91, 84, 87, 79, 93]. The intrinsic layer in these devices range from just 10 μm to 500 μm. CdTe has an even higher effective atomic number, 50, than GaAs, and an even wider bandgap, 1.5 eV. In principle, these properties suggest CdTe may be even more effective at absorbing ionising radiation while also capable of room temperature operation [92, 94, 95, 96].

This paper aims to design photodiodes which will be deployed into contaminated ground-water to determine the activity of ^{90}Sr directly. The detection efficiency must be maximised, defined as the ratio between the number of particles which deposit energy in the detector and the number of particles emitted [25]. The surface area, thickness and material composition of the detector are factors which will determine the detection efficiency. In this case the detector must be capable of fully absorbing the beta particles released during ^{90}Sr decay, up to 0.546 MeV, and ^{90}Y decay, up to 2.278 MeV. If the particles in question are of sufficient energy, they will simply pass right through the detector, while only depositing a fraction of their initial energy. While this can be recorded as a “hit” in the detector, and can be used to determine the activity of a source, the information will be insufficient for capturing a spectrum of emission.

4.3 Monte Carlo simulations

Geant4 is a Monte Carlo simulation code developed to model the propagation of radiation through matter [97]. Written in C++, Geant4 code has been used to simulate radiation-matter interactions in high-energy particle physics, medical and nuclear applications. The software traces radiation, step by step, as it traverses through matter. The probability of interactions with matter are described by probability distributions, known as cross-sections. Random number generation at the beginning of each step determines the outcome of the interaction. Data about the detector's response to radiation can then be collated and processed. The cross-sections are determined by the "physics list" which details the set of processes involved in the simulation. In this project a Geant4 model has been developed to simulate how beta radiation is absorbed in photodiodes in a groundwater borehole environment, and whether they are suitable for use as in situ beta detectors. This simulation used the FTFP BERT list which covers electron interactions up to 100 TeV.

4.3.1 Absorption of beta particles

The thickness of the detector is one of the factors which will determine how effectively it absorbs incident beta particles. Detectors of increasing thickness were modelled with 100 mm^2 surface areas. A beam of 1×10^7 0.546 MeV electrons was fired into the centre of the detector, from the surface, and the energy deposition of each particle was recorded. The results are displayed in Fig. B.1. As anticipated, Si fully absorbed significantly fewer particles than GaAs and CdTe at at lower thicknesses due to its lower atomic number. The detector only begins to fully absorb a small fraction, 1.766 % ± 0.004, of incident particles when the thickness is approximately 200 μm. CdTe outperformed GaAs in this range, however at 300 μm GaAs absorbed a higher percentage of particles completely. As the thickness of the detectors further increases, Si begins to absorb a greater proportion of particles and outperforms GaAs and CdTe at 800 μm. While GaAs and CdTe show diminishing returns as detector thickness is increased beyond 400 μm, Si does not exhibit the same behaviour in this

range, and is capable of fully absorbing 71.696% ± 0.027 of incident beta particles at 800 μm thickness. Meanwhile CdTe only fully absorbed 50.590% $\pm 0.023$of incident particles and GaAs 58.903% ± 0.024.

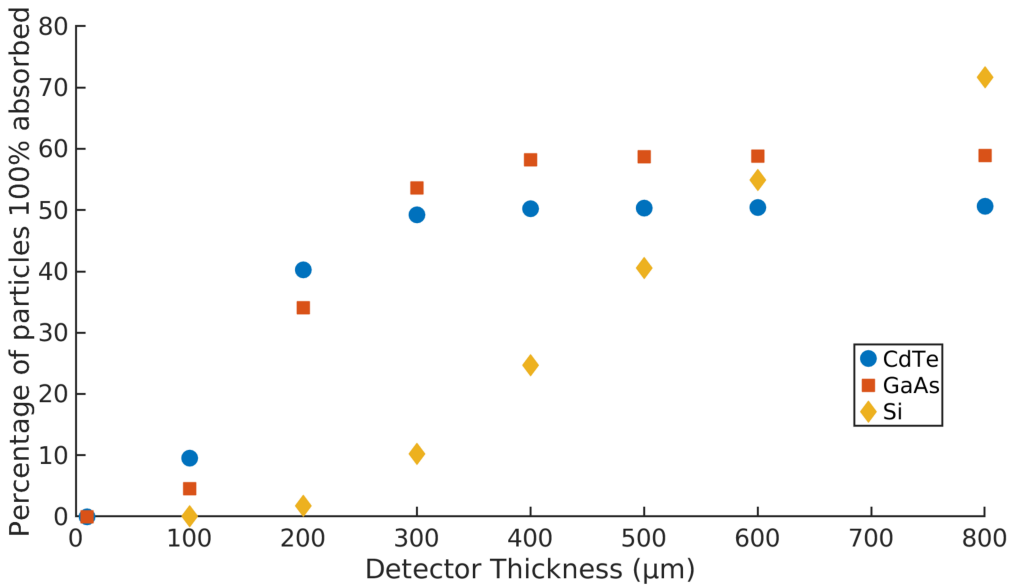

Figure 4.1: A comparison of complete 0.546 MeV beta particle absorption in GaAs (squares), CdTe (circles), and Si (diamonds) detectors of varying thickness. Errors are plotted, but not visible due to marker size.

In principle higher atomic number materials should absorb more radiation, however the simulation results can be explained by another factor related to the atomic number. As electrons interact with a surface they are prone to a phenomenon known as backscattering [25]. Electrons undergo erratic and sizeable deflections as they propagate through matter. Particles incident on the surface of the detector may deflect through such large angles that they simply rebound and leave the detector while only depositing a fraction of their energy. This phenomenon is more pronounced in high atomic number materials and this offers an explanation of the behaviour observed in Fig. B.1. A lower proportion of particles are backscattered by silicon, but as the material is inefficient at absorbing radiation of this type, the benefit is only seen at extreme volumes of material. CdTe is in theory the best absorber of radiation, but in this experiment its full benefit cannot be extracted. It outperforms GaAs at low thickness, but as a higher fraction of particles are backscattered, its absorption plateaus at a lower percentage of incident particles. To minimise the effects of backscattering and compare stopping

power of each material, a particle beam was generated from the centre, rather than at the surface of 800 μm thick detectors. In this simulation, GaAs fully absorbed 95.96 % $\pm 0.03\%$ of particles, CdTe 96.41 % $\pm 0.03\%$, and Si just 36.25 % $\pm 0.02\%$.

When ^{90}Sr decays via beta emission, it transmutes to ^{90}Y which itself decays by beta emission at 2.278 MeV. As a result, ^{90}Y contributes to the gross beta activity of the groundwater and therefore its presence must be quantified. Fig. 4.2 compares the ability of 100 mm^2 devices of varying thickness to fully absorb 1×10^7 beta particles at 2.278 MeV. While 400 μm seemed to be the point of diminishing returns for GaAs with 0.546 MeV particles, for 2.278 MeV only 0.430% $\pm 0.002\%$ are absorbed. CdTe, meanwhile, fully absorbs 1.480% $\pm 0.004\%$. Silicon detectors are essentially ineffective for particles of this energy, absorbing 0.0008 % $\pm 0.0002\%$. ^{90}Y quantification will require a detector thicker than 400 μm, with CdTe offering superior beta particle absorption than GaAs.

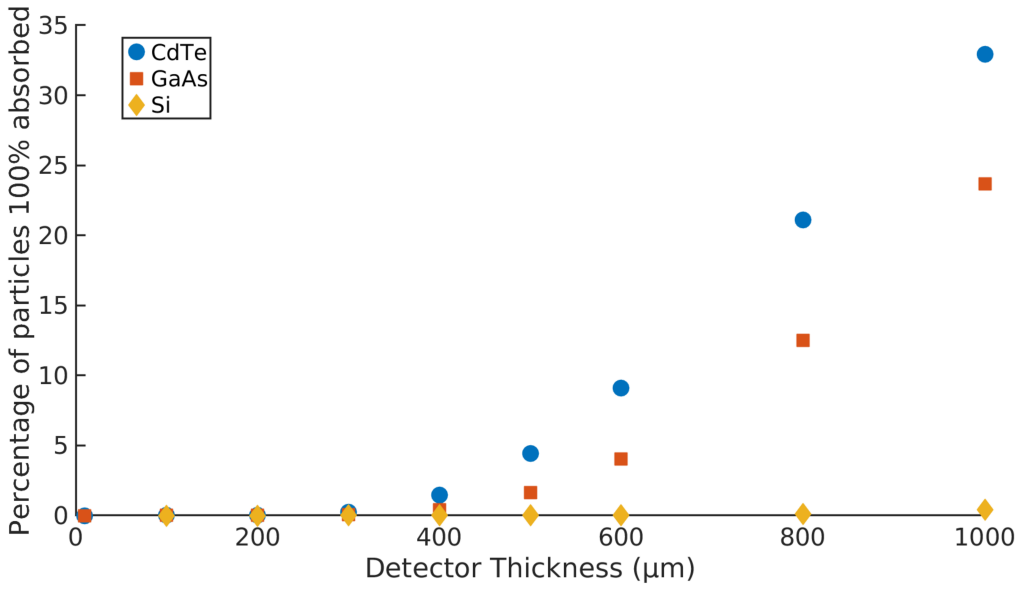

Figure 4.2: Fully absorbed 2.278 MeV beta particles in GaAs (squares), CdTe (circles) and Si (diamonds). Errors are plotted, but not visible due to marker size.

Beta particles take an erratic path through matter, therefore the width of the detector will influence its ability to absorb incident particles from a point source. To investigate the significance of this parameter detectors were modelled with a thickness of 400 μm and varying surface area from 10^{-4} mm^2 to 100 mm^2. The results of their interaction with 1×10^7 elec-

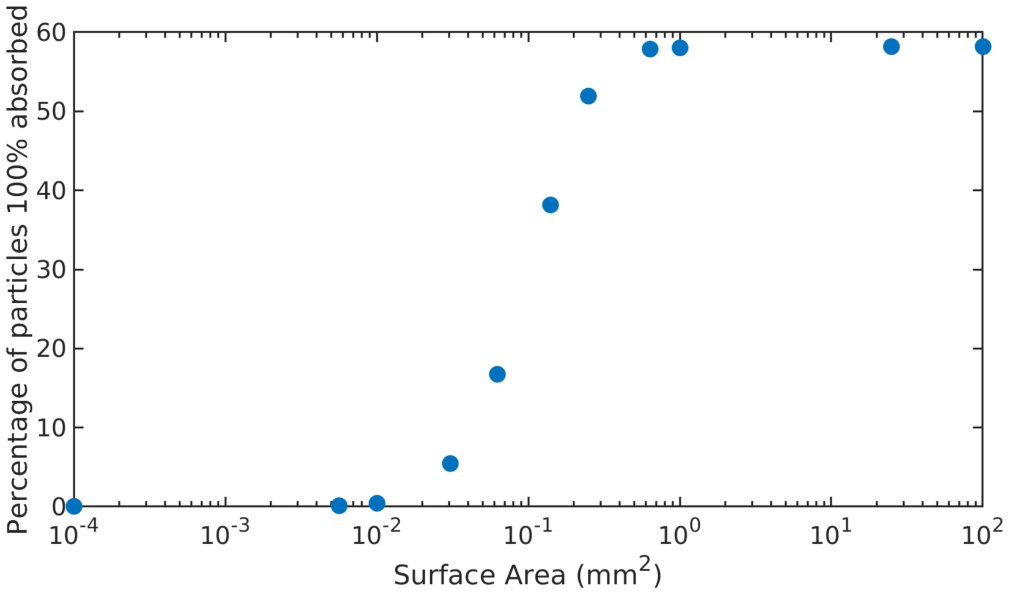

Figure 4.3: Complete 0.546 MeV beta particle absorption in 400 μm thick detectors of varying surface area.

trons at 0.546 MeV can be seen in Fig. 4.3. While the surface area is below 10^{-2} mm^2 the detector fails to record the full energy of incident particles at all. In the range between 10^{-2} mm^2 to 6.4 mm^2 the device becomes viable. Again, diminishing returns are seen when the surface area is further increased as the complete absorption of particles levels off out at approximately 58%.

4.3.2 Contaminated groundwater simulation

The simulations presented so far have examined point sources of radiation, however this research concerns the assay of contaminated groundwater. This scenario is modelled by simulating a 5 cm diameter and 2.5 cm deep cylinder of groundwater, populated with 10 $\times 10^7$ isotropic decaying ^{90}Sr ions. This simulation examined ^{90}Sr decay only. Four detectors of 400 μm thickness and varying surface area were investigated for their detection efficiency. The detectors were positioned at the surface of the water and the spectra collected after the run of particles is displayed in Fig. B.2. With a 1 mm^2 surface area, the detector only managed to record 163 hits leading to an incomplete spectrum; the maximum energy observed was 0.268 MeV. The 100 mm^2 detector counted a total of 13015 particles, with the counts

dropping below 5 after 0.458 MeV. The total counts observed scaled linearly with surface area. The vast majority of decay products did not reach the detector as they are either emitted in the wrong direction, or absorbed before they reach the device. This simulation highlights the importance of maximizing the number of particles striking the detector when counting from a scattered source.

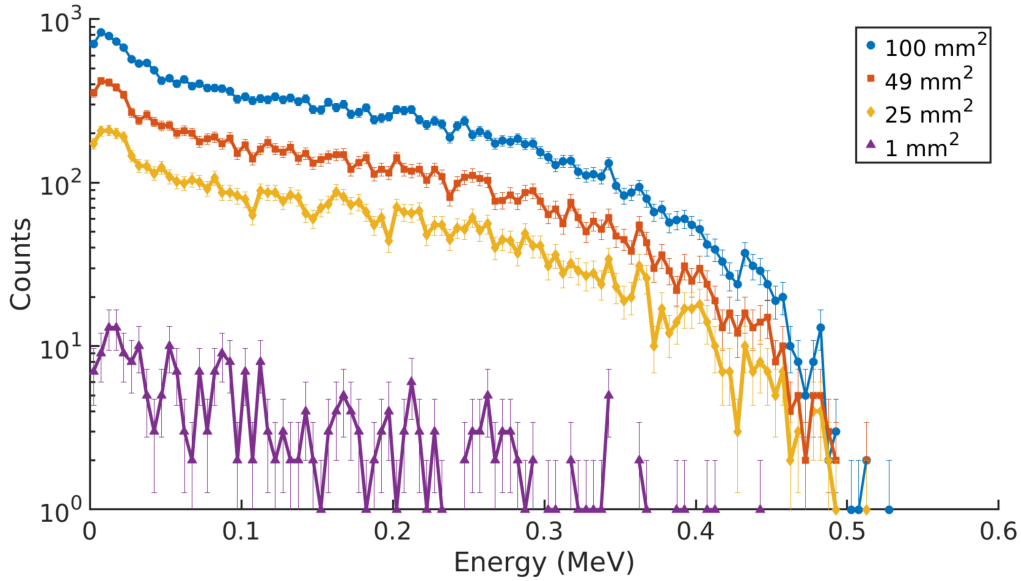

Figure 4.4: ^{90}Sr spectra observed in 400 μm thick GaAs detectors with increasing surface surface areas.

To examine the sensitivity to thickness, four 100 mm^2 GaAs detectors ranging from 0.4 mm to 2 mm were compared. The detectors were positioned at the surface of the water and the spectra they collected after the run of 10^8 ^{90}Sr and ^{90}Y ions had decayed is displayed in Figure 4.5. In this scenario, the 0.4 mm thick detector counted 196,515 particles but only counted 115 particles in the range from 1.725 MeV to 2.300 MeV, and therefore was inefficient at capturing the full spectrum of radiation. The thickest device detected 215,032 particles and counted 1,873 particles in the range from 1.725 MeV to 2.300 MeV. A peak can be seen at 0.302 MeV for the 0.4 mm thick device, likely a result of more energetic particles only depositing a fraction of their energy in the material. This peak is not observed in thicker detectors, but each spectrum features a peak approximately at 0.023 MeV as a result of backscattering. At greater thicknesses the spectra are distinguished by their absorption of

higher energy particles, from 1.150 to 2.3 MeV. As the thickness is increased from 0.75 mm to 1 mm, a 20.58 % increase in counts is observed, but as the thickness is then doubled to 2.0 mm only an 8.37 % increase in counts is seen.

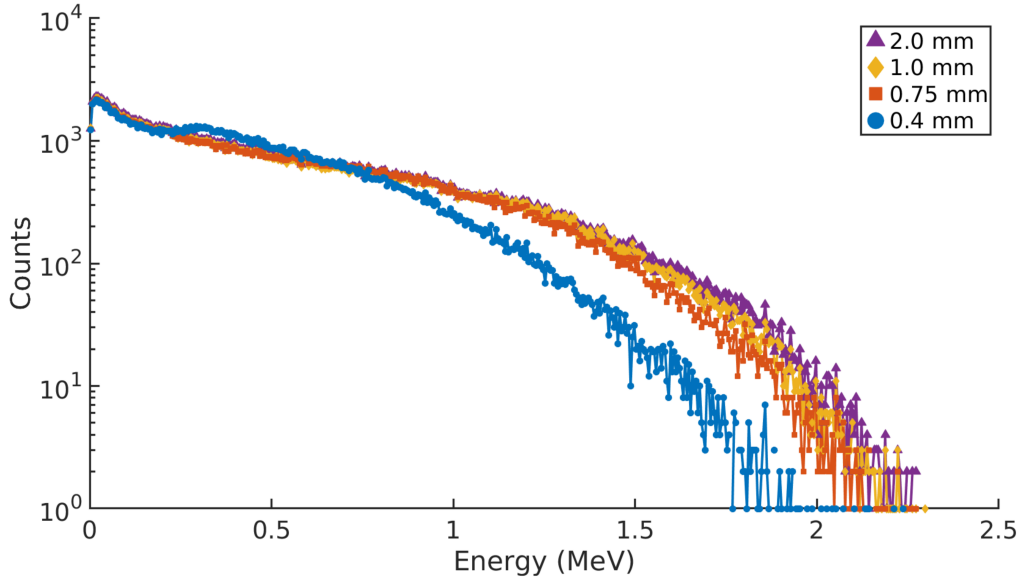

Figure 4.5: ^{90}Sr and ^{90}Y spectra observed in GaAs detectors with 100 mm^2 surface areas and varying thickness. Energy is resolved into 5 keV bins. Errors are omitted for visual clarity.

The full decay of 10^8 ^{90}Sr ions, was simulated for 100 mm^2 CdTe and GaAs detectors of 1 mm thickness to compare the spectra collected by each material. The spectra from these simulations are shown in Fig. 4.6. The GaAs detector counted 218,188 particles, and the CdTe detector 217,965. In this scenario the detectors therefore share virtually identical detection efficiency. The materials are distinguished by the shape of their spectra. A breakdown of the counts recorded in each quarter of the energy spectrum is displayed in Table 4.1. The CdTe detector features a higher and broader peak in the low energy range, centred at 0.013 MeV, fewer counts in the mid range, and greater counts in the high energy range. This can be attributed to the greater backscattering effect in CdTe, as low to mid range particles are more likely to backscatter while just depositing a fraction of their energy. Higher energy particles are more likely to be absorbed in CdTe, however this effect is limited as fewer particles are emitted in this range.

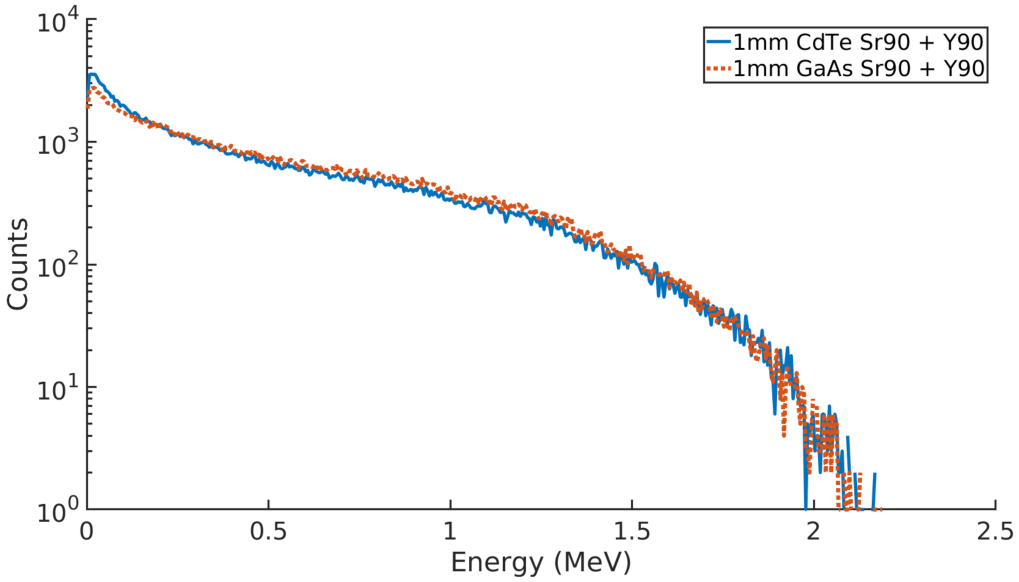

c

Figure 4.6: ^{90}Sr and ^{90}Y spectra observed in GaAs (red and dashed) and CdTe (blue and solid) detectors with 100 mm^2 surface areas and 1 mm thickness. Energy is resolved into 5 keV bins.

Table 4.1: Counts recorded in different energy ranges of the ^{90}Sr + ^{90}Y spectra observed in Fig. 4.6.

Material	0 - 0.575 MeV	0.575 - 1.150 MeV	1.150 - 1.725 MeV	1.725 - 2.300 MeV
GaAs	143,647 $\pm$ 379	55,448 $\pm$ 235	17,947 $\pm$ 134	1146 $\pm$ 34
CdTe	151,689 $\pm$ 389	49,258 $\pm$ 221	15,791 $\pm$ 126	1227 $\pm$ 35

4.4 Conclusions

The optimal design of a photodiode detector for the in situ measurement of ^{90}Sr has been investigated by modelling sensors and their absorption of beta radiation in a groundwater borehole scenario.

The complete absorption 0.546 MeV and 2.280 MeV beta particles in Si, GaAs and CdTe photodiodes was simulated to determine the most efficient absorber. The atomic number of a material both determines its ability to absorb ionising radiation and the propensity for that radiation to backscatter. The result is that as the thickness of GaAs and CdTe sensors increases, the complete absorption of 0.546 MeV beta particles plateaus. This occurs at approximately 300 μm and 400 μm for CdTe and GaAs sensors respectively. As backscattering

is not as prevalent in Si, it absorbed more radiation completely at 800 μm. Sensors 1 mm thick made from CdTe, GaAs and Si absorbed 32.92 %, 23.66 % and 0.413 % of 2.28 MeV particles completely. This eliminated Si as a candidate material in this application.

Detector geometry was optimised by modelling a cylinder of ^{90}Sr contaminated groundwater. The number of counts observed in the detector scaled linearly with surface area, and the optimal sensor modelled featured a surface area of 100 mm^2. It was found that the thickness of the detector should exceed 400 μm for absorption of high energy particles (1.150 to 2.30 MeV) released during ^{90}Y decay. However, doubling the thickness of the sensor from 1.0 mm to 2.0 mm only yielded an 8.37 % increase in counts for particles in this range. The benefit of this must be weighed against the defects associated with higher volume detectors. The thickness of compound semiconductors can be limited by defects which restrict the movement of charge carriers, reducing charge collection efficiency [92, 11].

The merits of CdTe and GaAs detectors were compared by modelling 1 mm thick and 100 mm^2 surface area detectors. Spectra from 10^8 decaying ^{90}Sr ions and the resulting ^{90}Y daughters were collected. Each material offered similar detection efficiency, but the shape of the spectra collected varied slightly. While CdTe offered marginally better absorption in the energy range from 1.725 - 2.3 MeV, the backscattering which resulted upon contact with lower energy particles produced a larger peak at low energies compared to that observed in the GaAs detector. The GaAs sensor counted 8,456 more particles above 0.575 MeV, exclusively the result of ^{90}Y decay. Ultimately this may identify GaAs as the prime material when counting from a mixed source.

5. Detector construction

Reprinted from: *G. Turkington, K. A. A. Gamage, J. Graham, Characterisation and suitability of a CdTe detector for strontium 90 assay in groundwater*, Nuclear Instruments and Methods in Physics Research Section A: Accelerators, Spectrometers, Detectors and Associated Equipment 997 (2021) 165155. doi:10.1016/j.nima.2021.165155. [21]

5.1 Abstract

This chapter presents a design of an in-situ detector for monitoring strontium 90 activity in groundwater at nuclear decommissioning sites. Current techniques for monitoring strontium 90 activity are lab-based and are time consuming, expensive and produce secondary waste. To alleviate these problems, a proof-of-concept detector has been developed which will be deployed in-situ, directly into groundwater boreholes. A compact detector was designed, housed in a waterproof casing and its initial performance as a strontium 90 detector in water was examined. A 10 x 10 x 1 mm cadmium telluride detector was paired with a appropriate charge sensitive amplifiers and readout systems to make a 118 x 83 x 40 mm sensor which was submersed in water. A 35.79 MBq collimated strontium 90 source was used to determine that the sensor was capable of counting beta particles from a range of 55.86 ± 5.40 mm. The detector was held at a reverse bias of 80 V for 290 minutes, the average counts observed in 5 minute intervals went from $1.32 \times 10^6 \pm 1.14 \times 10^3$ to $1.28 \times 10^6 \pm 1.13 \times 10^3$. However,

the results presented have established a viable proof-of-concept for an in-situ detector for strontium 90 assay in groundwater.

5.2 Introduction

Strontium 90, ^{90}Sr , is a by-product of nuclear fission and it is one of the prominent beta emitters found in nuclear waste at decommissioning sites such as Sellafield. It has a half-life of 28.8 years and decays via beta decay, releasing particles with energies up to 0.546 MeV. Its daughter yttrium 90, ^{90}Y , has a half-life of 64 hours and its decay releases beta particles with an end-point energy of 2.278 MeV [98]. ^{90}Sr shares similar chemical properties with calcium and can accumulate in calcium rich areas of the human body, such as bone structures, where irradiation can induce leukaemia and other bone cancers [33]. Contamination of groundwater at decommissioning sites is typically the result leaks from storage tanks, separation areas and ponds associated with fuel and waste storage. Fig. 5.1 depicts the scenario in which the detector will be deployed. ^{90}Sr which enters the ground may disperse and enter the groundwater table forming mobile plumes. At Sellafield Sr-90/Y-90 is the most common strong beta emitter in contaminated groundwater and greatly exceeds the WHO drinking water guidelines of 10 Bq/L [73] in many boreholes. While these waters are not exploited for drinking water purposes there is a long-term requirement to monitor the distribution and behaviour of this contamination on site.

Routine monitoring of ^{90}Sr is an expensive and time consuming process which produces secondary waste through collection of samples and laboratory analysis. Current techniques a require manual sampling from underground boreholes. Tests often take months to produce results, as groundwaters are stored for weeks to allow for ^{90}Y ingrowth, and many of the techniques require the use of hazardous solvents and acids [49].

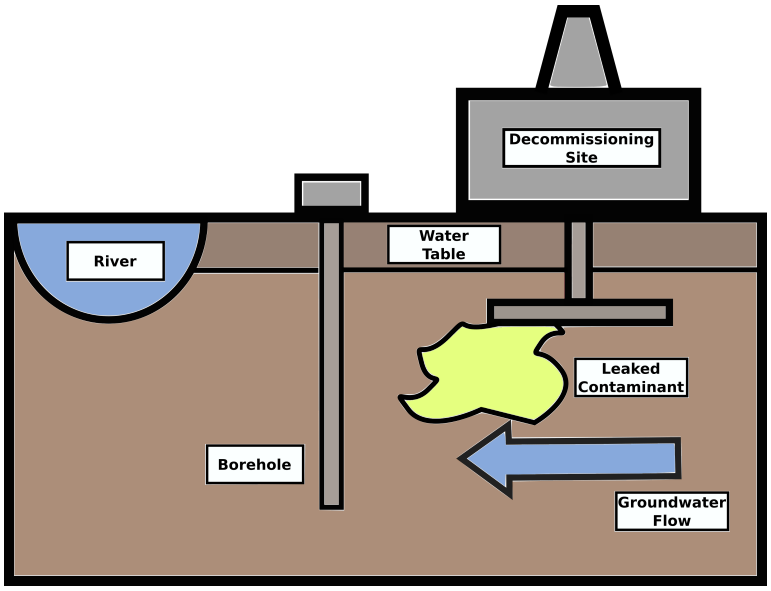

Figure 5.1: A depiction of the scenario in which the detector will be deployed. Waste from decommissioning sites leaks into the groundwater where it is monitored via boreholes.

This research is investigating the feasibility of a cadmium telluride (CdTe) in-situ detector for the assay of ^{90}Sr in groundwater. CdTe is a compound semiconductor material which has become popularised and it has many properties that make it a suitable material for the detection of ionising radiation. CdTe has a high effective atomic number, 50, which makes it an effective absorber of ionising radiationa and a wide bandgap, 1.44 eV, allowing for room temperature operation. It has gained traction in the fields of medical physics and astrophysics where it has been used to develop X-ray and gamma ray detectors [92]. However an increased atomic number is also associated with a higher rate of backscattering at the detector surface and this limits the number of particles completely absorbed within the detector.

As the detector must operate in a compact environment, it was important to use a detection medium which is small, capable of stopping the radiation of interest and does not require extensive cooling or other additional support systems. For these reasons, room temperature semiconductors were considered an appropriate candidate. A typical semiconductor detector consists of three layers. An anode, a cathode and an intrinsic layer of charge carriers. When beta radiation passed through the intrinsic layer, it does so through a series of Coulombic interactions which create electron-hole pairs. The number of charge carriers generated is

proportional to the energy deposited by the radiation in the detector. As the detector operates under a reverse bias voltage the electrons and holes are swept towards the anode and cathode respectively. The resulting current pulse can be detected, and its magnitude is equivalent to the energy lost by the radiation in the detector.

5.2.1 CdTe background information

Previous research has investigated the performance of detectors of varying dimensions and material composition for the detection of ^{90}Sr in groundwater [19]. CdTe and GaAs were identified as suitable materials for the task with similar properties and potential performance.

One of the drawbacks associated with CdTe is known as polarisation. This time-dependent effect occurs after the biasing of the diode and results in the reduction in photopeak amplitude, lessening couting rate and diminishing the energy resolution [99, 100]. Polarisation can occur in CdTe as a result of radiation flux incident on the detector or after the detector has been biased for some time [96]. This is a result of disruptions in the uniformity of electric field across the material stemming from alterations in charge trapping in deep level states [101]. Detectors polarised by the biasing voltage can recover after the applied voltage is removed for a short time [102]. The stability of CdTe detectors can otherwise be improved by increasing the biasing voltage or operating at low temperatures [99].

The detector will be deployed in boreholes at decommissioning sites, where it will monitor beta activity by being submersed directly into contaminated groundwater. Beta particles have a limited range in matter due to their Coulombic interaction with nearby atoms. Their path through matter is characterised by large deflections where significant fractions of their energy can be lost. This can be accompanied by the radiative Bremsstrahlung process, where low energy X-rays are emitted as the beta particle decelerates. Additionally, beta particles are emitted over a continuous energy spectrum. These properties have presented difficulties when designing beta detectors.

^{90}Sr is the predominant beta-emitter found at Sellafield and its activity tracks with total beta activity. Beta emitters can be split into two groups, strong and weak, depending on their emission energy. The weak category includes carbon-14, ^{14}C (0.156 MeV), technetium-99m ^{99m}Tc (0.141 MeV), and tritium. It is expected that these emitters will be too weak penetrate the protective layers of the detector in addition to traversing the groundwater [103]. The other chief beta emitter is caesium-137, ^{137}Cs, which decays via beta emission, up to 0.512 MeV, to barium-137m, ^{137m}Ba, which releases a 0.662 MeV gamma photon as it relaxes to its ground state. ^{137}Cs is generally found in low concentrations at Sellafield [104] with only one monitoring point exceeding the WHO safe water limit of 10 BqL^{-1}. By eliminating weak betas from entering the detector and considering the scarcity of other strong beta emitters, it may be the case that ^{90}Sr will be the only significant beta emitter which the detector is both sensitive and exposed to. Some research has suggested it may be possible to use gross measurement of activity in ground water to identify individual radionuclides by linear regression [105]. The time for completion for existing methods of groundwater monitoring is typically 1-2 months. This detector is being designed to produce results on a much smaller timescale, from 1 hour to 1 day, thereby providing information on a daily basis. This has the benefit of allowing decommissioning sites to examine the data quickly to determine whether beta activity is present or not, and rapidly respond to unexpected spikes in groundwater activity resulting from new leaks. This could be used to compliment existing techniques and allow for a selective approach with existing techniques such as liquid scintillation counting for closer examination of ^{90}Sr activity.

However, successful application of these technologies to in-situ monitoring will result in a significant reduction in secondary waste, long term costs and will also provide results allowing more detailed understanding of the response of ^{90}Sr to hydro-geological and geochemical perturbations to be assessed.

5.3 *Materials and methods*

Groundwater boreholes are up to 50 mm in diameter, and filled with water. Therefore a robust and compact detector must be designed to operate in this environment. The average annual groundwater temperature at Sellafield in 1997 was 10.67 °C [106]. This may be significant as some research has found that cooling to the region of 0-10 °C may have a significant affect on the stability of the detector and its performance over time [99].

5.3.1 CdTe diode

After considering the availability of semiconductor sensors on the market, and the feasibility of semiconductor fabrication, a 10 x 10 x 1 mm CdTe semiconductor detector was selected- (supplied by AcroRad, Japan). The CdTe detector is constructed in an Ohmic configuration with 20 nm thick platinum anodes and cathodes sandwiching a 1 mm thick CdTe crystal. This structure was mounted to an alumina substrate with gold wire bonds connecting to conductive pins which protruded from the bottom of the mount. An additional pin was used to ground the mount, which aided in reducing the noise present in the detector.

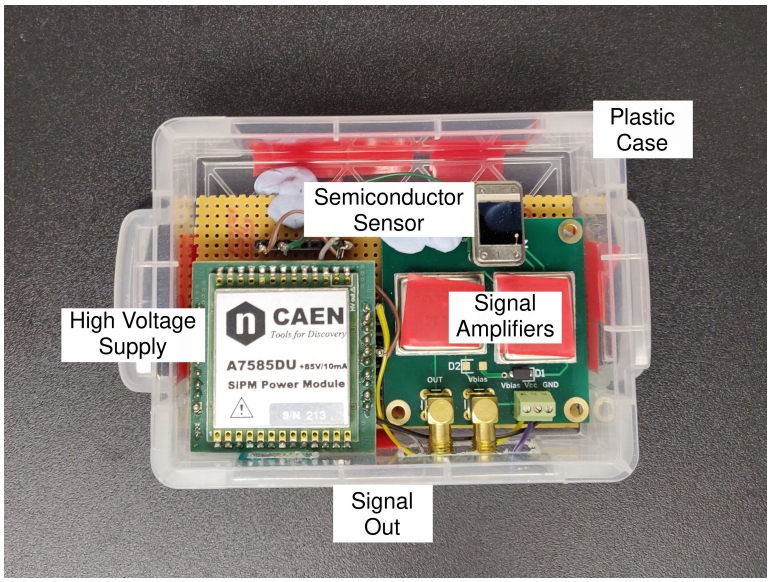

Figure 5.2: The constituent components of the detector as arranged in the case before it is sealed and submerged in water.

5.3.2 Electronics

The complete detector system is comprised of a few essential components. The current pulse produced by the CdTe semiconductor is amplified and shaped so that is more easily read by the counting system. This is achieved with a charge sensitive pre-amplifier (CSA), which acquires the signal from the detector while boosting the signal-to-noise ratio (SNR). The CSA sums the charge created within the detector on a feedback capacitor which releases an amplified current pulse, of amplitude V_o, from charge generated, Q_d, and capacitance C_f. This signal pulse is then shaped by a shaping amplifier, to produce a signal of Gaussian profile which is read by an analogue to digital converter (ADC) for signal processing. The CdTe sensor was paired with the α-CSA supplied by Micod with a capacitance, C_f of 1 pF and resistance, R_F, of 100 Mω. This produced current pulses with a sensitivity of 36 mV per MeV when paired with the CdTe diode. The amplifier was supplied with 5 V from a DC power supply.

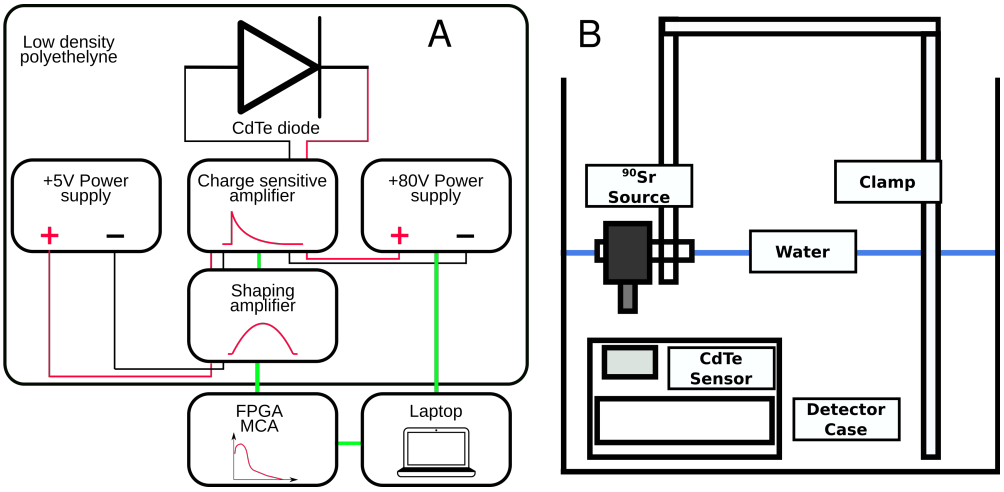

Figure 5.3: A) Depicts a schematic of the components in the detector and their function. B) displays the deployment of the detector underwater in the experimental setup

A CAEN (Italy) A7585D modular supply was mounted adjacent to the CSA. The CSA was connected to the high voltage output of the power supply and this was used to bias the attached semiconductor sensor. The CAEN power supply was programmed to supply a consistent 80 V bias to the CdTe diode. This bias was selected in accordance with manufacturer

guidelines for an Ohmic diode and helps to meet the performance and power requirements necessary for a small detector [107]. These components complete the sensitive part of the detector and the CdTe diode, amplifier and a CAEN power supply were housed in a 118 x 83 x 40 mm plastic box. Currently, this is larger than the required dimensions to fit into a borehole, however it would only take minor modifications to rearrange the components in a configuration which fits. A window was cut from the box above the CdTe sensor to reduce the attenuation of beta particles. The distance from the sensor to the window was 0.7 mm and this gap was filled with air. The complete detector system is illustrated in Fig. 5.6.

5.3.3 Attenuation due to waterproofing

To make the detector submersible in water, it was wrapped in two layers of low density polyethylene. This material was selected to ensure a water tight seal around the detector while keeping the attenuation of beta particles to a minimum by using a thin (0.027 mm) and low-density (0.91 g/cm^3) material [108]. The waterproof detector was attached to the bottom of a plastic container, which was filled with room temperature tap water. The water, plastic box, and metal clamp were all grounded. The output from the detector was recorded directly with the MCA connected to a laptop.

5.3.4 Data acquisition

A field programmable gate array (FPGA) is a type of microcontroller which consists of a series of logic gates that can be reprogrammed ad hoc. FPGAs are used to compile programs from a series of logic blocks, and as they are reprogrammable allow for quick iteration in program development and prototyping. Essentially this allows for large scale physical circuits to be modelled digitally on a small scale device. This flexibility means that FPGAs have become common place as a tool for instrument design. FPGAs typically have low power consumption and can be manufactured in small scale form factors. These qualities make FPGAs ideal for use in compact detectors.

FPGAs consist of reprogrammable logic blocks, and input/output (I/O) blocks which are reprogrammable. This hardware is interfaced with by software, or specifically a hardware description language (HDL). The two dominant HDLs are VHDL and Verilog, and these are packaged by the major manufacturers of FPGA chips, Intel and Xilinx, into user friendly graphical user interfaces (GUI). The HDLs are used to define the role of various logic blocks, which include addition, multiplication and accumulation, within the FPGA. Newer FPGA devices have incorporated memory storage, and use histograms to compile data. In this case, the FPGA was programmed off the shelf to function as a digital pulse processor to create a lightweight solution for a portable multichannel analyser. This was done with the software RayPanel, based on VHDL, which programs the device to function as a spectroscope.

Traditionally, pulse processing is done with analog components, for example an oscilloscope. FPGA technology allows this to be done digitally, eliminating the need for bulky analog electronics, reducing the sensitivity to thermal noise, and allows for the detection algorithm to easily be tuned to fit the purpose. In this case, digital processing consists of an initial analog conditioning stage for the signal acquired from the detector, the conditioned signal is then digitised by a fast ADC and a FPGA where the pulse is further processed and sorted into a histogram in accordance with its amplitude. The ADC samples at 100 MHz and the digital processing consists employs a trapezoidal filter [109] to categorise and bin pulses according to their height.

This programming used in this project based on open source code for a digital spectroscope, and is developed with the ISE WebPack (Xilinx Inc).ce with its amplitude. The ADC samples at 100 MHz and the digital processing consists employs a trapezoidal filter [109] to categorise and bin pulses according to their height. A peaking time of 5 μs and flat top time of 0.4 μs were found to perform the best for the CdTe detector. This was done in conjunction with software on a laptop, connected to the MCA via USB cable.

5.3.5 Source and background Count

A sealed and collimated ^{90}Sr source was used for these experiments. The aperture diameter on the collimator was 1 mm, barrel length 3.5 mm and the activity of the source at time of use was 35.79 MBq. When the source was submerged in water, it was wrapped in a thin nitrile layer to prevent water from entering the collimator and absorbing the radiation. There is uncertainty over the activity of the source before and after collimation. Therefore the experiment was designed in such a manner that the absolute activity of the source is not strictly relevant. Results in terms counts are framed in a relative sense. The question being asked is about the range over which the detector can be expected to identify ^{90}Sr decay above the background noise in the detector.

Experiments were carried out in the Nuclear Physics department at the University of Glasgow. A metal clamp was affixed to the plastic container and this was used to hold the collimated source above the detector, with the beam in alignment with the semiconductor sensor. This clamp allowed for the source to be positioned at different positions and distances from the sensor. While the detector was in use, it was covered with a light-proof sheet to prevent any interference of optical photons while the lighting in the lab was turned on. Several background count were taken, each of a duration of 5 minutes, equivalent to the counting time in many experiments. The average background count recorded in the detector was 48 $\pm$ 7 counts, equivalent to 0.16 counts per second. The background counts appeared to be randomly distributed, with all but two confined to the first 232 channels on the MCA.

5.3.6 Deployment in water

The detector was deployed into a a water filled container, to mimic the real world use-case for this device. This allowed the likely operating range of the detector through water to be characterised. The detector was fixed to the bottom of a 10 litre plastic contained which was with room temperature tap water. This simulated the deployment of the detector in groundwater and the ^{90}Sr source was positioned directly above the window to the semiconductor

sensor. Initially, the source was in contact with the dual layers of low-density polyethylene (LDPE) across the window. The counts in the detector were recorded for five minutes. The source was then moved vertically to increasing distances from the window, allowing for a larger volume of water to fill the space between the sensor to the collimator.

The performance of the detector over a longer duration of time was investigated. As mentioned previously, CdTe detectors can suffer from a degradation in performance after being biased or exposed to radiation for a period of time [99]. To investigate this, the detector was biased to 80 V and this remained consistent for the duration of 290 minutes. The ^{90}Sr was clamped in a single position above the detector level with the LDPE window. This meant the particles were transmitted through two layers of LDPE and a 0.7 cm air gap. The counts observed in the detector were recorded for five minutes at various intervals over the course of 290 minutes. The detector was covered with light-proof sheeting for the duration of the experiment while the ambient temperature of the room was held at a constant 20 °C.

5.4 Results

5.4.1 Attenuation due to waterproofing

The ^{90}Sr source was clamped at a distance of 12 mm from the surface of the plastic container and hits were recorded for 5 minutes. Compared with the uncovered detector, there was 9.36% decrease in counts, from $1.27 \times 10^6 \pm 1.13 \times 10^3$ to $1.16 \times 10^6 \pm 1.07 \times 10^3$. This is accounted for by particles scattering and being absorbed by the plastic layers between the collimator and detector. This decrease in counts is sufficiently low given the statistics involved in this experiment, however this may limit the effectiveness of the device when it comes to counting low activity sources. However, improvement could be achieved by removing one layer of LDPE, or trialling different lightweight and waterproof materials.

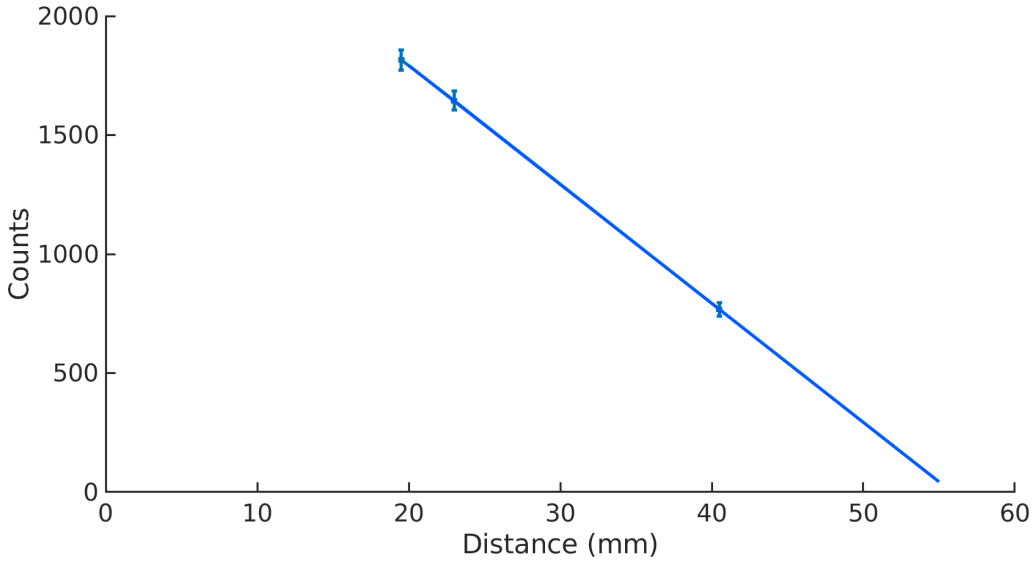

Figure 5.4: Counts observed in the detector after measurements at increasing distances in water. A linear least squares regression has been applied to 3 points of the graph to allow an estimate for the range over which the detector is effective, 55.86 $\pm$ 5.40 mm.

5.4.2 Detector performance and uncertainty

The counts in the detector were recorded over five minute intervals and plotted in Fig. 5.4. The counting time was selected to ensure a sufficient number of counts were collected to reduce statistical uncertainty. When the source was positioned directly at the window, 5.2 $\times$ 10^5 counts were observed in the detector and this drops off to 767 $\pm$ 28 counts at 40.0 mm. This provides a count which is significantly greater than the background rate for the detector. By performing a linear fit to the last 6 data points on the plot, it is estimated that the range for this detector in groundwater is approximately 55.86 $\pm$ 5.40 mm before the minimal detectable limit is reached. In this case, the minimal detectable limit, N_D, is defined as the minimum number of counts required to state with a 95% confidence level that radioactive decay has been detected above the presence of background noise, N_B, in the detector [25]. This is calculated with the following equation, the Currie Equation, which is derived from the Gaussian distributions which describe the statistical fluctuations in detector counting:

$$N_D = 4.653\sigma_{N_B} + 2.706 \tag{5.1}$$

This demonstrates that it is still reasonable to detect beta particles at range and this will be important in real world scenarios. The larger the volume of water the detector is sensitive to, the greater counting statistics it can generate. However, it should be noted that this experiment does not closely replicate the real world deployment of the detector. The collimated beam is considerably different to the colloid of radionuclides expected to be found in groundwater. However, the results produced here can be used to inform future experiments. This information will be useful when designing future experiments with contaminated groundwater, providing a guide for the necessary volumes of water required and provides information for determining the sensitivity and efficiency of the detector.

5.4.3 Detector performance over time

The results are plotted in Fig. 5.5. The mean number of counts recorded was $1.29 \times 10^6 \pm 1.13 \times 10^3$. The maximum number of counts, was the first measurement taken while the lowest $1.28 \times 10^6 \pm 1.13 \times 10^3$ was taken after 290 minutes. This represents a 3.26% decrease in counts. It is clear from Fig. 5.5 that the counts decline at a rate of 0.026 % per minute during the first 120 minutes, and the counts observed in the remaining 180 minutes were more steady only declining at a rate of 3.9×10^{-4} % per minute. The average counts over the first 120 minutes was 1.30 $\times 10^6$ compared with 1.28 $\times 10^6$ over the last 180 minutes.

The experiment was repeated but this time the reverse bias voltage applied to the detector was turned off between measurements. The results are plotted in Fig. 5.5, as a fraction of the maximum count recorded. The initial count sees the greatest number of hits in the detector, and this falls to 97.19 % after 290 minutes. The mean number of counts observed in the detector as a fraction of the maximum count was 98.16 %, which was greater than the

average of 97.52 % when the bias was applied between counts. A similar trend is seen here when both experiments are compared.

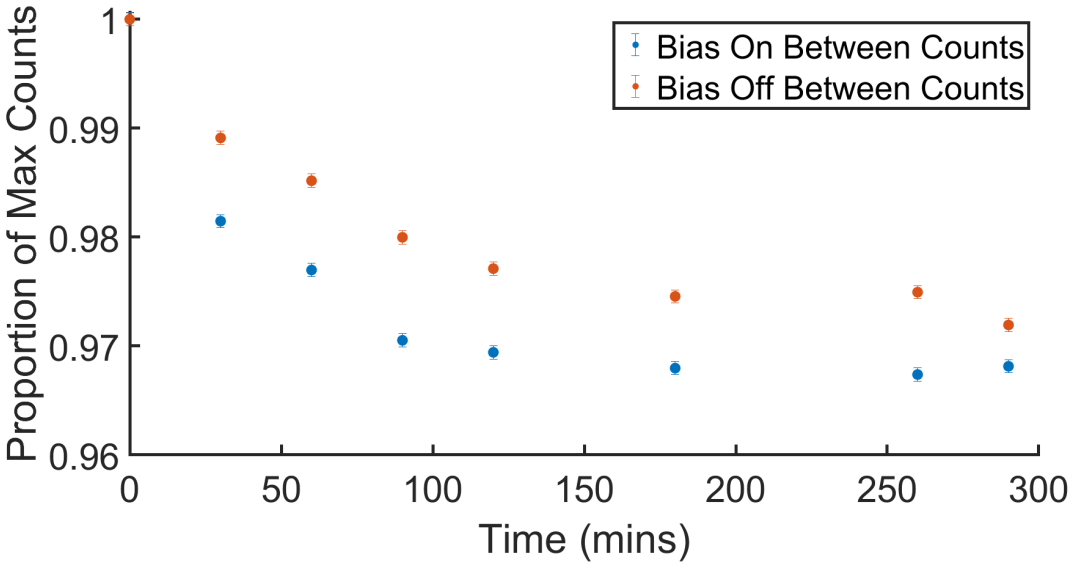

Figure 5.5: ^{90}Sr Counts recorded over 5 minute counting intervals during a 290 minute period, with the bias on and off between measurements.

Both experiments see a period rapid of decline, followed by relative stability. When the detector was unbiased between measurements, the number of counts reduced by approximately 0.021 % per minute but this declined to a loss of 0.0023 % per minute over the final 150 minutes of the experiment. This can be contrasted with when the bias was left on, there was a loss of 0.031 % counts per minute initially, followed by a loss of 8.30×10^{-4} % per minute.

Removing the bias from the detector between counts produced results with a higher average count as a proportion of the initial count. The instability in detector performance may be due to a number of factors including deviations in operating bias and variations in temperature [99] and some researchers have investigated radiation damage as a potential factor [110]. The detector is housed next to the 80 V power supply which generates heat as it operates and has an internal temperature monitor. While the detector is not submerged in water and operating in a 20 °C room, the temperature in the detector case averages at 31.01 °C. The power supply

used to bias the detector was used to monitor the internal temperature of the detector cavity over a 120 minute period while submerged in water. It was found that the temperature within the case rose from 24.49 °C to 26.62 °C . while the detector was submerged under water with a temperature of 14.8 °C . This heat produced creates an unstable environment for the detector [111], and may lead to variable detector performance until the temperature reaches equilibrium and detector performance stabilises. This instability in detector temperature may be interfering with counting performance over long periods of time. Turning the bias voltage off between measurements may have alleviated the build-up of heat within the detector case and allowed for a cooler and more stable environment for the detector. As noted [99], cooling the detector down to temperatures around 10 °C may produce beneficial effects when it comes to the consistency of detector performance over a long term operational period. As the groundwater at Sellafield has an average temperature of 10.67 °C , this may provide a suitable basis for some ambient cooling. Fluctuations in groundwater temperature should be accounted for in future development of the detector.

5.5 Conclusions

The detector presented has demonstrated its ability to detect the presence of a ^{90}Sr source. The results presented have demonstrated an operating range of over 40.0 mm in water from a 35.79 MBq ^{90}Sr source as the beta particles propagate through water. By performing a linear fit to the data points in Fig. 5.4, it is estimated that the range of beta particle for this detector in groundwater is approximately 55.86 ± 5.40 mm before the minimal detectable limit is reached. In the real world application, the source of beta particles will not be from a collimated beam, but randomly dispersed throughout the groundwater. Currently, this is difficult to replicate in a lab, but previous research [18] has indicated that this should be capable of detecting radiation within the interval of activities expected at nuclear decommissioning sites. As the detector is being designed to be deployed in-situ and provide measurements of

the groundwater activity, it is required to have stable performance over near real time. The detector was held at a reverse bias of 80 V for 290 minutes, the average counts observed in 5 minute intervals went from $1.32 \times 10^6 \pm 1.14 \times 10^3$ to $1.28 \times 10^6 \pm 1.13 \times 10^3$. This discrepancy may become important when detecting activities closer to the lowest detectable limit. It is anticipated that this is due to temperature changes as the detector operates and produces heat. The deployment of CdTe sensors into groundwater boreholes must account for variations in environmental conditions and, given the sensitivity of the detector to temperature, must accommodate for fluctuations in groundwater temperature.

5.6 Chapter 5b: water temperature variation

Turkington, G., Gamage, K. and Graham, J. (2019) A Proof-of-concept CdTe Detector for In-situ Measurement of Strontium-90 in Groundwater. 2019 IEEE Nuclear Science Symposium and Medical Imaging Conference (NSS/MIC 2019), Manchester, UK, 26 Oct - 02 Nov 2019.

5.7 Introduction

Strontium-90 is monitored routinely at nuclear decommissioning sites and it is commonly found to be the primary beta emitting radionuclide. Groundwater becomes contaminated after spills of nuclear waste and radionuclides such as ^{90}Sr leak into the environment[18]. Boreholes are installed in the groundwater table at decommissioning sites and water samples activity is measured by liquid scintillation. However, these procedures produce chemical waste, increase the exposure of workers, are time consuming and expensive. A CdTe detector has been developed which can be deployed in groundwater boreholes where beta decay is

measured directly. It is anticipated that the temperature of groundwater at Sellafield will have an average temperature of 10.1 °C and this is subject to some fluctuation. It has been demonstrated that CdTe performance has some sensitivity in relation to temperature and if operated in a temperature from 0-10 °C [112] detector stability may be achieved without the need for additional cooling. This may allow for greater flexibility in detector design when it is important to keep detector dimensions to a minimum.

5.8 Method

The complete detector was compiled with a few small and lightweight components. A 10 x 10 x 1 mm cadmium telluride detector was paired with a appropriate charge sensitive amplifiers and readout systems and placed in a 118 x 83 x 40 mm plastic container which was wrapped in two layers of low density polyethylene. The CdTe sensor was paired with the α-CSA supplied by Micod with a capacitance, C_f of 1 pF and resistance, R_F, of 100 M Ohms. The amplifier was supplied with 5 V from a DC power supply. A CAEN (Italy) A7585D modular supply was mounted adjacent to the CSA. The CSA was connected to the high voltage output of the power supply and this was used to bias the attached semiconductor sensor. The CAEN power supply was programmed to supply a consistent 80 V bias to the CdTe diode. A window was cut from the box above the CdTe sensor to reduce the attenuation of beta particles. The distance from the sensor to the window was 0.7 mm and this gap was filled with air. The complete detector system is photographed in Fig. 5.6.

A 12 L plastic container was filled with tap water and the detector was fixed to the bottom of the container to prevent movement. The container was filled with tap water and left in a 20 °C laboratory for 30 minutes. The temperature of the water was recorded every 5 minutes with a thermometer. A collimated strontium-90 source was clamped at a fixed position 0.7 cm above the detector, also submersed under water. The number of counts in the detector

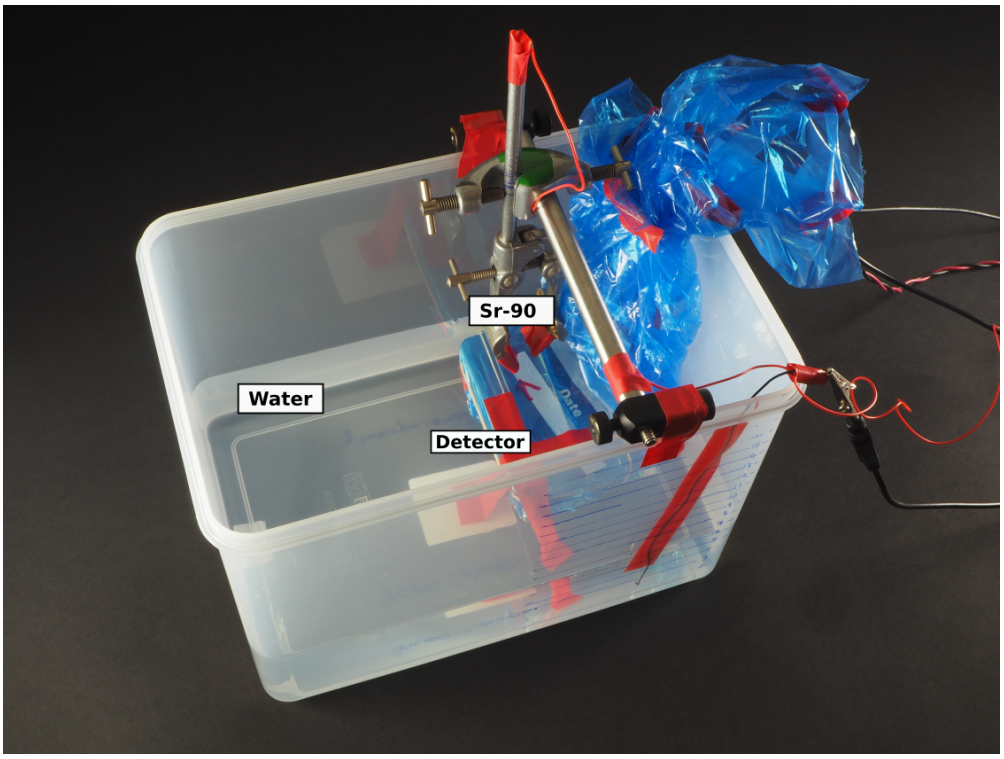

Figure 5.6: The complete detector set-up. The detector was placed under water in a 12 L container while a strontium-90 source was clamped above.

was collected in 5 minute intervals over a period of 120 minutes. The water was then cooled using ice. The counting procedure was replicated at the lower temperature. Meanwhile, the internal temperature of the sensor was monitored using the CAEN (Italy) A7585D power supply. Additionally, a mixture of synthetic groundwater was made with reference to [113]. The detector was placed in this mixture and a count from the source was taken and compared with tap water.

5.9 Results

The detector was tested in two scenarios, one where the temperature of the water had an average value of 14.3 °C and in another scenario where the temperature was 4.1 °C on average. Figure 5.7 plots the internal temperature of the detector over time in each scenario.

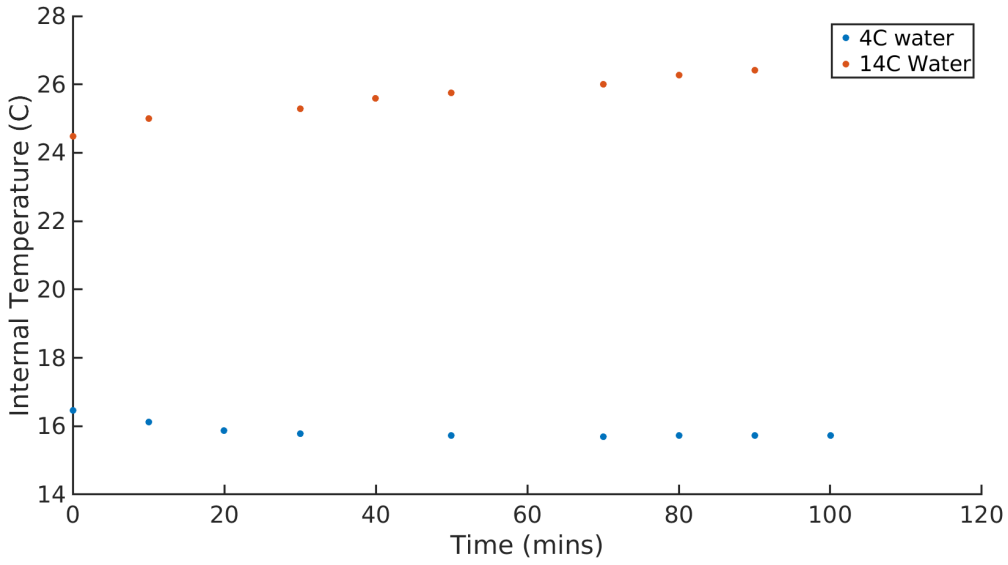

Figure 5.7: Internal temperature of the detector over time.

In the warmer water condition, the internal temperature of the detector was less stable, and was raised by 2.1 °C over the duration of the 120 minute period. Heat is generated inside the detector by the electronic components with the primary source of heat being the 80 V power supply used to bias the CdTe sensor.

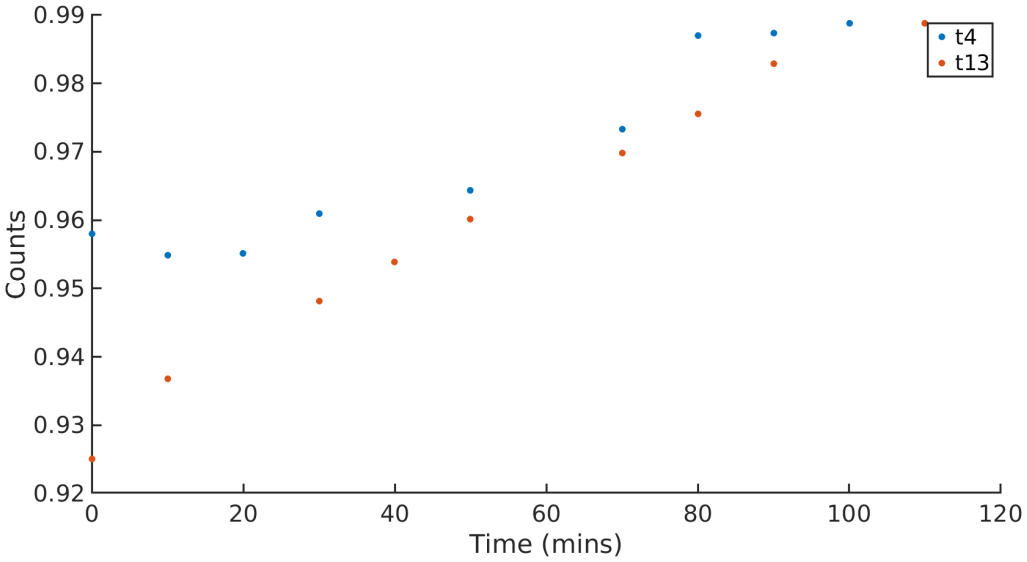

Figure 5.8: The averaged counts relative to the maximum count recorded in 5 minute counting periods while the detector was submerged in 4.1 °C water and 14.3 °C.

The experiments were repeated 3 times, over the course of many days. The activity of the strontium-90 source was 3.5 MBq, however the source was collimated with an aluminium barrel. To account for this, the results described here have been normalised and plotted as a fraction of the largest count recorded for each run. Figure 5.8 plots the averaged relative counts observed for each temperature condition. From this data it is observed that when the detector is placed in 4.1 °C water the counts observed are vary to a smaller degree the duration of the experiment. In both scenarios the most counts are observed at the end of the time period, and this may be due to the polarisation of the CdTe sensor over time [96]. However the detector in the 4.1 °C scenario deviates from this peak value by 4.0 % compared to a variation of 7.5 % in the 14.3 °C water scenario. The detector appears more stable in the 4.1 °C scenario.

The counts incident on the detector were recorded in both tap water and synthetic ground water scenarios. In each scenario the temperature of the water was maintained at 14.4 °C. The average number of counts in the tap water scenario was $7.127 \times 10^5 \pm 844$ and in the synthetic groundwater scenario was $7.129 \times 10^5 \pm 844$ showing no significant difference in results.

5.10 Conclusion

This paper has presented a novel detector for in-situ strontium-90 detection with a CdTe sensor. The deployment of CdTe sensors into groundwater boreholes must account for variations in environmental conditions and, given the sensitivity of the detector to temperature, a key factor will be the temperature of the groundwater. The stability of a CdTe detector in likely groundwater temperatures has been investigated and it has been demonstrated that the detector's performance was most stable at a water temperature of 4.1 °C. It is not expected that the salinity of the water will be a major contributing factor to detector performance.

6. Detector response to radionuclides

Reprinted from *G. Turkington, K. A. A. Gamage, J. Graham, The Simulated Characterization and Suitability of Semiconductor Detectors for Strontium 90 Assay in Groundwater*, Sensors 21 (3) (2021) 984. doi:10.3390/s21030984. [20]

6.1 Abstract

This paper examines the potential deployment of a cadmium telluride strontium-90 detector in groundwater boreholes at nuclear decommissioning sites. This is represents a novel approach to monitoring strontium-90 contamination at decommissioning sites such as Sellafield, and has the potential to reduce lifetime monitoring costs while providing information on a significantly reduced timescale. A Geant4 simulation was used to model the deployment of the detector in a contaminated groundwater borehole. It was found that the detector was sensitive to strontium-90, yttrium-90, caesium-137 and potassium-40 decay, some of the significant beta emitters found at Sellafield. However, the device showed no sensitivity to carbon-14 decay, due to the inability of the weak beta emission to penetrate both the groundwater and the detector shielding. The limit of detection for such a sensor when looking at solely strontium-90 decay would be 323 BqL^{-1} after a 1 hour measurement and 66 BqL^{-1} after a 24 hour measurement deployed in a groundwater borehole. Existing techniques are capable of examining strontium-90 decay below the World Health Organisations safe drinking water limit of 10 BqL^{-1}. A GaAs sensor with twice the surface area, but 0.3 % of the

thickness was modelled for comparison. Using this sensor, sensitivity was increased, such that the limit of detection for strontium-90 was 91 BqL^{-1} after 1 hour and 18 BqL^{-1} after 24 hours. However, this sensor sacrifices the potential to identify the present radionuclides by their end-point energy.

6.2 Introduction

At decommissioning sites, leaks and spills of nuclear waste leads to the introduction of radionuclides into the groundwater table. The concentrations of radionuclides in the groundwater can vary depending on the type of radionuclide, its source, and its permeability in different soils and structures. The concentrations of radionuclides across the site are monitored by samplying groundwater from boreholes and this data typically ignores variations in water depth [104]. The majority of beta emitters found at Sellafield are found in the separation area, where plutonium and uranium were separated from spent fuel. In 2016, the highest annual average total beta found in a borehole was 105,553 BqL^{-1}, with a maximum result of 124,000 BqL^{-1}. These wells are particularly active due to their location net to legacy waste storage, a location in which there were considerable leaks in the 1970s [104].

In general beta emitters are split into two categories, strong and weak, depending on their decay energy. In the strong category, ^{90}Sr is the single largest contributor to total beta activity and its activity maps with the total beta activity on the site. ^{90}Sr is a fission product and decays via the emission of a beta particle up to 0.546 MeV to ^{90}Y which itself decays by beta emission up to 2.28 MeV. The other strong beta emitter of interest is caesium-137, ^{137}Cs, a fission product which decays by beta emission to the metastable isomer barium-137, which returns to its ground state via the emission of a 0.661 MeV photon. At Sellafield, ^{137}Cs is typically found in very low concentrations with only one sampled borehole's annual average exceeding the WHO drinking water guideline of 10 BqL^{-1}. Some beta emitters emit

at much lower energies and are therefore more difficult to detect. This category includes tritium, carbon-14 (^{14}C), and naturally occurring potassium-40 (^{40}K). ^{14}C can be produced in nuclear reactors and is found in boreholes in the Sellafield separation area, with the highest annual average concentration being 43,825 BqL^{-1} however only 10 wells exceeded the WHO drinking water limit [104]. ^{14}C has a maximum decay energy of just 0.156 MeV.

Table 6.1: Activities of the prominent beta emitters found at Sellafield in 2016

Radionuclide	Average activity BqL^{-1}	Maximum activity BqL^{-1}	WHO Drinking water limit BqL^{-1}
^{90}Sr	-	59,000	10
^{137}Cs	6160	30	n/a
^{14}C	1287	24,246	16,260
^{40}K	632	11,663	n/a
Tritium	136	2,438	1,620

This research investigates the potential real-world performance of a cadmium telluride, CdTe, detector which is deployed directly into a groundwater borehole. Current methods for monitoring ^{90}Sr contamination require manual sampling of water from boreholes and analysis in laboratories with techniques such as ionic separation and liquid scintillation counting [49]. This can take months to produce results, is time consuming and produces secondary waste. The proposed detector will directly measure ^{90}Sr contamination in the groundwater after its insertion into groundwater boreholes, thereby providing results in a more timely and cost effective manner. The detector in this research has been designed to be sensitive to ^{90}Sr decay [114] and utilises a 10 x 10 x 1 mm CdTe sensor supplied by Acrorad (Japan). This detector has an Ohmic configuration and operates with a bias voltage of 80 V. CdTe is a semiconductor cmpound with established use as an X-ray detector and can be used in solar panels [92, 29]. The atomic number of CdTe is 50 and it has a bandgap of 1.44 eV. This means that it is effective at absorbing ionising radiation and has potential to work at room temperature [29].

Beta particles have a short range in matter due to the Coulombic interactions which occur as they are scattered by nearby atoms. This, and the continuous nature of beta emission, has presented difficulties when it comes to designing beta detectors. This research is concerned

with how these difficulties will affect the data it is possible to collect with an in-situ detector deployed directly into groundwater.

6.3 The detection of typical beta emitters found at nuclear decommissioning sites

This detector is being designed to specifically look for ^{90}Sr contamination in groundwater, however it is unlikely to be found in isolation. Realistically other radionuclides will be present, and this may include ^{137}Cs, ^{90}Y , ^{14}C, ^{40}K and tritium. As outlined above, these radionuclides emit radiation at very different energies and may be distributed differently throughout the environment due to their sorption properties [115]. Therefore, it is important to consider the sensitivity of the detector to the radionuclides likely to be found in the groundwater at decommissioning sites. As it is difficult to identify the origin of a beta particle, it is important to know which radionuclides are contributing to the total counts seen in the detector.

6.3.1 Simulation layout

Geant4 is a Monte Carlo simulation code developed to examine the interaction between radiation and matter [97]. Written in C++, Geant4 code has been used to simulate radiation-matter interactions in high-energy particle physics, medical and nuclear applications. The software tracks radiation, step by step, as it travels through matter. At each step, the probability which step next occurs is determined by probability distributions, known as cross-sections. At the beginning of a step a number is randomly generated and this is used to determine whether the particle interacts with matter, and in what way, or otherwise proceeds along its path. When particles interact with the sensitive layer of the detector, the information about that interaction is stored and can be used for analysis. The phyics used in the

simulation are described by "physics lists" which are predefined mathematical models which are used to calculate the outcome of interactions. This simulation used the FTFP BERT list which allows electron interactions up to 100 TeV, uses a maximum step length of 0.65 mm, an energy threshold of 900 keV, and a low energy limit of 1 eV.

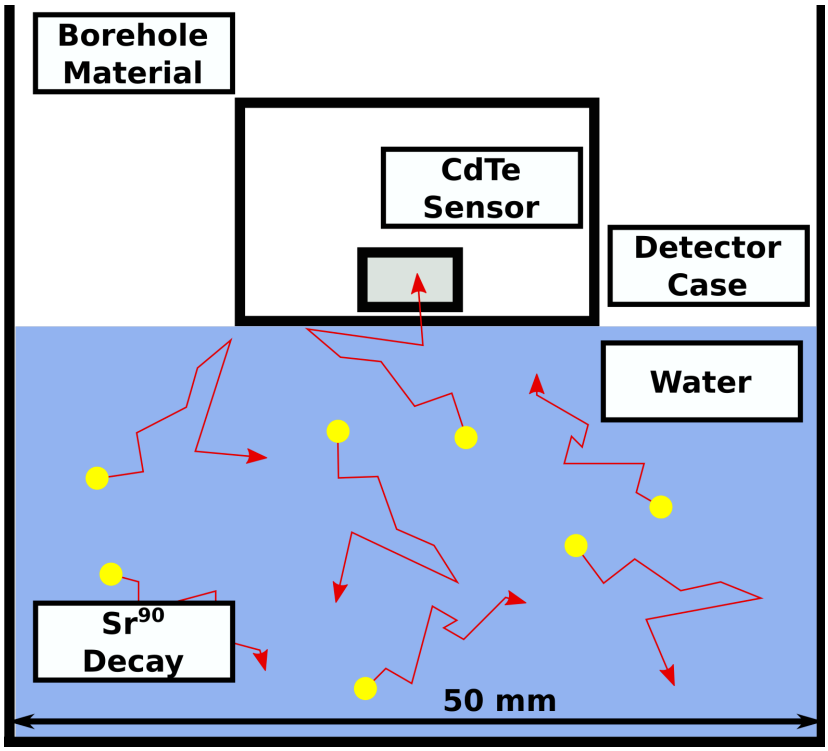

Figure 6.1: The simulation scenario illustrated. The detector is deployed to the surface of contaminated groundwater. Decaying radionuclides are randomly distributed throughout the water

The real world use-case of the detector was modelled with a Geant4 simulation, Fig. 6.1. A section of a groundwater borehole has been coded to model the surrounding soil, plastic piping, groundwater and the detector's casing and sensor. A cylinder with a 5 cm diameter and 5 cm height was modelled and populated sufficient radionuclide to match likely values found at Sellafield. In this experiment, a 1 hour counting time was simulated for each concentration of radionuclide. The decaying atoms are randomly populated throughout the groundwater. In this simulation the detector consists of a 10 x 10 x 1 mm CdTe detector with 20 nm thick platinum Ohmic contacts on either side. The detector is sealed by two layers of low density polyethelyne (LDPE), a thin and waterproof plastic which protects the sensor

and electronics from the groundwater but also attenuates incoming beta particles. There is a 1 mm gap between the sensor and the LDPE which is filled with air. In the simulation individual radionuclides are randomly distributed through the groundwater and decay, emitting the radiation in a random direction. The sensor is placed at the surface of the water where it counts beta particles which strike its surface and records the energy they deposit as they are either fully absorbed or scatter before this can happen.

6.3.2 Sensitivity to radionuclides

Some of the pure beta emitting radionuclides found at Sellafield are ^{90}Sr , ^{90}Y , ^{14}C, and naturally occurring ^{40}K. It's important to establish the detector's sensitivity to these radionuclides to establish whether they contribute to the detector's response function. This will give insight into the viability of this detector in the real world, and give insight into the difficulty of examining ^{90}Sr decay in the presence of other radionuclides. In this section, the detector has been exposed to each of these radionuclides in a scenario which represents an exposure time of 1 hour. The number of counts in the detector for different radionuclides at different activities is displayed in Table 6.2.

Table 6.2: The number of counts observed in the detector for different radionuclides and activities after a 1 hour counting period.

Activity Bq L^{-1}	^{90}Sr Counts	^{90}Y Counts	^{40}K Counts	^{14}C Counts	^{137}Cs
100,000	12,752	242,593	162,060	0	78013
10,000	1287	24,246	16,260	0	7842
1,000	136	2,438	1,620	0	792
100	10	246	172	0	73
10	1	6	18	0	10
1	0	1	0	0	1

The detector is unable to detect any ^{14}C counts, even at high concentrations of 100,000 BqL^{-1}. This indicates that maximum decay energy of the radionuclide is an important factor in how sensitive the detector is to the radionuclide. Betas emitted by ^{14}C are of such low energy, on average 0.049 MeV, that they are absorbed in the groundwater or detector casing before they are able to reach the sensor. This is notable because ^{14}C can be found in high

concentrations at Sellafield, up to 10,000s of BqL^{-1}. If the detector is blind to this activity it will have some significant implications. It means that a total beta count of high and low energy emitters is not be possible. However, this could be advantageous as weak betas are automatically filtered out of the detector response function, meaning it is only sensitive to the higher energy emitters which are of primary interest. The data shows that there is sensitivity to ^{90}Sr , ^{90}Y and ^{40}K in this scenario. It can be observed that the higher the energy of the decay, the more sensitive the detector is to the radionuclide. However, ^{40}K is only found in almost negligible quantities at Sellafield, with a maximum result of 1.0 BqL^{-1} in 2016 [104]. It is not certain whether ^{90}Sr and ^{90}Y would exist in secular equilibrium as data is not collected to monitor ^{90}Y concentrations in groundwater. This could be a significant factor in detector performance as ^{90}Y decay overlaps with ^{90}Sr decay in energy. If these radionuclides are found in secular equilibrium and their activity is 100,000 BqL^{-1}, the number of ^{90}Y counts observed is 20.28 times that of ^{90}Sr . This is due to the higher average emission energy of ^{90}Y , and its likelier transmission through water. ^{137}Cs is typically found at low activities in the separation area of Sellafield, in the region of 10 - 40 BqL^{-1}, and as such is likely going to be undetected and only add to the noise in the detector. The characteristic peak from the 32 keV decay is visible in the collected spectrum, enabling the identification of the radionuclide when it is present in sufficient activities. In conclusion, it is expected that when the detector is deployed into groundwater it will not be sensitive to weak beta emitters such as ^{14}C, but has sensitivity to strong betas like ^{90}Sr , ^{90}Y , ^{40}K and ^{137}Cs.

6.4 Low detectable limit and error propagation

The limit of detection of a detector describes the fewest number of counts which can be detected reliably by the system. This property is particularly relevant in the case of monitoring radionuclide activity at decommissioning sites, as it describes the lowest activity which can be detected. There are two aspects to consider when defining the detection limits of a detec-

tor, whether the sample is radioactive or not, and whether we can quantitatively measure its activity. This section shall consider the limit of detection for the sensor, and the the length measurement required to achieve it.

In a simple case where a decision must be made whether a borehole contains radioactivity, the number of counts from the sampled water, N_T, and the number of counts from the background, N_B, are subtracted to produce a result, N_S, which can be compared with a critical level, L_C. This is used to determine the likelihood of measured counts representing true activity and not fluctuations in statistical noise. The minimum detectable activity, α, is calculated with the following equation where N_D is defined as the minimum number of counts needed to ensure that the detector does not produce a false-negative rate that exceeds 5% [25].

$$\alpha = \frac{4.653\sigma_{N_B} + 2.706}{feT} \tag{6.1}$$

Where f is the radiation yield per disintegration, e is the absolute detection efficiency and T is the time taken to count the sample. When this formula is applied to ^{90}Sr and ^{90}Y , the expected low detectable limits are 569 BqL^{-1} and 35 BqL^{-1} respectively. The safe drinking water limit for ^{90}Sr is 10 BqL^{-1}. This suggests that, in its current state, the detector would be unsuited for monitoring radiation close to or at the safe limits. Performance would improve by eliminating some of the background noise, which can be achieved by refining the electronic design and accounting for temperature control systems in the detector. A reduction in background noise of 50 % would reduce the lower detectable limit by 29 %, to 406 BqL^{-1} leaving it still significantly short of the safe drinking water limit. Alternatively, the counting time for the detector could be increased. The results of this are documented in Table 6.3. By increasing the measurement time to 24 hours the LOD would be significantly reduced, to 66 BqL^{-1}, while still obtaining results on a daily basis. The background noise in the detector

would have to be significantly reduced, by up to 98 % for the detector performance to reach the safe water drinking limit.

Table 6.3: The limit of measurement for ^{90}Sr in the CdTe detector for increasing lengths of measurement.

Length of Measurement	Limit of Detection (BqL^{-1})
10 minutes	799
1 hour	323
24 hours	66
48 hours	46
168 hours	25

These results suggest that the detector is unlikely to compete with traditional methods for monitoring ^{90}Sr contamination in terms of precision. If truly instant results are required, the detector could be applied to monitor activity levels in highly concentrated areas above 800 Bq^{-1}. By increasing the counting time to 48 hours, or more, the detector can assess lower activity levels which approach the safe drinking water limits. This would still produce results in quicker fashion than traditional techniques and would allow for faster scanning of large areas to identify possible spikes in activities or new leaks. Operating over such a time period may present additional challenges such as detector stability over time [116], changes in temperature and power requirements.

The spectra of ^{90}Sr at different concentrations is plotted in Fig. 6.2 with a normalised spectrum of emitted ^{90}Sr decay. The maximum energy is shifted from 0.514 MeV to 0.403 MeV, a shift of 21.6 % at 100,000 BqL^{-1}. This shift increases to 25.5 % and 41.0 % for 10,000 BqL^{-1} and 1,000 BqL^{-1} respectively. This is due to particles depositing some of their energy in the water and the casing of the detector. A similar shift in ^{90}Y spectra is seen although to a less significant extent. In that case, the maximum energy shifts by 7 % from the maximum at 100,000 BqL^{-1} to 22.8 % at 1,000 BqL^{-1}. The response function of the detector to different activity levels is distributed differently. This is explained by the lower attenuation of high energy particles. This effect, along with scattering on the detector surface distorts the spectrum and skews it towards lower energy particles. As the activity decreases and the

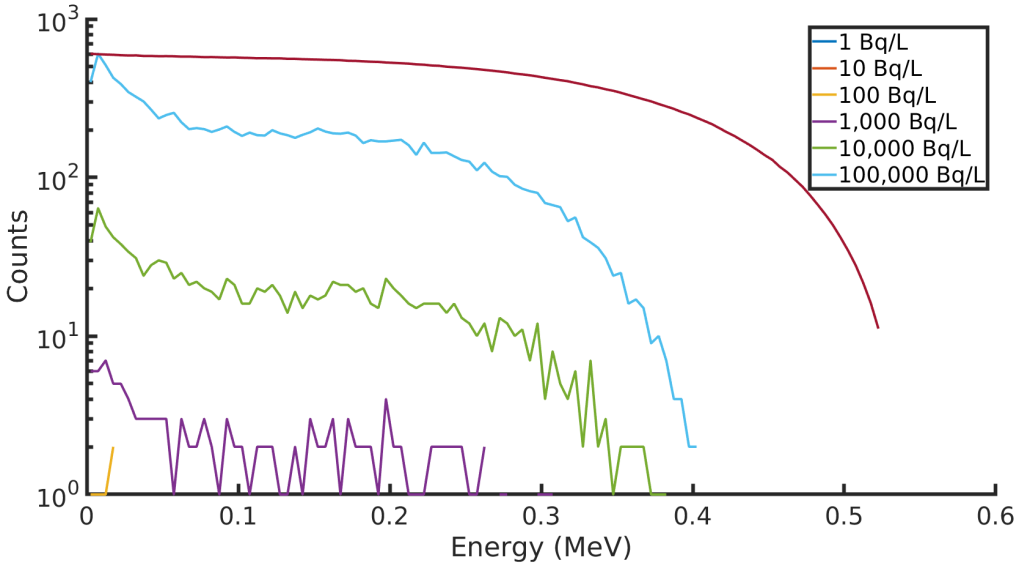

Figure 6.2: ^{90}Sr decay counted in a CdTe detector in a groundwater borehole simulation at different activities.

spectra begin to shift to the left, the distribution of the response function changes too. The peak at the lower energy points in the spectrum is no longer seen and the counts become more evenly distributed across the energy distribution in the spectrum.

Table 6.4: The counts observed in a GaAs sensor for various radionuclides found at Sellafield, and the percentage increase compared to the CdTe sensor.

Activity Bq L^{-1}	Sr90 Counts	Y90 Counts	K40 Counts	^{14}C Counts
100,000	28,428 (+222 %)	834,089 (344 %)	505,585 (311 %)	0
10,000	2859 (+222 %)	83,203 (343 %)	50,438 (310 %)	0
1,000	321 (+236 %)	8,130 (333 %)	5,080 (313 %)	0
100	32 (+320 %)	802 (326 %)	506 (294 %)	0
10	3	81	58	0
1	1	15	10	0

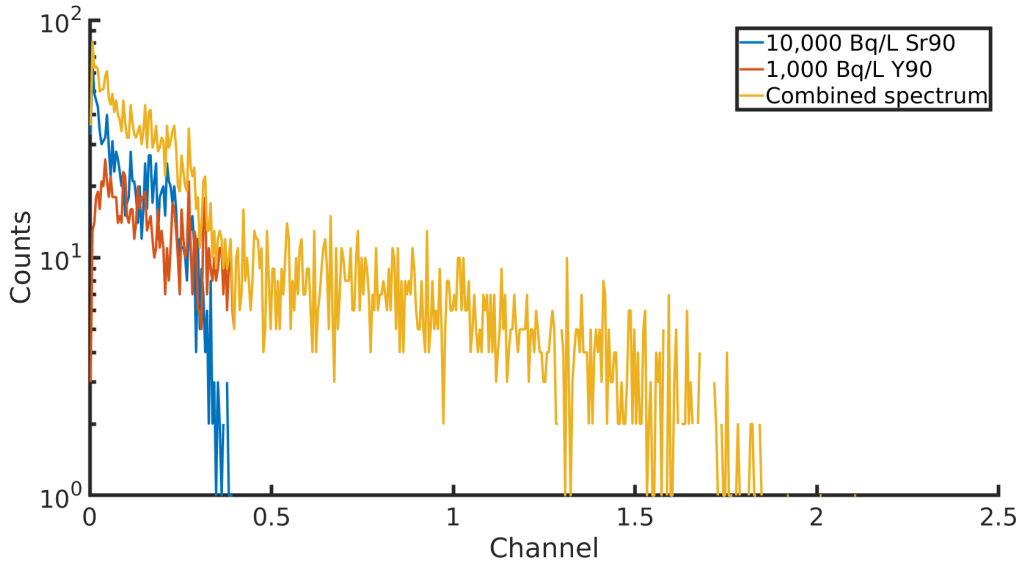

Figure 6.3: ^{90}Sr and ^{90}Y counts recorded recorded in a CdTe detector in a groundwater borehole simulation. The maximum decay energies are reduced as the particles are attenuated in water and the detector casing. The combined spectrum is plotted in yellow.

6.5 GaAs detector

The previous sections assesses a 10 x 10 x 1 mm CdTe sensor, but other sensors types are available. One such sensor is a gallium-arsenide, GaAs, sensor with a surface area of 2 cm^2 and a much thinner sensitive layer at 3 μm. This sensor is designed for solar panel usage and therefore has a larger surface area. This detector may be applied for the purposes of radionuclide monitoring, and its larger surface area, different material and thinner sensitive layer provides a contrast in approach to the CdTe sensor.

The same experiments were repeated with the GaAs sensor. The range of activities found at Sellafield for radionuclides are shown in Table 6.4 with the percentage increase compared to the counts in the CdTe sensor. Notably, the counting rate is much higher and this is due to the larger surface area of the sensor. This becomes particularly pertinent at the activities from 1-100 BqL^{-1}. The GaAs detector is proportionally more sensitive to ^{90}Y decay than ^{90}Sr decay. However, in spite of the larger surface area the GaAs detector is still unable to detect ^{14}C decay and is sensitive to the same radionuclides, ^{90}Sr , ^{90}Y and ^{40}K.

Table 6.5: The limit of measurement for ^{90}Sr in the GaAs detector for increasing lengths of measurement.

Length of Measurement	Limit of Detection (BqL^{-1})
10 minutes	226
1 hour	91
24 hours	18
48 hours	13
168 hours	7

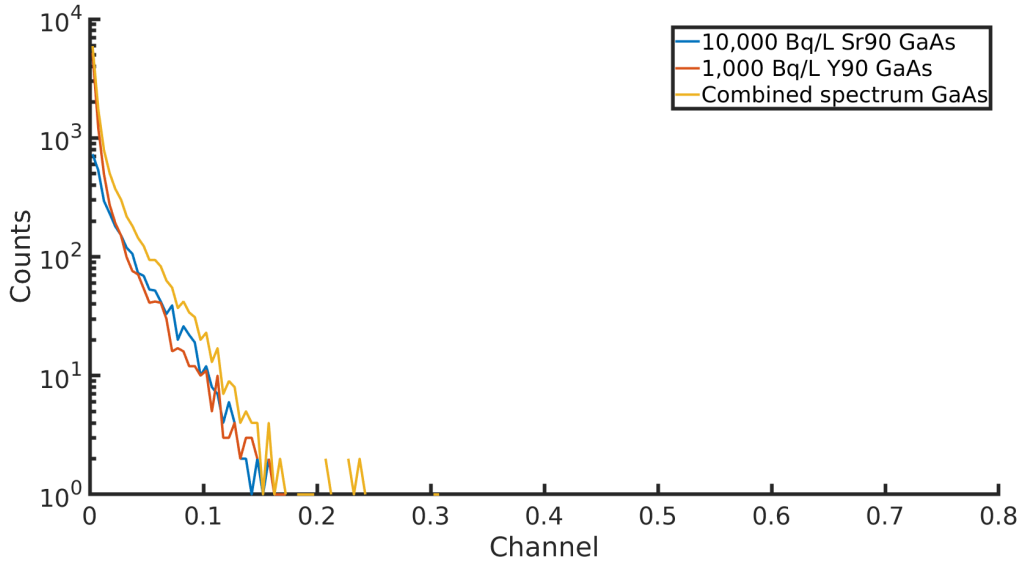

Figure 6.4: ^{90}Sr and ^{90}Y counts recorded recorded in a GaAs detector in a groundwater borehole simulation. The combined spectrum is plotted in yellow.

If it is assumed that the same level of background is present for the GaAs sensor, the LOD is significantly lower when compared to the CdTe detector. Table 6.5 describes the LOD of the GaAs sensor as the measurement time is increased. This means it is a more viable detector for monitoring contamination close to the safe water drinking limit and results can be achieved within a 48 hour period. The detector is more sensitive when it comes to simply counting the beta decay in the groundwater, however the response function of the detector to radiation is significantly different to the CdTe sensor. Although ^{90}Y may be counted after ingrowth as a method of estimating ^{90}Sr activity in groundwater, the activity of ^{90}Y in groundwater is not recorded. This is due to the weeks it takes for ^{90}Sr analysis to happen and the short decay time of ^{90}Y . It is unclear whether ^{90}Y and ^{90}Sr occur in groundwater in secular equilibrium or

whether this ratio is disrupted by other factors such as their sorption onto different materials in the ground. Fig. 6.3 plots the detector response to a 10:1 ratio ^{90}Sr and ^{90}Y and their combined spectra. As previously indicated, the detector is more sensitive to ^{90}Y decay and there are approximately twice as many ^{90}Y counts as ^{90}Sr counts in these spectra. Fig. 6.4 plots the spectrum captured by the detector for a groundwater mixture containing 10,000 BqL^{-1} of ^{90}Sr and 1000 BqL^{-1} of ^{90}Y . There is little distinction between the two sources in terms of channel number in the detector and it would be impossible to identify the presence of both radionuclides by looking at the energy deposits. The detector would lose its ability to distinguish between ^{90}Sr and ^{90}Y decay. This can be seen by comparing Fig. 6.3 with Fig. 6.4. The spectrum produced in the GaAs detector is compressed and shifted to the left, only a few counts of ^{90}Y 90 exceed the energy deposit produced by ^{90}Sr . This reduces the possibility of identifying radionuclides by their energy deposit in the detector.

6.6 Conclusions

An in-situ ^{90}Sr detector was modelled to examine its potential performance and sensitivity in a real-world scenario. This technique requires the detector to be deployed directly into a groundwater borehole where it directly counts beta decay from radionuclides. This will eliminate the requirement for chemical separation and pre-treatment necessary for other techniques, such as liquid scintillation counting. Geant4 was used to model a groundwater borehole scenario, and the deployment of the detector into water contaminated with ^{90}Sr , ^{90}Y , ^{137}Cs, ^{14}C and ^{40}K. A 10 x 10 x 1 mm CdTe sensor was contrasted with a 20 mm x 20 mm x 3μm GaAs sensor.

The CdTe detector was found to be sensitive to strong beta emitters, ^{90}Sr , ^{90}Y , ^{137}Cs, and ^{40}K, with that sensitivity increasing with the average emission energy of the radionuclide in question. However there was no sensitivity to ^{14}C, a weak emitter, but one which contributes

significantly to the total beta counts found at Sellafield. The GaAs sensor was more sensitive in terms of counts to each radionuclide, but was similarly blind to weak beta emitters. Therefore, such a detector is unlikely to be effective as a counter for total beta activity.

The limit of detection for the CdTe sensor and ^{90}Sr decay was found to be 323 BqL^{-1} after a 1 hour measurement and 66 BqL^{-1} after a 24 hour measurement. Meanwhile, the GaAs sensor had a lower limit of detection of 91 BqL^{-1} and 18 BqL^{-1} in 1 and 24 hours respectively. Existing techniques are capable of examining ^{90}Sr decay below the World Health Organisations safe drinking water limit of 10 BqL^{-1}. This has the benefit of allowing decommissioning sites to examine the data quickly to determine whether beta activity is present or not, and rapidly respond to unexpected spikes in groundwater activity resulting from new leaks. This could be used to compliment existing techniques and allow for a selective approach with existing techniques such as liquid scintillation counting for closer examination of ^{90}Sr activity. Additionally this would allow for rapid scanning of large areas of land and be used to pinpoint locations of peak activity.

7. Identification of beta emitting radionuclides

Reprinted from: *G. Turkington, K. A. A. Gamage, J. Graham, The Simulation of In-Situ Groundwater Detector Response as a Means of Identifying Beta Emitting Radionuclides by Linear Regression Analysis*, Sensors 21 (17) (2021) 5732. 10.3390/s21175732. [22]

7.1 Abstract

The in-situ characterisation of strontium-90 contamination of groundwater at nuclear decommissioning sites would represent a novel and cost-saving technology for the nuclear industry. However, beta particles are emitted over a continuous spectrum and it is difficult identify radionuclides due to the overlap of their spectra and the lack of characteristic features. This can be resolved by using predictive modelling to perform a maximum-likelihood estimation of the radionuclides present in a beta spectrum obtained with a semiconductor detector. This is achieved using a linear least squares linear regression and relating experimental data with simulated detector response data. In this case, by simulating a groundwater borehole scenario and the deployment of a cadmium telluride detector within it, it is demonstrated that it is possible to identify the presence of ^{90}Sr , ^{90}Y , ^{137}Cs and ^{235}U decay. It is determined that the optimal thickness of the CdTe detector for this technique is in the range of 0.1 to 1 mm. The influence of suspended solids in the groundwater is also investigated. The average and

maximum concentrations of suspended particles found at Sellafield do not significantly deteriorate the results. It is found that applying the linear regression over two energy windows improves the estimate of ^{90}Sr activity in a mixed groundwater source. These results provide validation for the ability of in-situ detectors to determine the activity of ^{90}Sr in groundwater in a timely and cost-effective manner.

7.2 Introduction

This research aims to develop a methodology for estimating the ^{90}Sr activity in contaminated groundwater at nuclear decommissioning sites as measured by a cadmium telluride (CdTe)[117, 118] detector that is deployed in a groundwater borehole. There is demand in the nuclear decommissioning industry to develop new ^{90}Sr monitoring techniques that can reduce the lifetime monitoring costs of the radionuclide [18, 119, 120, 121, 122, 123]. The aim is to design techniques that are safer, produce less secondary waste and can be completed rapidly without the need for specialised laboratory techniques. Currently, groundwater samples are taken from underground boreholes, treated, placed into storage and, eventually, the radionuclides in the groundwater are analysed using radiochemical separation and liquid scintillation counting. However, these stages could be bypassed with the deployment of an in-situ semiconductor detector. In order to compete with existing techniques, an in-situ detector should be able to identify the activity of individual radionuclides. This paper reports on a technique that allows for the activity of individual radionuclides to be determined using a gross measurement of the activity in the borehole and predictive modelling. Each radionuclide's contribution to the total activity is estimated by relating the gross spectrum to the simulated detector response to each radionuclide in the scenario.

There are two main challenges to consider when designing a beta detector. The first is that beta particles have a limited range in matter and are easily attenuated as they travel through

the environment [124]. The consequence of this is that the detection medium must be placed very close to the source of the radiation [125]. This is the reason that liquid scintillation is one of the primary beta detection techniques [49]. By mixing the sample of radionuclides and the scintillator together, the likelihood of interaction between beta radiation and the scintillator is sufficiently high. Liquid scintillation counters are able to achieve a low limit of detection, below the guideline value for drinking water. Alternatively, this research has taken advantage of the development of high-quality, high-density and high-energy-resolution semiconductors to design a compact detector that can be immersed directly in contaminated groundwater. Using a thin layer of waterproofing, the detector can be deployed in contaminated groundwater while keeping the attenuation of the radiation spectrum minimal.

The other challenge is that beta decay results in particles that are emitted over continuous spectra and terminate at an end-point energy. This presents difficulties when identifying beta emitters from a mixed source of radiation. When ^{90}Sr decays via beta emission, it is a result of an excess of neutrons in the nucleus, one of which will convert into a proton, a beta particle and an anti-neutrino. The emission of the anti-neutrino during beta decay is significant as the energy released by the nuclear decay is shared between both particles, resulting in the continuous spectrum of emission. As a result, it is difficult to determine the origin of a particular beta particle in a mixed spectrum and, consequently, the radionuclides in the sample. By contrast, gamma emission occurs as electrons fall between fixed energy levels in the nucleus [25]. This results in characteristic energy peaks in the emission spectra, from which the associated radionuclides can be easily identified. As it is not practical to perform radiochemical separation in situ, the detection of ^{90}Sr will require the acquisition of a gross beta spectrum and predictive model to identify the constituent radionuclides. This method posits that the total spectrum measured with the detector comprises the summation of the detector response to each individual radionuclide. By simulating the detector response to the constituent radionuclides, a linear regression model can be applied to make a maximum-likelihood estimate of the radionuclides present in the groundwater and their activities.

7.2.1 Background literature

Predictive modelling techniques have been developed for applications with different detector types. A simulation-based linear regression approach to radionuclide identification has been demonstrated in other research [126, 127]. S. Grujic et al. [128] report on using the Monte Carlo simulation package MCNP [129] to simulate the response function of a semiconductor Si detector to identify ^{90}Sr contamination in water samples taken from spent nuclear fuel storage pools. In this case, a PIPS (passivated implanted planar silicon) detector with a surface area of 1.197 cm and a thickness of 502 µm is simulated. In this research, the gross radiation spectrum is considered to be the sum of the individual radiation spectra, modified by the response function of the detector—as described in Equation (7.1).

$$\sum_{n=1}^{N} A_n R_{n,i} = C_i i = i_L, i_U \tag{7.1}$$

where i is the lower and upper channel number of the multichannel analyser in the detector, N is the number of unknown radionuclides with unknown activities in the sample, A_n is the activity of the radionuclide that must be determined [Bq], $R_{n,i}$ is the simulated response function of the detector to radionuclide n in channel i, and C_i is the gross beta spectrum that is measured with the detector in the configuration as modelled in the simulation. This equation can be used to form a system of linear equations that are resolved using the least squares with linear inequality constraints method [130]. In this study, the groundwater sample was placed in a Petri dish below the detector and the scenario was modelled in MCNP. The researchers used the least squares method to identify an activity of 166.3 $\pm$ 13.4 Bq cm^{-3} for ^{137}Cs in a mixed sample with ^{90}Sr . The activity of ^{137}Cs in the sample was found to be 179.8 $\pm$ 10.5 Bq cm^{-3} using a calibrated GX5020 germanium (Ge) detector.

E. Bai et al. conducted an investigation into the use of portable gamma detectors for identifying radionuclides in public spaces and at checkpoint searches with the goal of identifying

nuclear weapons. In this case, the researchers were interested in poorly resolved gamma spectra from unknown radionuclides, where there may be potential overlap of gamma emission or sufficient attenuation of their characteristic peaks to mask their presence. They proposed a technique where the detector repsonse is modelled, but they presented a two-stage algorithm consisting of a linear regression stage and a subsampling stage based on majority voting [105]. The detection algorithm is based on a similar equation to Equation (7.1). In typical gamma detection, a peak fitting algorithm is used to fit a Gaussian function to peaks in detected gamma spectrum, and the energies of these peaks are used to identify the radionuclides from a database of radionuclides. The scenario that the researchers address is when the gamma peaks are masked by noise or so poorly resolved that peak fitting may fail. The generated system of equations was resolved using a least absolute shrinkage and selection operator (LASSO) algorithm with a subsampling stage implemented to successfully reduce the rate of false positive errors. Predictive modelling is increasingly being used in other fields to overcome the deficiencies in detector technology as a means to implement remote sensors for monitoring environmental quality [131, 132, 133, 134]

7.3 Methodology

The radionuclide identification procedure presented in this research comprises two sections. First, the detector response is simulated [135], and second, a system of equations is constructed that relates the detector response to individual radionuclides to the gross radiation spectrum that is measured. A linear regression is applied to the system of equations to provide an estimate of the activity of the radionuclides in the groundwater.

7.3.1 Groundwater radiation model

The gross radiation spectrum collected with an in-situ detector comprises contributions from each individual radionuclide present in the groundwater. This can be expressed by a linear relationship, as written in the form of Equation (7.2).

$$\mathbf{M} = R\mathbf{N} \tag{7.2}$$

M is a vector containing the gross spectrum of radiation measured with a CdTe detector deployed in a groundwater borehole. **N** is an $n \times k$ matrix that details the detector response to each individual radionuclide, where k is the number of radioactive sources and n is the number of channels in the detector. The relative activities of the radionuclides, R, are unknown and can be found by solving Equation (7.2) computationally using linear regression[136]. In this case, the iteratively weighted least squares method is used [137].

7.3.2 Detector response simulation

In nuclear radiation spectroscopy, the spectrum that is output by a detector is an approximation of the true emission spectrum released by radionuclides. These two spectra can be related by a response function. There are two aspects that contribute to the response function. Firstly, the radiation must interact physically with the environment en route to the detector and this leads to attenuation of the spectrum. This process is simulated using the Monte Carlo software, Geant4 [138]. Secondly, the contribution of electronic noise and statistical variations in electron-hole production [25] within the semiconductor must be modelled, and this is achieved with a Gaussian broadening of the detector output generated by Geant4.

This is expressed in Equation 7.3[139].

$$\int_0^{E_{min}} R(S,E)N(E)dE = M(S) \tag{7.3}$$

$$0 \leq E \leq E_{max}, 0 \leq S \leq S_{max} \tag{7.4}$$

In this equation, N(E) is the emission spectrum, M(S) is the measured radiation spectrum, R(S,E) is the response function, S is the signal value, and E is the radiation energy. This equation has the form of a Fredholm integral equation and can be rewritten as a system of linear equations; see Equation (7.2).

The groundwater borehole environment in which the detector will be deployed was modelled with a Geant4 simulation; see Figure 7.1. The purpose of the simulation is to model the decay of radionuclides and the interaction of the released radiation with the environment and the detector. A typical groundwater borehole at Sellafield comprises a plastic inner layer with 5 cm diameter and is surrounded by a silicon filtering layer, which is installed to keep contaminants out of groundwater samples. The interior of the borehole was filled with water to a depth of 5 cm, with the detector positioned at the surface.

The detector design consists of a 10 $\times$ 10 $\times$ 1 mm CdTe detector with 20 nm thick platinum Ohmic contacts on either side. The detector is sealed with two layers of low-density polyethelyne (LDPE), a thin and waterproof plastic, which protects the detector and electronics from the groundwater but also attenuates incoming beta particles. There is a 1 mm gap between the detector and the LDPE that is filled with air.

To generate data to fill the response matrix, **N**, the groundwater was populated with the equivalent of 100,000 BqL^{-1} ^{90}Sr , ^{90}Y , ^{137}Cs, ^{40}K for 5 h of measurement in the borehole. This simulation used the FTFP BERT physics list, which allows electron interactions up to 100 TeV and uses a maximum step length of 0.65 mm, an energy threshold of 900 keV and a low energy limit of 1 eV.

$$FWHM = a + b\sqrt{(E + cE^2)} \tag{7.5}$$

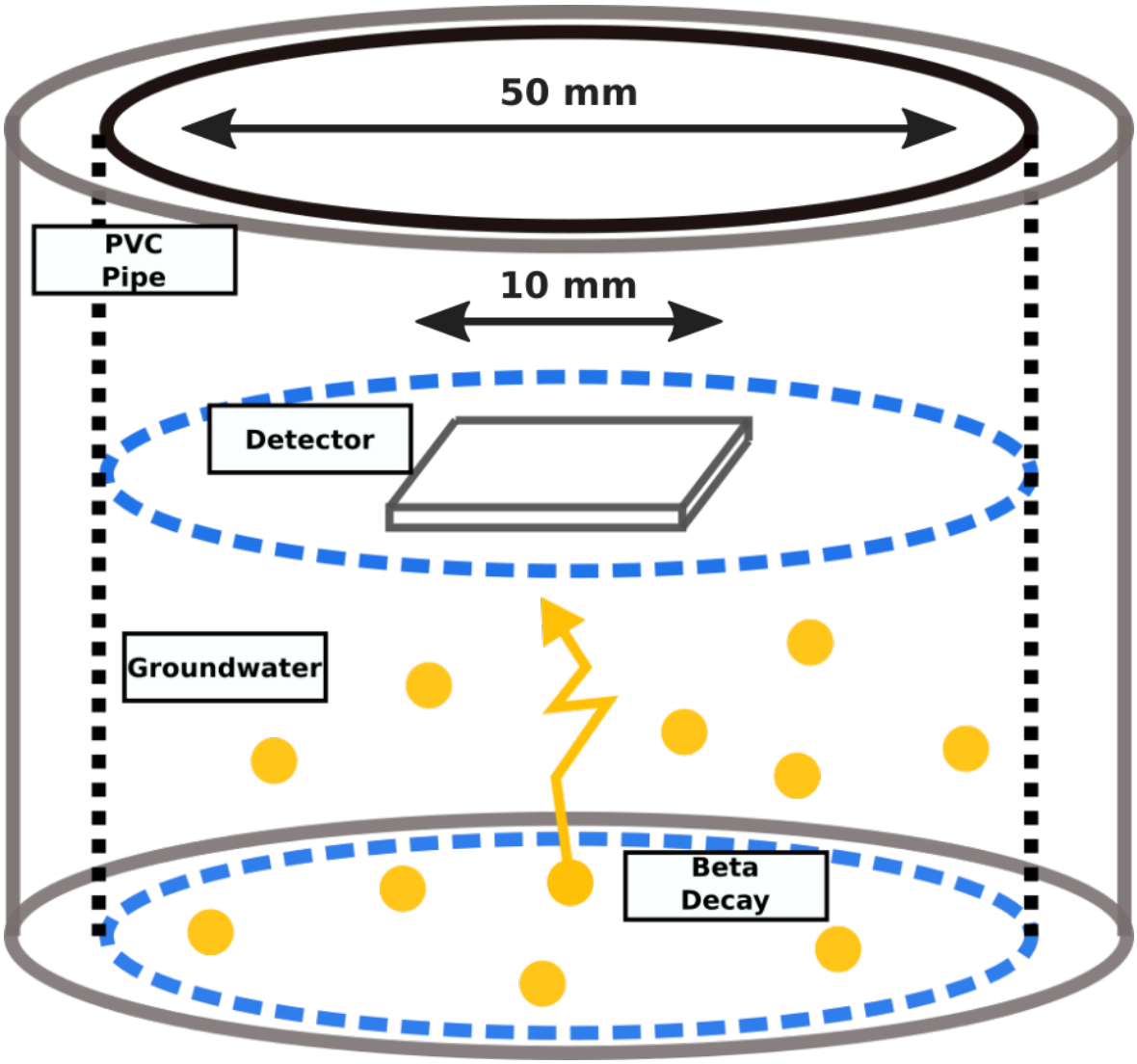

Figure 7.1: The scenario simulated in the simulation. A PVC pipe, with a 5 cm diameter, comprises the innermost layer of the borehole and it is surrounded by silicon. The detector is deployed in contact with the water, which is populated randomly with decaying radionuclides.

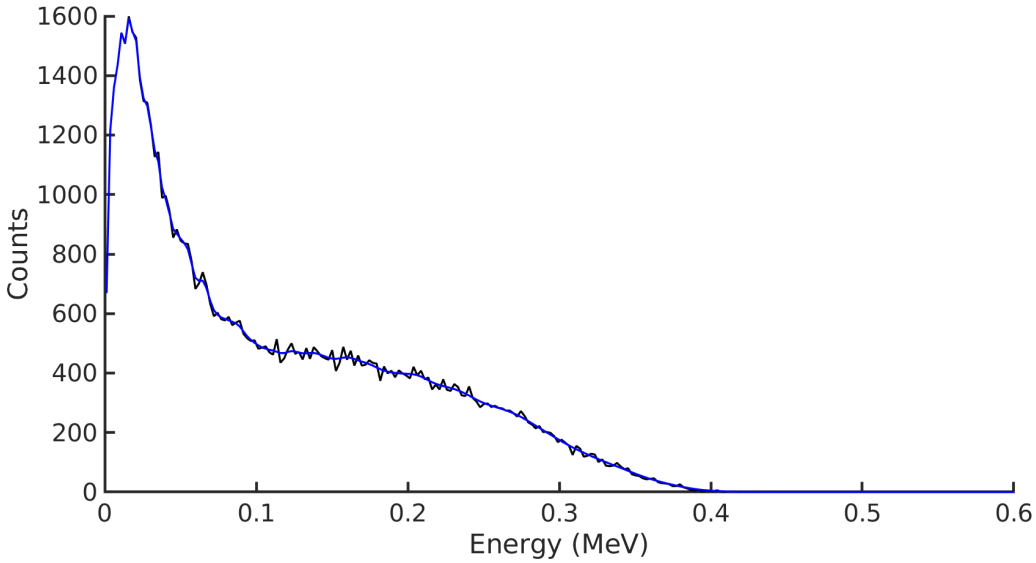

Figure 7.2: The simulated ^{90}Sr spectrum acquired with the CdTe detector in the groundwater scenario, black, with the Gaussian broadening applied, blue.

A Geant4 simulation tracks radiation as it travels through matter and calculates the energy physically deposited in the material body of a radiation detector. However, the reality of radiation detection is more complicated. To make the simulated detector response more realistic, a Gaussian broadening was applied to the data. Manufacturer data were used to plot the correlation between the full width half-maximum (FWHM) and the gamma peaks of Am, ^{57}Co,^{137}Cs. The coefficients a, b and c were determined from Equation (7.5) and were used to apply a Gaussian broadening to the simulated spectra, as seen in Figure 7.2.

7.4 Results

The goal of this section is to demonstrate the deconvolution of a gross beta spectrum and evaluate the methodology to establish whether it can identify ^{90}Sr activity in a contaminated groundwater environment.

This technique is dependent on a priori knowledge of the radionuclides expected to be found in a groundwater borehole at a nuclear decommissioning site. If a radionuclide is not in-

cluded in the response matrix, its presence cannot be determined. On the other hand, it is necessary to evaluate whether including many radionuclides in the response matrix can lead to false positives or otherwise distort the estimates of radionuclide activity. In Table 7.1, a borehole simulation is populated with ^{90}Sr activity from 100,000 BqL^{-1} to 100 BqL^{-1}. The response matrix, X, is populated with just ^{90}Sr and ^{90}Y initially, but ^{137}Cs, ^{40}K, and ^{235}U are added in stages so that their effect on the estimated ratio of ^{90}Sr and ^{90}Y can be compared. This has demonstrated that the regression technique is effective at determining the ratio of ^{90}Sr present in the groundwater down to activities as low as 100 BqL^{-1}. The inclusion of the additional radionuclides into the response matrix does not produce any significant false positive values in the results and only alludes to a small deviation in the estimation of activity.

Table 7.1: Results of analysis of a pure ^{90}Sr mixture of decreasing activity with different radionuclides included in the detector response matrix.

^{90}Sr Activity BqL^{-1}	X[^{90}Sr ^{90}Y]	X[^{90}Sr ^{90}Y ^{137}Cs]	[^{90}Sr ^{90}Y ^{137}Cs ^{40}K ^{235}U]
100,000	[1.0000 0.0000]	[1.0000 0.0000 0.0000]	[1.0000 0.0000 0.0000 0.0000 0.0000]
10,000	[0.1017 0.0001]	[0.1010 0.0000 0.0000]	[0.1001 0.0001 0.0000 0.0000 0.0001]
1,000	[0.0125 0.0000]	[0.0111 0.0000 0.0000]	[0.0114 0.0004 0.0000 0.0000 0.0002]
100	[0.0019 0.0000]	[0.0021 0.0000 0.0000]	[0.0021 0.0000 0.0000 0.0002 0.0000]

Table 7.2 demonstrates the ability to resolve ^{90}Sr from ^{90}Y decay at varying activity levels in groundwater. In reality, it is not well understood how these two radionuclides exist within the groundwater itself. The elements have different chemical properties, which means they interact with the environment differently; ^{90}Sr and ^{90}Y have different sorption rates in soil and move through the groundwater system at different rates. When a groundwater sample is collected, significant time passes between sampling and activity determination, which means that secular equilibrium is achieved at the point of counting. The spectrum of this mixture is plotted in Figure 7.3. Here, the measured spectrum is plotted in black. The gamma peak from ^{137}Cs can be seen at 662 keV, with the X-ray photopeak protruding at the start of the spectrum. The long tail is due to beta emission from ^{90}Y . Because ^{90}Y decay results in more energetic particles, it produces a higher count-rate for the same activity when compared with ^{90}Sr . This means that the ^{90}Y spectrum is more well-defined for low activities, and this

reflects the results shown in Table 7.2, where the ratio of ^{90}Y is reproduced more reliably at low counts compared to ^{90}Sr . However, it is still possible to identify the presence of ^{90}Sr in strongly ^{90}Y -contaminated groundwater. This scenario is unlikely to occur in reality, but serves as verification of the effectiveness of the technique.

^{90}Sr and ^{90}Y are not the only radionuclides found in contaminated groundwater at nuclear decommissioning sites; therefore, the deconvolution of a gross radiation spectrum may contain contributions from gamma emitters such as ^{137}Cs and even alpha emitters such as ^{235}U. The detector's response to these radionuclides has been simulated and the deconvolution of ^{137}Cs is presented in Table 7.3. ^{137}Cs decay comprises beta decay up to an end-point energy of 0.512 MeV and gamma emission at 0.662 MeV. ^{137}Cs is not typically found in high groundwater concentrations at Sellafield due to its strong sorption onto soil, with a maximum activity of 41.8 BqL^{-1}. The results demonstrate the ability to deconvolve ^{137}Cs activity from a mixture of high activity ^{90}Sr and low activity ^{90}Sr .

Table 7.2: The ratios of ^{90}Sr and ^{90}Y mixed to different activities as determined by linear regression analysis.

^{90}Sr Activity BqL^{-1}	^{90}Y Activity BqL^{-1}	^{90}Sr Ratio	^{90}Y Ratio
100,000	100,000	1.0000	1.0000
100,000	10,000	1.0390	0.0974
100,000	1,000	1.0125	0.0011
100,000	100	0.9963	0.0003
100	100,000	0.0022	1.0000
100	10,000	0.00411	0.0973
100	1,000	0.0015	0.0108
100	100	0.0000	0.0001

Finally, this method was applied to a realistic mixture of radionuclides that may be found in a groundwater borehole, as shown in Table 7.4. The results are reported with a 95% confidence interval. There is agreement between the simulated activity and the calculated activity as a result of the deconvolution of the gross spectrum. ^{235}U was correctly not identified in the sample and the activities of ^{137}Cs, ^{90}Sr and ^{90}Y were resolved despite the common overlap between their beta emission. The estimated activity of ^{90}Sr 12.03 $\pm$ 0.56 kBq L^{-1} which leaves some discrepancy between the true and calculated activity. This is largely down to

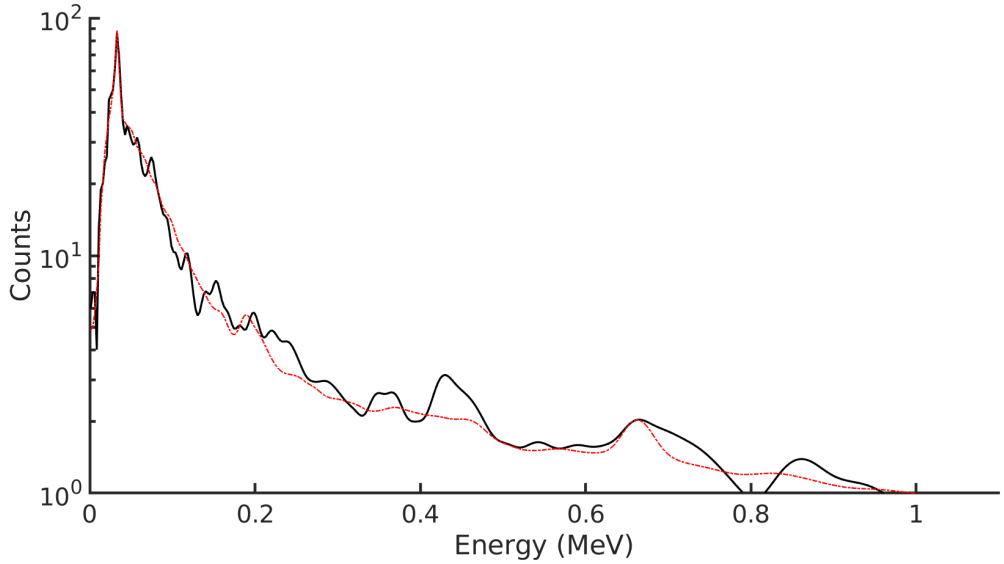

Figure 7.3: The spectrum corresponding to the radionuclide mix in Table 7.4 output by the detector is plotted in black, and the reconstructed spectrum resulting form the linear regression is plotted in red.

Table 7.3: The ratios of ^{90}Sr and ^{137}Cs mixed to different activities as determined by linear regression analysis.

^{90}Sr Activity BqL^{-1}	^{137}Cs Activity BqL^{-1}	^{90}Sr Ratio	^{137}Cs Ratio
100,000	100,000	1.0000	1.0000
100,000	10,000	0.9686	0.1004
100,000	1,000	0.9810	0.0104
100,000	100	1.0072	0.0011
100	100,000	0.0022	1.0000
100	10,000	0.0000	0.1000
100	1,000	0.0000	0.0103
100	100	0.0094	0.0011

difficulties in resolving ^{90}Sr and ^{90}Y spectra. ^{90}Y emission is more energetic and therefore less likely to be fully absorbed in the groundwater.

Table 7.4: The estimate of ^{90}Sr , ^{90}Y , and ^{137}Cs activity from a realistic groundwater borehole

Radionuclide	Simulated Activity (kBq L^{-1})	Calculated Activity (kBq L^{-1})
^{90}Sr	10.00	12.29 ± 0.56
^{90}Y	1.00	0.74 ± 0.05
^{137}Cs	0.10	0.12 ± 0.004
^{235}U	0	0.00

7.4.1 Alternative detector

The previous sections describe the use of a $10 \times 10 \times 1$ mm CdTe detector that was designed specifically for monitoring ^{90}Sr contamination, but the results of applying this technique to other detectors' configurations should be considered. A 1 mm detector is relatively unusual and detectors on the market are typically much thinner; indeed, thin solar cell panels may even be appropriated as radiation detectors. This section will consider the use of such detectors and evaluate whether they are viable for the linear regression technique. CdTe detectors of decreasing thickness were exposed to a simulated groundwater scenario containing 10kBq L^{-1} of ^{90}Sr , 1 kBq L^{-1} of ^{90}Y and 0.1 kBq L^{-1} of ^{137}Cs. The results of the simulations are displayed in Table 7.5. The 0.003 mm thick detector categorically produces the least agreement and it completely fails to estimate the activity of ^{90}Sr in the groundwater. The material is not thick enough to sufficiently resolve in incident radiation upon its surface and as such produces highly compressed spectra. These spectra become impossible to distinguish from one another, which leads to the results seen in Table 7.5. Therefore, it is determined that in order to perform this technique, the thickness of the detector should fall within the range of 1 mm to 0.01 mm.

Of the detectors that fall into this range, it is notable that the detector with 0.1 mm thickness produces results that are closest to the true activities in the sample. This is somewhat paradoxical but can be explained by the effect of backscattering particles. Beta particles incident on a surface are prone to backscattering, where they only deposit a fraction of their energy

Table 7.5: The estimate of ^{90}Sr , ^{90}Y , and ^{137}Cs activity from a realistic groundwater borehole using a 3 μm GaAs detector.

Thickness (mm)	^{90}Sr (kBq L^{-1})	^{90}Y (kBq L^{-1})	^{137}Cs(kBq L^{-1})
1.0	12.03 $\pm$ 0.56	1.03 $\pm$ 0.14	0.12 $\pm$ 0.04
0.5	12.11 $\pm$ 0.52	0.99 $\pm$ 0.04	0.083 $\pm$ 0.003
0.1	10.42 $\pm$ 0.42	0.99 $\pm$ 0.02	0.099 $\pm$ 0.004
0.01	12.72 $\pm$ 0.91	0.93 $\pm$ 0.01	0.11 $\pm$ 0.013
0.003	0.00 $\pm$ 1.10	0.89 $\pm$ 0.01	5.81 $\pm$ 0.30

and leave the detector before they are fully absorbed. This effect produces a peak in both the ^{90}Sr and ^{90}Y spectra collected with these detectors. When the detector is very thin, this peak is very pronounced. As the thickness of the detector increases, an increasing number of particles are distributed at higher channel numbers in the detector. This effect produces a second peak that is present in the 0.1 mm thick detector, but not in the 0.5 and 1 mm thick detectors. This characteristic of the spectrum in the 0.1 mm detector means that the regression can more easily resolve the ^{90}Sr and ^{90}Y spectra.

7.4.2 Impact of suspended solids

The groundwater found in monitoring boreholes commonly contains small concentrations of suspended solids, such as minerals and rock, which may remain from the drilling process or from inflow from the surrounding geological formation. To consider any potential influence of these particles on the measurement of radionuclides, these non-radionuclide components were added to the simulation based on analysis of measured particle concentrations, turbidity analysis and analysis of representative rock data.

The components considered include sodium, potassium, iron, calcium, magnesium, iron, aluminium, silicon and oxygen [140]. These components were distributed uniformly throughout the groundwater simulation, in accordance with the average and maximum monitored values. The results are reported in Table 7.6. When the groundwater contains the average concentration of all the components, 40 mg L^{-1}, the estimated activity of ^{90}Sr is 10.09 $\pm$ 0.55 kBq L^{-1}, and returns a result of 9.74 $\pm$ 0.51 kBq L^{-1} for the maximum concentration at

300 mg L^{-1}. Therefore, it is not determined that these concentrations of components in the groundwater influenced the determination of the activity. The variation between the reported results is due to the random nature of radioactive decay and some inconsistency in the linear regression technique used.

Table 7.6: The estimate of ^{90}Sr , activity from a realistic groundwater borehole with different concentrations of suspended non-radionuclide particles.

Total Concentration mg L^{-1}	Estimation of 10 kBq L^{-1} ^{90}Sr Activity
Average 40	10.09 ± 0.55
Maximum 300	9.74 ± 0.51

Suspended solid concentrations can reach much higher levels than presented here; however, these can be considered to indicate a poorly designed or installed borehole or one requiring maintenance before a detector could be deployed.

7.4.3 Activity determination by energy Windows: other improvements

As seen in Table 7.4, there is room for improvement in the determination of ^{90}Sr activity from a mixed source. One reason for this poor performance is the overlap of all the spectra up to the ^{90}Sr end-point energy of 0.546 MeV. It has already been noted that the presence of an artificial peak in the ^{90}Y spectrum can improve this deconvolution. As this peak is not present in detectors thicker than 0.5 mm, the estimation of the activities can be improved by performing a linear regression over two energy windows, low and high. The low energy window is classified as the energies up to 0.546 MeV and the high energy window contains all subsequent energies recorded in the detector. Therefore, no ^{90}Sr decay is present in the high energy window and this window can be used to determine the activities of ^{90}Y and ^{137}Cs independently from ^{90}Sr activity. The reconstructed ^{90}Y and ^{137}Cs spectra are then subtracted from the low energy window which allows the activity of ^{90}Sr to be determined independently of higher-energy radionuclides. This technique was applied to a groundwater simulation containing 10.0 kBq L^{-1} ^{90}Sr , 1.0 kBq L^{-1} of ^{90}Y and 0.1 kBq L^{-1} of ^{137}Cs and the results are displayed in Table 7.7. In this case, the estimated activity of ^{90}Sr is erroneous by a margin of 0.77 kBq L^{-1} compared with 2.29 kBq L^{-1}. This demonstrates

that performing a linear regression over a high energy and low energy window can improve the estimation of ^{90}Sr activity in a mixed groundwater source.

Table 7.7: The estimate of ^{90}Sr , ^{90}Y , and ^{137}Cs activity from a realistic groundwater borehole

Radionuclide	Simulated Activity (kBq L^{-1})	Calculated Activity (kBq L^{-1})
^{90}Sr	10.00	10.77 ± 0.21
^{90}Y	1.00	1.06 ± 0.03
^{137}Cs	0.10	0.10 ± 0.01
^{235}U	0	0.00

The purpose of an in-situ detector is to collect results rapidly, and, as such, the previous spectra were collected over a time period of 5 h. Increasing this time period would result in spectra with a greater number of total counts. In Table 7.8, the results of determining 10 kBq\ L activity over increasing time periods are presented. The results are consistent and it is not apparent that increasing the counting time is a factor in achieving estimates that are closer to the true ^{90}Sr activity. Additionally, increasing the number of counts in the a priori matrix, X, makes no discernible difference to the estimated activity for the same 10 kBq\ L ^{90}Sr activity over a 5 h period.

Table 7.8: The estimate of ^{90}Sr activity for increasing lengths of measurement, and therefore counts.

Length of measurement (hours)	Simulated Activity (kBq L^{-1})	Calculated Activity (kBq L^{-1})
5	10.00	10.05 ± 0.09
10	10.00	9.84 ± 0.03
24	10.00	9.69 ± 0.04

7.5 Conclusions

The issue of quantifying ^{90}Sr activity in groundwater boreholes with an in-situ detector has been presented and addressed by simulating the detector response and using a linear regression to estimate the activity of the radionuclides present. The response function of a CdTe detector to ^{90}Sr , ^{90}Y ^{137}Cs and ^{235}U contamination in a groundwater borehole was simulated

using the Monte Carlo software package Geant4. These response functions were used to create a database from which the detector's response can be predicted. This method can be used to estimate ^{90}Sr activity as low as 100 BqL^{-1}, and it can be applied to identify ^{90}Sr activity among a background of ^{90}Y , ^{137}Cs, ^{40}K and ^{235}U. It was shown that including additional radionuclides in the response function matrix does not significantly degrade the estimate of ^{90}Sr activity. It was determined that detectors with thickness in the range of 0.1 to 1 mm can be used to apply this technique.

The issue of suspended solids in the groundwater was examined. The commonly found particles at Sellafield are sodium, potassium, iron, calcium, magnesium, iron, aluminium, silicon and oxygen, and these were included in the groundwater simulation at average and maximum concentrations. For these concentrations, the particles were not found to influence the results of radionuclide activity estimation.

One of the main impediments to beta spectroscopy is the overlapping of spectra that do not have characteristic features. This was resolved by applying the linear regression technique to two energy windows, determined by the end-point energy for ^{90}Sr emission. Using this approach, the ^{90}Sr activity in a 10.0 kBq L^{-1} ^{90}Sr , 1.0 kBq L^{-1} ^{90}Y and 0.1 kBq L^{-1} ^{137}Cs mixed source was estimated as 10.77 $\pm$ 0.21 kBq L^{-1}.

These results have demonstrated how detector simulation and data regression can be used to enable in-situ semiconductor detectors to estimate ^{90}Sr , ^{90}Y , ^{137}Cs and ^{235}U activity in groundwater. However, some shortcomings are still present. Future research will investigate whether the application of different linear regression techniques can be used to improve the results. Some success may be found by incorporating different approaches to weighting to reduce the influence of outliers in the regression. The incorporation of other techniques, such as peak finding, may help to refine the results generated with this approach.

8. Discussion and conclusion

8.1 Summary

The development of novel radiation detectors is an essential field of research for the nuclear decommissioning industry and its aim of monitoring nuclear waste contamination at legacy sites. In this thesis a novel in-situ ^{90}Sr detector has been developed, and its potential use has been demonstrated. This involved several stages: research, design, characterisation and simulation of in-situ deployment. This culminated in the development of a novel in-situ semiconductor detector which served as proof-of-concept for this approach to monitoring ^{90}Sr contamination in groundwater.

The first step in the project was to perform a comprehensive literature review of the existing ^{90}Sr monitoring methods to understand how they work and identify areas in which they can be improved. The major problems which concern beta detection are that the particles have a short range in matter and are emitted over a continuous spectrum. Existing techniques have adapted to these challenges by taking samples from the field and performing radiochemical separation followed by liquid scintillation counting in the lab. This approach generates high quality results but it is time consuming and produces secondary waste. This thesis discusses the mitigation of these problems by presenting the development of a novel detector which is designed to be to deployed in a groundwater borehole for in-situ monitoring. Such a detector must have a small form factor, less than 5 cm width, be waterproof and mobile. After a review of potential detector media, it was decided that room temperature semiconductors offered a viable solution to the problem.

A comparison of different semiconductor materials was the next stage in the project. There are many different materials which can be used to construct semiconductor detectors including gallium arsenide, cadmium telluride and silicon. These materials were compared through literature review and more specifically Geant4 simulations, see Chapter 4. Through modelling semiconductor materials, it was possible to examine how the materials interact with beta radiation on a fundamental level and this lead the design of the semiconductor detector in terms of the physical dimensions required to absorb ^{90}Sr emission, namely the thickness of the detector. It was found that higher density materials could absorb more of the energy from beta particles but an increase in atomic number also corresponded with an increase in backscattering which ultimately reduces the sensitivity of the detector in terms of counts. Both CdTe and GaAs were determined to be suitable room temperature semiconductor materials for an in-situ ^{90}Sr detector and offered better performance than Si for this application. It was found that the optimal design of the semiconductor would be 1 mm thick with a surface area of at least 10 mm^2.

A CdTe panel, supplied by Acrorad, was used as the medium for the ^{90}Sr detector. The 10 x 10 x 1 mm panel was paired with appropriate charge sensitive amplifiers, a FPGA chip to digitally process the signal and interface with a computer, a programmable on-board power-supply and simple casing with water-proofing. This resulted in a detector unit which was submersible and was found to be sensitive to a collimated ^{90}Sr source up to a range of 55.86 $\pm$ 5.40 mm in water. This served as the basis for demonstrating the experimental viability of the detector however the Covid-19 pandemic halted further experiments at this point.

In order to replicate laboratory experiments a Geant4 simulation was developed to investigate the deployment of the detector in a borehole scenario and determine its sensitivity to the radionuclides which are found at a decommissioning site. A section of a borehole was modelled including the soil, sand, plastic pipe and groundwater which was populated with various radionuclides. It was found that the detector was sensitive to ^{90}Sr , ^{90}Y , ^{137}Cs, ^{14}C, and ^{40}K, some of the predominant beta emitters found at Sellafield. The detector was

not sensitive to low energy beta emitters like ^{14}C as they were significantly attenuated by the water and waterproof casing of the detector. When solely looking at ^{90}Sr decay it was estimated that a minimum detectable limit of 323 Bq/L was achieved for a 1 hour measurement, improving to 66 Bq/L with a 24 hour measurement. This means that this approach can be competitive with existing techniques which can produce a limit of detection under the WHO's safe drinking water guideline of 10 Bq/L but on a much shorter time scale. Using a more readily available GaAs sensor with a wider surface area and thinner sensitive layer, the detectable limit fell to 18 Bq/L however such a detector would sacrifice the ability to resolve the end-point energy of high energy beta particles.

The final section of the research dealt with one of the key issues facing in-situ detection of ^{90}Sr , the task of identifying ^{90}Sr activity from a background of mixed beta radiation. In existing techniques, this is achieved by using radiochemical separation in a lab, but this produces secondary waste and it would be difficult to adapt these techniques to an in-situ scenario. An alternative approach is to use predictive modelling to perform a maximum-likelihood estimation of the radionuclides present in the beta spectrum obtain with the detector. This was done by simulating the detector's response to radionuclides such as ^{90}Sr , ^{90}Y , ^{137}Cs, and ^{235}U. This data is used to form a linear relationship between the modelled individual responses and the gross beta spectrum measured with the detector. Using this approach, it was possible to identify the presence of these radionuclides from a mixed source measurement. Different detector designs were tested and it was ascertained that the optimal thickness of a CdTe detector for this approach is in the range of 0.1 mm to 1 mm. The technique demonstrated here points a way forward for in-situ detectors to identify and determine the activity of radionuclides in a mixed source.

8.2 Outlook

The detector developed in this research has provided insight into how beta radiation can be detected in-situ using a compact semiconductor detector which is deployed into groundwater boreholes. This avoids the need for sample collection and treatment yet is capable of producing results on a shorter time-scale. This was achieved by developing a small detector which can be easily deployed in hard to reach areas and using predictive modelling to identify the radionuclides present in a sample.

By deploying this type of detector in groundwater boreholes across a decommissioning site, the beta activity in the groundwater could be monitored in near real time, particularly in high activity areas, and this could allow for rapid response to spikes in activity. Additionally, as the detector is compact its use can be adapted to other environments and applications such as waste pipes, rivers or other commercial security scenarios where the geometry is tight and it's difficult to place a detector. However, the predictive modelling technique must be adapted to each environment as the radiation emitted will behave differently depending on its material interactions. Different geometries and materials will produce a unique detector response for each scenario.

One of the primary challenges facing in-situ beta detection is the identification of radionuclides present in the medium being monitored. The solution proposed in this research is to use a predictive modelling technique based on linear regression. Chapter 7 demonstrated the potential of this approach as a viable technique and performing the analysis over different energy windows was proven to improve the results. This could be further developed by the modification of the detector to include different sensor types. One approach explored in this research was to use a thin and flexible semiconductor material wrapped around the surface of the detector, this was modelled with a Geant4 simulation. Alternatively, a different detector type such as a scintillator paired with a SiPM (Silicon photomultiplier) could be implemented

to capture more low-energy beta particles. Another approach could see shielding introduced into the detector to limit the absorption of low energy beta particles.

8.3 Future work

This research has demonstrated the potential for an in-situ beta detector for monitoring ^{90}Sr contamination in groundwater boreholes but in order to ready the detector for field use further development is required. This includes improving the detector hardware and developing computer software for radioisotope identification.

The effects of temperature were only briefly considered in this research, where the detector was immersed in ice cooled water. In general semiconductor detectors perform better in cooler conditions, and in this regard a groundwater borehole environment provides some welcomed cooling. However future research will characterise the detector performance as the external temperature varies and the internal temperature rises after prolonged operation. This could be stabilised by mounting the CdTe panel on a heat sync and pairing it with an internal temperature sensor. By monitoring the internal and external temperature, the reverse-bias voltage can be changed as appropriate to maintain the performance of the detector.

One of the unexplored aspects of this detector is the physical deployment of the detector in a borehole and the transmission of the data it generates. The detector must be lowered into the borehole by a mechanism or deployed permanently and this will depend on the needs of the decommissioning site's requirements. Remote transmission of data could be achieved with wireless transmission and this would benefit site workers by reducing their time spent on the field and exposed to radiation. Additionally, a more sustainable waterproof solution for the detector should be explored. The difficulty is in having a material that is radiation resistant, thin, low density yet able to resist water and does not significantly attenuate the ^{90}Sr

emission. Inspiration for this solution can be taken from solar cells where weather protection is achieved by either applying thin layers of polymers or glass which is sufficiently thin such that it is flexible and resilient.

The performance of the detector could be improved by increasing the surface area of the semiconductor. This would reduce the lower detectable limit. This was demonstrated in the thesis by the simulation of thin and flexible semiconductor detectors. Such a detector can be flexed around a the body of the detector, but this approach reduces the volume of water the detector is exposed to and therefore the number of beta particles entering the detector. Alternatively, the conventional CdTe sensor can be made larger but this brings complications in terms of the bias voltage and leakage current. It may be possible to combine two different sensors to get a more complete measurement of the full range of radiation incident on the detector. This could be a case of simply adding an additional CdTe detector to increase the surface area, or the introduction of another semiconductor material with different properties and sensitivities. In some regards, the predictive modelling technique can minimise the need to improve detector performance as a consistent response is more important than absolute sensitivity.

These results have demonstrated how detector simulation and linear regression can be used to enable in-situ semiconductor detectors to estimate ^{90}Sr , ^{90}Y , ^{137}Cs and ^{235}U activity in groundwater. However, some shortcomings are still present. Future research will investigate the application of different linear regression techniques can be used to improve the results and be used to optimise the performance of the technique. Some success may be found by incorporating different approaches to weighting to reduce the influence of outliers in the regression. The incorporation of other techniques, such as peak finding, may help to refine the results generated with this approach.

Bibliography

[1] How is radioactive waste produced? | UK Radioactive Waste Inventory (UKRWI), https://ukinventory.nda.gov.uk/about-radioactive-waste/how-is-radioactive-waste-produced/.

[2] HPaul, English: Beta spectrum of RaE (Apr. 2015).

[3] Tubas-en, English: Cs-137 decay diagram.

[4] Kolbasz, English: English translation of Caesium-137 Gamma Ray Spectrum-de.svg (Mar. 2015).

[5] U. W, The Uranium series. (May 2009).

[6] Qwerty123uiop, English: Schematic view of a photomultiplier coupled to a scintillator, illustrating detection of gamma rays (30 November 2013, 21:25:28).

[7] F. band structure, English: Simple diagram of semiconductor band structure, showing a few bands on either side of the band gap. Redrawn from bitmap using vector graphics. (Apr. 2015).

[8] A. Grau Malonda, L. Rodriguez Barquero, A. Grau Carles, Radioactivity determination of 90Y, 90Sr and 89Sr mixtures by spectral deconvolution, Nuclear Instruments and Methods in Physics Research Section A: Accelerators, Spectrometers, Detectors and Associated Equipment 339 (1-2) (1994) 31–37. doi:10.1016/0168-9002(94)91774-4.

[9] J. Olfert, X. Dai, S. Kramer-Tremblay, Rapid determination of Sr-90/Y-90 in water samples by liquid scintillation and Cherenkov counting, Journal of Radioanalytical and Nuclear Chemistry 300 (1) (2014) 263–267. doi:10.1007/s10967-013-2913-0.

[10] A. V. Tyazhev, D. L. Budnitsky, O. B. Koretskay, V. A. Novikov, L. S. Okaevich, A. I. Potapov, O. P. Tolbanov, A. P. Vorobiev, GaAs radiation imaging detectors with an active layer thickness up to 1mm, Nuclear Instruments and Methods in Physics Research Section A: Accelerators, Spectrometers, Detectors and Associated Equipment 509 (1) (2003) 34–39. doi:10.1016/S0168-9002(03)01545-6.

[11] M. Veale, S. Bell, D. Duarte, M. French, A. Schneider, P. Seller, M. Wilson, A. Lozinskaya, V. Novikov, O. Tolbanov, A. Tyazhev, A. Zarubin, Chromium compensated gallium arsenide detectors for X-ray and γ-ray spectroscopic imaging, Nuclear Instruments and Methods in Physics Research Section A: Accelerators, Spectrometers, Detectors and Associated Equipment 752 (2014) 6–14. doi:10.1016/j.nima.2014.03.033.

[12] A. M. Barnett, J. E. Lees, D. J. Bassford, Direct detection of Tritium and Carbon-14 beta particles with GaAs photodiodes, Journal of Instrumentation 7 (09) (2012) P09012. doi:10.1088/1748-0221/7/09/P09012.

[13] G. Lioliou, X. Meng, J. S. Ng, A. M. Barnett, Characterization of gallium arsenide X-ray mesa p-i-n photodiodes at room temperature, Nuclear Instruments and Methods in Physics Research Section A: Accelerators, Spectrometers, Detectors and Associated Equipment 813 (2016) 1–9. doi:10.1016/j.nima.2015.12.030.

[14] V. B. Chmill, A. V. Chuntonov, A. V. Smol, A. P. Vorobiev, S. S. Khludkov, A. A. Koretski, L. S. Okaevitch, A. I. Potapov, V. E. Stepanov, O. P. Tolbanov, K. M. Smith, Particle detector based on GaAs. Radiation hardness and spatial resolution, Nuclear Instruments and Methods in Physics Research Section A: Accelerators, Spectrometers, Detectors and Associated Equipment 409 (1) (1998) 247–250. doi:10.1016/S0168-9002(97)01272-2.

[15] A. Šagátová, B. Zaťko, F. Dubecký, T. Ly Anh, V. Nečas, K. Sedlačková, M. Pavlovič, M. Fülöp, Radiation hardness of GaAs sensors against gamma-rays, neutrons and electrons, Applied Surface Science 395 (2017) 66–71. doi:10.1016/j.apsusc.2016.08.167.

[16] IAEA Safety Standards: Classification of Radioactive Waste—No. GSG-1 (2009).

[17] M. I. Ojovan, 1 - Radioactive waste characterization and selection of processing technologies, in: M. I. Ojovan (Ed.), Handbook of Advanced Radioactive Waste Conditioning Technologies, Woodhead Publishing Series in Energy, Woodhead Publishing, 2011, pp. 1–16. doi:10.1533/9780857090959.1.

[18] G. Turkington, K. A. A. Gamage, J. Graham, Beta detection of strontium-90 and the potential for direct in situ beta detection for nuclear decommissioning applications, Nuclear Instruments and Methods in Physics Research Section A: Accelerators, Spectrometers, Detectors and Associated Equipment 911 (2018) 55–65. doi:10.1016/j.nima.2018.09.101.

[19] G. Turkington, K. A. A. Gamage, J. Graham, Direct measurement of strontium 90 in groundwater: Geometry optimisation of a photodiode based detector, Journal of Instrumentation 14 (10) (2019) P10018–P10018. doi:10.1088/1748-0221/14/10/P10018.

[20] G. Turkington, K. A. A. Gamage, J. Graham, The Simulated Characterization and

Suitability of Semiconductor Detectors for Strontium 90 Assay in Groundwater, Sensors 21 (3) (2021) 984. doi:10.3390/s21030984.

[21] G. Turkington, K. A. A. Gamage, J. Graham, Characterisation and suitability of a CdTe detector for strontium 90 assay in groundwater, Nuclear Instruments and Methods in Physics Research. Section A: Accelerators, Spectrometers, Detectors, and Associated Equipment 997. doi:10.1016/j.nima.2021.165155.

[22] G. Turkington, K. A. A. Gamage, J. Graham, The Simulation of In-Situ Groundwater Detector Response as a Means of Identifying Beta Emitting Radionuclides by Linear Regression Analysis, Sensors 21 (17) (2021) 5732. doi:10.3390/s21175732.

[23] M. F. L'Annunziata, Radiation Physics and Radionuclide Decay, in: Handbook of Radioactivity Analysis, Elsevier, 2012, pp. 1–162. doi:10.1016/B978-0-12-384873-4.00001-3.

[24] W. R. Leo, Techniques for Nuclear and Particle Physics Experiments: A How-to Approach, 2nd Edition, Springer-Verlag, Berlin Heidelberg, 1994. doi:10.1007/978-3-642-57920-2.

[25] G. F. Knoll, Radiation Detection and Measurement, 3rd Edition, Wiley, New York, 2000.

[26] J. Verplancke, P. F. Fettweis, R. Venkataraman, B. M. Young, H. Schwenn, Chapter 5 - Semiconductor Detectors, in: M. F. L'Annunziata (Ed.), Handbook of Radioactivity Analysis (Third Edition), Academic Press, Amsterdam, 2012, pp. 299–362. doi:10.1016/B978-0-12-384873-4.00005-0.

[27] P. N. Luke, M. Amman, Room-Temperature Replacement for Ge Detectors—Are We There Yet?, IEEE Transactions on Nuclear Science 54 (4) (2007) 834–842. doi:10.1109/TNS.2007.903184.

[28] S.-D. Chun, S.-H. Park, D. H. Lee, Y. K. Kim, J. H. Ha, S. M. Kang, Y. H. Cho, D.-G. Hong, J. K. Kim, Property of a CZT Semiconductor Detector for Radionuclide Identification, Journal of Nuclear Science and Technology 45 (sup5) (2008) 421–424. doi:10.1080/00223131.2008.10875879.

[29] P. M. Johns, J. C. Nino, Room temperature semiconductor detectors for nuclear security, Journal of Applied Physics 126 (4) (2019) 040902. doi:10.1063/1.5091805.

[30] A. Panahifar, D. M. L. Cooper, M. R. Doschak, 3-D localization of non-radioactive strontium in osteoarthritic bone: Role in the dynamic labeling of bone pathological changes, Journal of Orthopaedic Research 33 (11) (2015) 1655–1662. doi:10.1002/jor.22937.

[31] M. Zamburlini, A. Pejović-Milić, D. R. Chettle, C. E. Webber, J. Gyorffy, In vivo

study of an x-ray fluorescence system to detect bone strontium non-invasively, Physics in Medicine & Biology 52 (8) (2007) 2107. doi:10.1088/0031-9155/52/8/005.

[32] V. Chiste, Table de Radionucleides, http://www.lnhb.fr/nuclides/Sr-90_tables.pdf (May 2005).

[33] S. H. Wallace, S. Shaw, K. Morris, J. S. Small, A. J. Fuller, I. T. Burke, Effect of groundwater pH and ionic strength on strontium sorption in aquifer sediments: Implications for ^{90}Sr mobility at contaminated nuclear sites, Applied Geochemistry 27 (8) (2012) 1482–1491. doi:10.1016/j.apgeochem.2012.04.007.

[34] H. Tazoe, H. Obata, T. Yamagata, Z. Karube, H. Nagai, M. Yamada, Determination of strontium-90 from direct separation of yttrium-90 by solid phase extraction using DGA Resin for seawater monitoring, Talanta 152 (2016) 219–227. doi:10.1016/j.talanta.2016.01.065.

[35] J. Small, S. Wallace, I. Burke, Strontium-90 mobility in contaminated nuclear facilities and groundwater, NNL Science 1 (2) (2014) 26.

[36] N. Kavasi, S. Sahoo, A. Sorimachi, S. Tokonami, T. Aono, S. Yoshida, Measurement of Sr-90 in soil samples affected by the Fukushima Daiichi Nuclear Power Plant accident, Journal of Radioanalytical and Nuclear Chemistry 303 (3) (2015) 2565–2570. doi:10.1007/s10967-014-3649-1.

[37] S. K. Sahoo, N. Kavasi, A. Sorimachi, H. Arae, S. Tokonami, J. W. Mietelski, E. Łokas, S. Yoshida, Strontium-90 activity concentration in soil samples from the exclusion zone of the Fukushima daiichi nuclear power plant, Scientific Reports 6 (2016) 23925. doi:10.1038/srep23925.

[38] L. Pages, E. Bertel, H. Joffre, L. Sklavenitis, Energy loss, range, and bremsstrahlung yield for 10-keV to 100-MeV electrons in various elements and chemical compounds, Atomic Data and Nuclear Data Tables 4 (Journal Article) (1972) 1–27. doi:10.1016/S0092-640X(72)80002-0.

[39] N. A. Chieco, The Procedures Manual of the Environmental Measurements Laboratory, U.S. Department of Energy I (28) (1997) 524.

[40] A. N. Anthemidis, K.-I. G. Ioannou, Recent developments in homogeneous and dispersive liquid–liquid extraction for inorganic elements determination. A review, Talanta 80 (2) (2009) 413–421. doi:10.1016/j.talanta.2009.09.005.

[41] D. M. Beals, W. G. Britt, J. P. Bibler, D. A. Brooks, Radionuclide analysis using solid phase extraction disks, Journal of Radioanalytical and Nuclear Chemistry 236 (1-2) (1998) 187–191. doi:10.1007/BF02386340.

[42] E. P. Horwitz, M. L. Dietz, D. E. Fisher, Separation and preconcentration of stron-

tium from biological, environmental, and nuclear waste samples by extraction chromatography using a crown ether, Analytical Chemistry 63 (5) (1991) 522–525. doi:10.1021/ac00005a027.

[43] M. F. L'Annunziata, M. J. Kessler, Chapter 7 - Liquid Scintillation Analysis: Principles and Practice, in: M. F. L'Annunziata (Ed.), Handbook of Radioactivity Analysis (Third Edition), Academic Press, Amsterdam, 2012, pp. 423–573. doi:10.1016/B978-0-12-384873-4.00007-4.

[44] C. K. Kim, A. Al-Hamwi, A. Törvényi, G. Kis-Benedek, U. Sansone, Validation of rapid methods for the determination of radiostrontium in milk, Applied Radiation and Isotopes 67 (5) (2009) 786–793. doi:10.1016/j.apradiso.2009.01.036.

[45] M. Uesugi, R. Watanabe, H. Sakai, A. Yokoyama, Rapid method for determination of ^{90}Sr in seawater by liquid scintillation counting with an extractive scintillator, Talanta 178 (2018) 339–347. doi:10.1016/j.talanta.2017.09.041.

[46] Ryszard Broda and Philippe Cassette and Karsten Kossert, Radionuclide metrology using liquid scintillation counting, Metrologia 44 (4) (2007) S36.

[47] ISO 5667-11:2009, Water quality – Sampling – Part 11: Guidance on sampling of groundwaters, Tech. rep., International Organization for Standardization (2009).

[48] ISO 5667-3:2012, Water quality – Sampling - Part 3: Preservation and handling of water samples, Tech. rep., BSI Standards Institution (2012).

[49] N. Vajda, C.-K. Kim, Determination of radiostrontium isotopes: A review of analytical methodology, Applied Radiation and Isotopes 68 (12) (2010) 2306–2326. doi:10.1016/j.apradiso.2010.05.013.

[50] M. Rodríguez, J. A. Suárez, A. G. Espartero, Separation of radioactive strontium by extraction using chromatographic resin, Nuclear Instruments and Methods in Physics Research Section A: Accelerators, Spectrometers, Detectors and Associated Equipment 369 (2) (1996) 348–352. doi:10.1016/S0168-9002(96)80007-6.

[51] N. Vajda, A. Ghods-Esphahani, E. Cooper, P. R. Danesi, Determination of radiostrontium in soil samples using a crown ether, Journal of Radioanalytical and Nuclear Chemistry 162 (2) (1992) 307–323. doi:10.1007/BF02035392.

[52] T. Jabbar, K. Khan, M. S. Subhani, P. Akhter, Determination of ^{90}Sr in environment of district Swat, Pakistan, Journal of Radioanalytical and Nuclear Chemistry 279 (2) (2009) 377–384. doi:10.1007/s10967-007-7277-5.

[53] J. J. Surman, J. M. Pates, H. Zhang, S. Happel, Development and characterisation of a new Sr selective resin for the rapid determination of ^{90}Sr in environmental water samples, Talanta 129 (2014) 623–628. doi:10.1016/j.talanta.2014.06.041.

[54] S. Dulanska, B. Remenec, L. Matel, D. Galanda, A. Molnar, Pre-concentration and determination of Sr-90 in radioactive wastes using solid phase extraction techniques, Journal of Radioanalytical and Nuclear Chemistry 288 (3) (2011) 705–708. doi:10.1007/s10967-011-1019-9.

[55] Ž. Grahek, G. Karanović, M. Nodilo, Rapid determination of ^{89,90}Sr in wide range of activity concentration by combination of yttrium, strontium separation and Cherenkov counting, Journal of Radioanalytical and Nuclear Chemistry 292 (2) (2012) 555–569. doi:10.1007/s10967-011-1441-z.

[56] J. Ometáková, S. Dulanská, L. Mátel, B. Remenec, A comparison of classical ^{90}Sr separation methods with selective separation using molecular recognition technology products AnaLig® SR-01 gel, 3M Empore™ Strontium Rad Disk and extraction chromatography Sr®Resin, Journal of Radioanalytical and Nuclear Chemistry 290 (2) (2011) 319–323. doi:10.1007/s10967-011-1338-x.

[57] H. H. Ross, Measurement of beta-emitting nuclides using Cerenkov radiation, Analytical Chemistry 41 (10) (1969) 1260–1265. doi:10.1021/ac60279a011.

[58] S. C. Scarpitta, I. M. Fisenne, Cerenkov counting as a complement to liquid scintillation counting, Applied Radiation and Isotopes 47 (8) (1996) 795–800. doi:10.1016/0969-8043(96)00061-9.

[59] D. Brajnik, S. Korpar, G. Medin, M. Starič, A. Stanovnik, Measurement of ^{90}Sr activity with Cherenkov radiation in a silica aerogel, Nuclear Instruments and Methods in Physics Research Section A: Accelerators, Spectrometers, Detectors and Associated Equipment 353 (1) (1994) 217–221. doi:10.1016/0168-9002(94)91642-X.

[60] D. D. Rao, S. T. Mehendarge, S. Chandramouli, A. G. Hegde, U. C. Mishra, Application of Cherenkov radiation counting for determination of ^{90}Sr in environmental samples, Journal of Environmental Radioactivity 48 (1) (2000) 49–57. doi:10.1016/S0265-931X(99)00053-3.

[61] I. Coha, S. Neufuss, Ž. Grahek, M. Němec, M. Nodilo, J. John, The effect of counting conditions on pure beta emitter determination by Cherenkov counting, Journal of Radioanalytical and Nuclear Chemistry 310 (2) (2016) 891–903. doi:10.1007/s10967-016-4853-y.

[62] J. M. Torres, J. F. García, M. Llauradó, G. Rauret, Rapid determination of strontium-90 in environmental samples by single Cerenkov counting using two different colour quench curves, Analyst 121 (11) (1996) 1737–1742. doi:10.1039/AN9962101737.

[63] S. Tsroya, O. Pelled, U. German, R. Marco, E. Katorza, Z. Alfassi, Color quench correction for low level Cherenkov counting, 5th International Conference on Radionuclide Metrology - Low-Level Radioactivity Measurement Techniques ICRM-LLRMT'08 67 (5) (2009) 805–808. doi:10.1016/j.apradiso.2009.01.038.

[64] M. Capogni, P. De Felice, A prototype of a portable TDCR system at ENEA, Applied Radiation and Isotopes 93 (2014) 45–51. doi:10.1016/j.apradiso.2014.03.021.

[65] R. Broda, P. Cassette, K. Kossert, Radionuclide metrology using liquid scintillation counting, Metrologia 44 (4) (2007) S36. doi:10.1088/0026-1394/44/4/S06.

[66] P. Cassette, J. Bouchard, The design of a liquid scintillation counter based on the triple to double coincidence ratio method, Nuclear Instruments and Methods in Physics Research Section A: Accelerators, Spectrometers, Detectors and Associated Equipment 505 (1) (2003) 72–75. doi:10.1016/S0168-9002(03)01023-4.

[67] Hidex 300 SL, http://hidex.com/products/hidex-300-sl/.

[68] P. Cassette, M. Capogni, L. Johansson, K. Kossert, O. Nähle, J. Sephton, P. D. Felice, Development of portable Liquid Scintillation counters for on-site primary measurement of radionuclides using the Triple-To-Double Coincidence Ratio method, in: 2013 3rd International Conference on Advancements in Nuclear Instrumentation, Measurement Methods and Their Applications (ANIMMA), 2013, pp. 1–7. doi:10.1109/ANIMMA.2013.6727876.

[69] O. Nähle, Q. Zhao, C. Wanke, M. Weierganz, K. Kossert, A portable TDCR system, Applied Radiation and Isotopes 87 (2014) 249–253. doi:10.1016/j.apradiso.2013.11.084.

[70] F. Vacap, G. Manjón, M. Garcia-León, Efficiency calibration of a liquid scintillation counter for ^{90}Y cherenkov counting, Nuclear Instruments and Methods in Physics Research Section A: Accelerators, Spectrometers, Detectors and Associated Equipment 406 (2) (1998) 267–275. doi:10.1016/S0168-9002(98)91986-6.

[71] M. Tayeb, X. Dai, E. C. Corcoran, D. G. Kelly, Evaluation of interferences on measurements of ^{90}Sr/^{90}Y by TDCR Cherenkov counting technique, Journal of Radioanalytical and Nuclear Chemistry 300 (1) (2014) 409–414. doi:10.1007/s10967-013-2910-3.

[72] D. Offin, G. Toon, G. Bolton, Review of Remote Systems for Monitoring Radionuclides in Groundwater, National Nuclear Decommissioning Authority NNL 13748 (3) (2016) 55.

[73] World Health Organization, Guidelines for Drinking-Water Quality., 2017.

[74] D. S. McGregor, Semiconductor Counters, in: C. Grupen, I. Buvat (Eds.), Handbook of Particle Detection and Imaging, Springer Berlin Heidelberg, Berlin, Heidelberg, 2012, pp. 377–410. doi:10.1007/978-3-642-13271-1-16.

[75] S. V. Bulyarskiy, A. V. Lakalin, I. E. Abanin, V. V. Amelichev, V. V. Svetuhin, Optimization of the parameters of power sources excited by β-radiation, Semiconductors

51 (1) (2017) 66–72. doi:10.1134/S1063782617010055.

[76] F. Dubecký, A. Perd'ochová, P. Ščepko, B. Zat'ko, V. Sekerka, V. Nečas, M. Sekáčová, M. Hudec, P. Boháček, J. Huran, Digital X-ray portable scanner based on monolithic semi-insulating GaAs detectors: General description and first "quantum" images, Nuclear Instruments and Methods in Physics Research Section A: Accelerators, Spectrometers, Detectors and Associated Equipment 546 (1) (2005) 118–124. doi:10.1016/j.nima.2005.03.020.

[77] P. H. Gooda, W. B. Gilboy, High resolution alpha spectroscopy with low cost photodiodes, Nuclear Instruments and Methods in Physics Research Section A: Accelerators, Spectrometers, Detectors and Associated Equipment 255 (1) (1987) 222–224. doi:10.1016/0168-9002(87)91105-3.

[78] G. Bertuccio, Prospect for energy resolving X-ray imaging with compound semiconductor pixel detectors, Nuclear Instruments and Methods in Physics Research Section A: Accelerators, Spectrometers, Detectors and Associated Equipment 546 (1) (2005) 232–241. doi:10.1016/j.nima.2005.03.015.

[79] G. Lioliou, M. D. C. Whitaker, A. M. Barnett, High temperature GaAs X-ray detectors, Journal of Applied Physics 122 (24) (2017) 244506. doi:10.1063/1.5005878.

[80] H. Spieler, Oxford University Press, Semiconductor Detector Systems, Vol. 12.;12;, Oxford University Press, Oxford, 2005.

[81] K. Afanaciev, M. Bergholz, P. Bernitt, G. Chelkov, J. Gajewski, M. Gostkin, C. Grah, R. Heller, H. Henschel, A. Ignatenko, Z. Krumshteyn, S. Kulis, W. Lange, W. Lohmann, D. Mokeev, V. Novikov, M. Ohlerich, A. Rosca, A. Sapronov, R. Schmidt, S. Schuwalow, O. Tolbanov, A. Tyazhev, Chalmers University of Technology, N. E. Department of Applied Physics, Chalmers tekniska högskola, N. teknik Institutionen för teknisk fysik, Investigation of the radiation hardness of GaAs sensors in an electron beam, JOURNAL OF INSTRUMENTATION 7 (11) (2012) P11022–P11022. doi:10.1088/1748-0221/7/11/P11022.

[82] V. K. Dixit, S. K. Khamari, S. Manwani, S. Porwal, K. Alexander, T. K. Sharma, S. Kher, S. M. Oak, Effect of high dose γ-ray irradiation on GaAs p-i-n photodetectors, Nuclear Instruments and Methods in Physics Research Section A: Accelerators, Spectrometers, Detectors and Associated Equipment 785 (2015) 93–98. doi:10.1016/j.nima.2015.03.008.

[83] N. A. Naz, U. S. Qurashi, M. Z. Iqbal, Arsenic antisite defects in p-GaAs grown by metal-organic chemical-vapor deposition and the EL2 defect, Journal of Applied Physics 106 (10) (2009) 103704. doi:10.1063/1.3243162.

[84] C. Erd, A. Owens, G. Brammertz, M. Bavdaz, A. Peacock, V. Lämsä, S. Nenonen, H. Andersson, N. Haack, Hard X-ray test and evaluation of a prototype 32×32 pixel

gallium–arsenide array, Nuclear Instruments and Methods in Physics Research Section A: Accelerators, Spectrometers, Detectors and Associated Equipment 487 (1) (2002) 78–89. doi:10.1016/S0168-9002(02)00949-X.

[85] K. Adomi, J. I. Chyi, S. F. Fang, T. C. Shen, S. Strite, H. Morkoç, Molecular beam epitaxial growth of GaAs and other compound semiconductors, Thin Solid Films 205 (2) (1991) 182–212. doi:10.1016/0040-6090(91)90301-D.

[86] P. J. Sellin, G. Rossi, M. J. Renzi, A. P. Knights, E. F. Eikenberry, M. W. Tate, S. L. Barna, R. L. Wixted, S. M. Gruner, Performance of semi-insulating gallium arsenide X-ray pixel detectors with current-integrating readout, Nuclear Instruments and Methods in Physics Research Section A: Accelerators, Spectrometers, Detectors and Associated Equipment 460 (1) (2001) 207–212. doi:10.1016/S0168-9002(00)01117-7.

[87] X. Wu, T. Peltola, T. Arsenovich, A. Gädda, J. Härkönen, A. Junkes, A. Karadzhinova, P. Kostamo, H. Lipsanen, P. Luukka, M. Mattila, S. Nenonen, T. Riekkinen, E. Tuominen, A. Winkler, Processing and characterization of epitaxial GaAs radiation detectors, Nuclear Instruments and Methods in Physics Research Section A: Accelerators, Spectrometers, Detectors and Associated Equipment 796 (2015) 51–55. doi:10.1016/j.nima.2015.03.028.

[88] Casino, http://www.gel.usherbrooke.ca/casino/index.html.

[89] G. Lioliou, A. M. Barnett, Gallium Arsenide detectors for X-ray and electron (beta particle) spectroscopy, Nuclear Instruments and Methods in Physics Research Section A: Accelerators, Spectrometers, Detectors and Associated Equipment 836 (2016) 37–45. doi:10.1016/j.nima.2016.08.047.

[90] Recent developments in Geant4, Nuclear Instruments and Methods in Physics Research Section A: Accelerators, Spectrometers, Detectors and Associated Equipment 835 (2016) 186–225. doi:10.1016/j.nima.2016.06.125.

[91] A. Šagátová, B. Zaťko, V. Nečas, F. Dubecký, T. Ly Anh, K. Sedlačková, P. Boháček, Z. Zápražný, From single GaAs detector to sensor for radiation imaging camera, Applied Surface Science 461 (2018) 3–9. doi:10.1016/j.apsusc.2018.06.269.

[92] S. Del Sordo, L. Abbene, E. Caroli, A. M. Mancini, A. Zappettini, P. Ubertini, Progress in the Development of CdTe and CdZnTe Semiconductor Radiation Detectors for Astrophysical and Medical Applications, Sensors 9 (5) (2009) 3491–3526. doi:10.3390/s90503491.

[93] S. V. Chernykh, A. V. Chernykh, S. I. Didenko, F. M. Baryshnikov, N. Burtebayev, G. I. Britvich, A. P. Chubenko, V. G. Guly, Y. N. Glybin, T. K. Zholdybayev, J. T. Burtebayeva, M. Nassurlla, GaAs detectors with an ultra-thin Schottky contact for spectrometry of charged particles, Nuclear Instruments and Methods in Physics Research Section A: Accelerators, Spectrometers, Detectors and Associated Equipment

845 (2017) 52–55. doi:10.1016/j.nima.2016.06.038.

[94] S. H. Shin, G. T. Niizawa, J. G. Pasko, G. L. Bostrup, F. J. Ryan, M. Khoshnevisan, C. I. Westmark, C. Fuller, P-I-N CdTe Gamma Ray Detectors by Liquid Phase Epitaxy (LPE), IEEE Transactions on Nuclear Science 32 (1) (1985) 487–491. doi:10.1109/TNS.1985.4336879.

[95] G. C. Sun, H. Samic, J. C. Bourgoin, D. Chambellan, O. Gal, P. Pillot, A comparison between GaAs and CdTe for X-ray imaging, IEEE Transactions on Nuclear Science 51 (5) (2004) 2400–2404. doi:10.1109/TNS.2004.834719.

[96] J. Becker, M. W. Tate, K. S. Shanks, H. T. Philipp, J. T. Weiss, P. Purohit, D. Chamberlain, J. P. C. Ruff, S. M. Gruner, Characterization of CdTe sensors with Schottky contacts coupled to charge-integrating pixel array detectors for X-ray science, Journal of Instrumentation 11 (12) (2016) P12013–P12013. doi:10.1088/1748-0221/11/12/P12013.

[97] Geant4, http://www.geant4.org/geant4/.

[98] Nuclear Data – Table – Laboratoire National Henri Becquerel.

[99] M. Niraula, A. Nakamura, T. Aoki, Y. Tomita, Y. Hatanaka, Stability issues of high-energy resolution diode type CdTe nuclear radiation detectors in a long-term operation, Nuclear Instruments and Methods in Physics Research Section A: Accelerators, Spectrometers, Detectors and Associated Equipment 491 (1) (2002) 168–175. doi:10.1016/S0168-9002(02)01175-0.

[100] A. Cola, I. Farella, The polarization mechanism in CdTe Schottky detectors, Applied Physics Letters 94 (10) (2009) 102113. doi:10.1063/1.3099051.

[101] D. Vartsky, M. Goldberg, Y. Eisen, Y. Shamai, R. Dukhan, P. Siffert, J. Koebel, R. Regal, J. Gerber, Radiation induced polarization in CdTe detectors, Nuclear Instruments and Methods in Physics Research Section A: Accelerators, Spectrometers, Detectors and Associated Equipment 263 (2-3) (1988) 457–462. doi:10.1016/0168-9002(88)90986-2.

[102] R. Bell, G. Entine, H. Serreze, Time-dependent polarization of CdTe gamma-ray detectors, Nuclear Instruments and Methods 117 (1) (1974) 267–271. doi:10.1016/0029-554X(74)90408-X.

[103] G. Choppin, J.-O. Liljenzin, J. Rydberg, C. Ekberg, Absorption of Nuclear Radiation, in: Radiochemistry and Nuclear Chemistry, Elsevier, 2013, pp. 163–208. doi:10.1016/B978-0-12-405897-2.00007-0.

[104] Sellafield Groundwater Monitoring Annual Data Review 2016, https://assets.publishing.service.gov.uk/government/uploads/system/uploads/attachment_data/

_Annual_Data_Review_2016.pdf (2016).

[105] E.-W. Bai, K.-s. Chan, W. Eichinger, P. Kump, Detection of radionuclides from weak and poorly resolved spectra using Lasso and subsampling techniques, Radiation Measurements 46 (10) (2011) 1138–1146. doi:10.1016/j.radmeas.2011.08.020.

[106] A. P. Fraser Harris, C. I. McDermott, O. Kolditz, R. S. Haszeldine, Modelling groundwater flow changes due to thermal effects of radioactive waste disposal at a hypothetical repository site near Sellafield, UK, Environmental Earth Sciences 74 (2) (2015) 1589–1602. doi:10.1007/s12665-015-4156-6.

[107] M. Funaki, Y. Ando, R. Jinnai, A. Tachibana, R. Ohno, Development of CdTe detectors in Acrorad (2015) 8.

[108] V. R. Sastri, 6 - Commodity Thermoplastics: Polyvinyl Chloride, Polyolefins, and Polystyrene, in: V. R. Sastri (Ed.), Plastics in Medical Devices (Second Edition), William Andrew Publishing, Oxford, 2014, pp. 73–120. doi:10.1016/B978-1-4557-3201-2.00006-9.

[109] V. T. Jordanov, G. F. Knoll, Digital synthesis of pulse shapes in real time for high resolution radiation spectroscopy, Nuclear Instruments and Methods in Physics Research Section A: Accelerators, Spectrometers, Detectors and Associated Equipment 345 (2) (1994) 337–345. doi:10.1016/0168-9002(94)91011-1.

[110] M. Ruat, C. Ponchut, Defect signature, instabilities and polarization in CdTe X-ray sensors with quasi-ohmic contacts, Journal of Instrumentation 9 (04) (2014) C04030–C04030. doi:10.1088/1748-0221/9/04/C04030.

[111] I. Farella, G. Montagna, A. M. Mancini, A. Cola, Study on Instability Phenomena in CdTe Diode-Like Detectors, IEEE Transactions on Nuclear Science 56 (4) (2009) 1736–1742. doi:10.1109/TNS.2009.2017020.

[112] M. Niraula, A. Nakamura, T. Aoki, Y. Tomita, Y. Hatanaka, Stability issues of high-energy resolution diode type CdTe nuclear radiation detectors in a long-term operation, Nuclear Instruments and Methods in Physics Research Section A: Accelerators, Spectrometers, Detectors and Associated Equipment 491 (1) (2002) 168–175. doi:10.1016/S0168-9002(02)01175-0.

[113] E. J. Smith, W. Davison, J. Hamilton-Taylor, Methods for preparing synthetic freshwaters, Water Research 36 (5) (2002) 1286–1296. doi:10.1016/S0043-1354(01)00341-4.

[114] G. Turkington, K. A. A. Gamage, J. Graham, Optimising sensor geometry of a photodiode based detector for the direct detection of strontium 90 in groundwater, Journal of Physics: Conference Series 1643 (2020) 012210. doi:10.1088/1742-6596/1643/1/012210.

[115] W.-S. Kim, S. Han, J. Ahn, W. Um, Investigation of 3H, 99Tc, and 90Sr transport in fractured rock and the effects of fracture-filling/coating material at LILW disposal facility, Environmental Geochemistry and Health 41 (1) (2019) 411–425. doi:10.1007/s10653-018-0123-y.

[116] M. Niraula, A. Nakamura, T. Aoki, Y. Tomita, Y. Hatanaka, Stability issues of high-energy resolution diode type CdTe nuclear radiation detectors in a long-term operation, Nuclear Instruments and Methods in Physics Research Section A: Accelerators, Spectrometers, Detectors and Associated Equipment 491 (1) (2002) 168–175. doi:10.1016/S0168-9002(02)01175-0.

[117] A. Cola, I. Farella, Electric Field and Current Transport Mechanisms in Schottky CdTe X-ray Detectors under Perturbing Optical Radiation, Sensors 13 (7) (2013) 9414–9434. doi:10.3390/s130709414.

[118] S. U. Egarievwe, U. N. Roy, C. A. Goree, B. A. Harrison, J. Jones, R. B. James, Ammonium Fluoride Passivation of CdZnTeSe Sensors for Applications in Nuclear Detection and Medical Imaging, Sensors 19 (15) (2019) 3271. doi:10.3390/s19153271.

[119] J. Venara, M. Ben Mosbah, C. Mahé, J. Astier, S. Adera, M. Cuozzo, V. Goudeau, Design and development of a portable β-spectrometer for 90Sr activity measurements in contaminated matrices, Nuclear Instruments and Methods in Physics Research Section A: Accelerators, Spectrometers, Detectors and Associated Equipment 953 (2020) 163081. doi:10.1016/j.nima.2019.163081.

[120] M. Nancekievill, J. Espinosa, S. Watson, B. Lennox, A. Jones, M. J. Joyce, J.-i. Katakura, K. Okumura, S. Kamada, M. Katoh, K. Nishimura, Detection of Simulated Fukushima Daichii Fuel Debris Using a Remotely Operated Vehicle at the Naraha Test Facility, Sensors 19 (20) (2019) 4602. doi:10.3390/s19204602.

[121] P. G. Martin, J. Moore, J. S. Fardoulis, O. D. Payton, T. B. Scott, Radiological Assessment on Interest Areas on the Sellafield Nuclear Site via Unmanned Aerial Vehicle, Remote Sensing 8 (11) (2016) 913. doi:10.3390/rs8110913.

[122] J. Kim, K. T. Lim, K. Ko, E. Ko, G. Cho, Radioisotope Identification and Nonintrusive Depth Estimation of Localized Low-Level Radioactive Contaminants Using Bayesian Inference, Sensors 20 (1) (2020) 95. doi:10.3390/s20010095.

[123] I. K. Ukaegbu, K. A. A. Gamage, M. D. Aspinall, Nonintrusive Depth Estimation of Buried Radioactive Wastes Using Ground Penetrating Radar and a Gamma Ray Detector, Remote Sensing 11 (2) (2019) 141. doi:10.3390/rs11020141.

[124] T. T. Alton, S. D. Monk, D. Cheneler, Beta particle energy spectra shift due to self-attenuation effects in environmental sources, Nuclear Engineering and Technology 49 (7) (2017) 1483–1488. doi:10.1016/j.net.2017.05.001.

[125] U. Lee, W. N. Choi, J. W. Bae, H. R. Kim, Fundamental approach to development of plastic scintillator system for in situ groundwater beta monitoring, Nuclear Engineering and Technology 51 (7) (2019) 1828–1834. doi:10.1016/j.net.2019.05.006.

[126] P. Kump, E.-W. Bai, K.-S. Chan, W. Eichinger, Detection of shielded radionuclides from weak and poorly resolved spectra using group positive RIVAL, Radiation Measurements 48 (2013) 18–28. doi:10.1016/j.radmeas.2012.11.002.

[127] S. R. White, K. T. Wood, P. G. Martin, D. T. Connor, T. B. Scott, D. A. Megson-Smith, Radioactive Source Localisation via Projective Linear Reconstruction, Sensors 21 (3) (2021) 807. doi:10.3390/s21030807.

[128] S. Grujić, M. Milošević, U. Kozmidis-Luburić, I. Bikit, Monte Carlo simulation of beta radiation response function for semiconductor Si detector, Nuclear Instruments and Methods in Physics Research Section A: Accelerators, Spectrometers, Detectors and Associated Equipment 654 (1) (2011) 288–292. doi:10.1016/j.nima.2011.06.070.

[129] Los Alamos National Laboratory: MCNP Home Page, https://mcnp.lanl.gov/.

[130] C. L. Lawson, R. J. Hanson, Solving Least Squares Problems, Classics in Applied Mathematics, Society for Industrial and Applied Mathematics, 1995. doi:10.1137/1.9781611971217.

[131] I. Vajs, D. Drajic, N. Gligoric, I. Radovanovic, I. Popovic, Developing Relative Humidity and Temperature Corrections for Low-Cost Sensors Using Machine Learning, Sensors 21 (10) (2021) 3338. doi:10.3390/s21103338.

[132] J. Venkatraman Jagatha, A. Klausnitzer, M. Chacón-Mateos, B. Laquai, E. Nieuwkoop, P. van der Mark, U. Vogt, C. Schneider, Calibration Method for Particulate Matter Low-Cost Sensors Used in Ambient Air Quality Monitoring and Research, Sensors 21 (12) (2021) 3960. doi:10.3390/s21123960.

[133] B. Jeon, J. Kim, E. Lee, M. Moon, G. Cho, Pseudo-Gamma Spectroscopy Based on Plastic Scintillation Detectors Using Multitask Learning, Sensors 21 (3) (2021) 684. doi:10.3390/s21030684.

[134] D. Czerwinski, J. Gęca, K. Kolano, Machine Learning for Sensorless Temperature Estimation of a BLDC Motor, Sensors 21 (14) (2021) 4655. doi:10.3390/s21144655.

[135] A. Tomal, J. Santos, P. Costa, A. Lopez Gonzales, M. Poletti, Monte Carlo simulation of the response functions of CdTe detectors to be applied in x-ray spectroscopy, Applied Radiation and Isotopes 100 (2015) 32–37. doi:10.1016/j.apradiso.2015.01.008.

[136] M. J. Neuer, Spectral identification of a 90Sr source in the presence of masking nuclides using Maximum-Likelihood deconvolution, Nuclear Instruments and Methods in Physics Research Section A: Accelerators, Spectrometers, Detectors and Associ-

ated Equipment 728 (2013) 73–80. doi:10.1016/j.nima.2013.06.013.

[137] P. J. Green, Iteratively Reweighted Least Squares for Maximum Likelihood Estimation, and Some Robust and Resistant Alternatives, Journal of the Royal Statistical Society: Series B (Methodological) 46 (2) (1984) 149–170. doi:10.1111/j.2517-6161.1984.tb01288.x.

[138] S. Agostinelli, J. Allison, K. Amako, J. Apostolakis, H. Araujo, P. Arce, M. Asai, D. Axen, S. Banerjee, G. Barrand, F. Behner, L. Bellagamba, J. Boudreau, L. Broglia, A. Brunengo, H. Burkhardt, S. Chauvie, J. Chuma, R. Chytracek, G. Cooperman, G. Cosmo, P. Degtyarenko, A. Dell'Acqua, G. Depaola, D. Dietrich, R. Enami, A. Feliciello, C. Ferguson, H. Fesefeldt, G. Folger, F. Foppiano, A. Forti, S. Garelli, S. Giani, R. Giannitrapani, D. Gibin, J. J. Gómez Cadenas, I. González, G. Gracia Abril, G. Greeniaus, W. Greiner, V. Grichine, A. Grossheim, S. Guatelli, P. Gumplinger, R. Hamatsu, K. Hashimoto, H. Hasui, A. Heikkinen, A. Howard, V. Ivanchenko, A. Johnson, F. W. Jones, J. Kallenbach, N. Kanaya, M. Kawabata, Y. Kawabata, M. Kawaguti, S. Kelner, P. Kent, A. Kimura, T. Kodama, R. Kokoulin, M. Kossov, H. Kurashige, E. Lamanna, T. Lampén, V. Lara, V. Lefebure, F. Lei, M. Liendl, W. Lockman, F. Longo, S. Magni, M. Maire, E. Medernach, K. Minamimoto, P. Mora de Freitas, Y. Morita, K. Murakami, M. Nagamatu, R. Nartallo, P. Nieminen, T. Nishimura, K. Ohtsubo, M. Okamura, S. O'Neale, Y. Oohata, K. Paech, J. Perl, A. Pfeiffer, M. G. Pia, F. Ranjard, A. Rybin, S. Sadilov, E. Di Salvo, G. Santin, T. Sasaki, N. Savvas, Y. Sawada, S. Scherer, S. Sei, V. Sirotenko, D. Smith, N. Starkov, H. Stoecker, J. Sulkimo, M. Takahata, S. Tanaka, E. Tcherniaev, E. Safai Tehrani, M. Tropeano, P. Truscott, H. Uno, L. Urban, P. Urban, M. Verderi, A. Walkden, W. Wander, H. Weber, J. P. Wellisch, T. Wenaus, D. C. Williams, D. Wright, T. Yamada, H. Yoshida, D. Zschiesche, Geant4—a simulation toolkit, Nuclear Instruments and Methods in Physics Research Section A: Accelerators, Spectrometers, Detectors and Associated Equipment 506 (3) (2003) 250–303. doi:10.1016/S0168-9002(03)01368-8.

[139] A numerical method for solving the Fredholm integral equation of the first kind and its application to restore the folded radiation spectrum, Nuclear Instruments and Methods in Physics Research Section A: Accelerators, Spectrometers, Detectors and Associated Equipment 255 (1-2) (1987) 152–155. doi:10.1016/0168-9002(87)91091-6.

[140] Elemental composition of [REDACTED] sediments., Tech. Rep. LP04074/06/11/01, National Nuclear Laboratory (2009).

Appendices

B. Optimising sensor geometry of a photodiode based detector for the direct detection of strontium 90 in groundwater.

Turkington, G., Gamage, K. A. A. and Graham, J. (2020) Optimising sensor geometry of a photodiode geometry based beta detector for the direct detection of strontium 90 in groundwater. Journal of Physics: Conference Series, 1643, 012210. (doi: 10.1088/1742-6596/1643/1/012210)

B.1 Abstract

Strontium-90, as one of the primary beta emitting radionuclides produced during nuclear fission, strontium-90 contaminates groundwater at nuclear decommissioning sites after leaks and spills. Its presence in the groundwater presents a long-term site risk, and its activity must be routinely monitored. Existing techniques see groundwater samples collected from deep underground boreholes and sent to remote labs for analysis. These procedures are expensive, time consuming and produce chemical waste, whereby eliminating the need for sample collection and treatment, the net lifetime monitoring costs of strontium 90 can be reduced.

In this paper authors present an optimisation of a beta detector, based on submersible photodetector, which can be used in real-time, in-situ beta detection. In order to directly detect and characterise strontium 90 in groundwater, it is essential to maximise the number of beta particles incident on the photodiode surface and ensure that they are fully absorbed within the sensitive region of the detector. This work has developed a Geant4 software framework for investigating the energy deposition by beta particles on photodiode detectors. A series of simulations have been performed to investigate radiation absorption in silicon, cadmium telluride and gallium arsenide detectors. Variations in sensitive area and detector thickness were modelled to determine their suitability for strontium-90 detection in groundwater. The optimal detector geometry of gallium arsenide photodiodes was further investigated. The simulation results and analysis suggest that the optimal detector will feature a large surface area, at least 1 cm^2, and an intrinsic layer approximately 400 μm thick.

B.2 Introduction

Leaks of waste at nuclear decommissioning sites have resulted in the contamination of the groundwater table as radionuclides enter the environment. Strontium 90, the principle beta emitting radionuclide found at decommissioning sites, has a half-life of 28.8 years and decays at 0.546 MeV. s daughter, Yttrium 90, decays at 2.278 MeV with a significantly shorter half-life of 64 hours [32]. Nuclear sites must plan the routine monitoring of ^{90}Sr for decades and current techniques are time consuming, produce secondary waste and are expensive. Currently groundwater samples are taken from underground boreholes and analysis is performed in off-site laboratories. Samples are radiochemically treated, and activity is measured by liquid scintillation, Cherenkov or proportional gas counting methods [49]. By detecting radiation directly and in situ, the need for sample collection can be eliminated which may reduce the worker dose and lifetime monitoring costs [18]. This paper proposes the optimal

physical characteristics for a photodiode detector for in situ ^{90}Sr measurement in groundwater.

Photodiodes have been used to detect ionising radiation. Photodiodes are semiconductor materials produce a current pulse in response to ionising radiation when operating under a reverse bias voltage. Incident radiation separates electron-hole pairs within the intrinsic region, producing a current pulse in proportion to the energy deposited by the incident particle. Photodiodes are comprised of multiple layers, as positively, p, and negatively, n, doped layers are brought together, charge separates and an intrinsic, i, layer is created. The intrinsic layer is the sensitive region and responsible for charge generation as ionising radiation is absorbed within the detector. The intrinsic layer can be formed by placing a layer of undoped semiconductor between p and n regions, forming a p-i-n junction, or the deposition of metal contacts onto the semiconductor material, forming an ohmic or Schottky diode.

Many different semiconductor materials can be used to fabricated photodiodes. Each material has unique properties and therefore the most appropriate one for each application must be considered. Silicon is the most widely available and used semiconductor. Its low atomic number, 14, and narrow bandgap, 1.17 eV, mean that silicon detectors are often cooled to minimise thermal noise [25]. GaAs has a higher atomic number, 32, and a bandgap of 1.42 eV which makes it viable at room temperature [78]. In recent years, GaAs photodiodes have been developed as gamma and X-ray detectors[91, 93, 79, 84, 87]. CdTe has an even higher atomic number, 50, than GaAs, and an even wider bandgap, 1.5 eV. CdTe may be a more effective absorber of ionising radiation with low nosie operation at room temperature [94, 95, 96].

B.3 Monte Carlo simulations

This research consists of Monte Carlo simulations aimed at finding the most effective semiconductor material for absorbing beta radiation released during ^{90}Sr decay. The goal is to develop a novel detector which is deployed into contaminated groundwater directly. The ratio between the number of particles which deposit energy in the detector and the number of particles emitted should be amplified through detector design. In this case the detector must be capable of fully absorbing the beta particles released during ^{90}Sr decay, up to 0.546 MeV, and ^{90}Y decay, up to 2.278 MeV. If the detector is too thin it will fail to register a significant portion of the particles incident on its surface and will be inefficient at determining the activity of the source of radiation. Simulations are carried out with Geant4, a Monte Carlo simulation code written in C++.

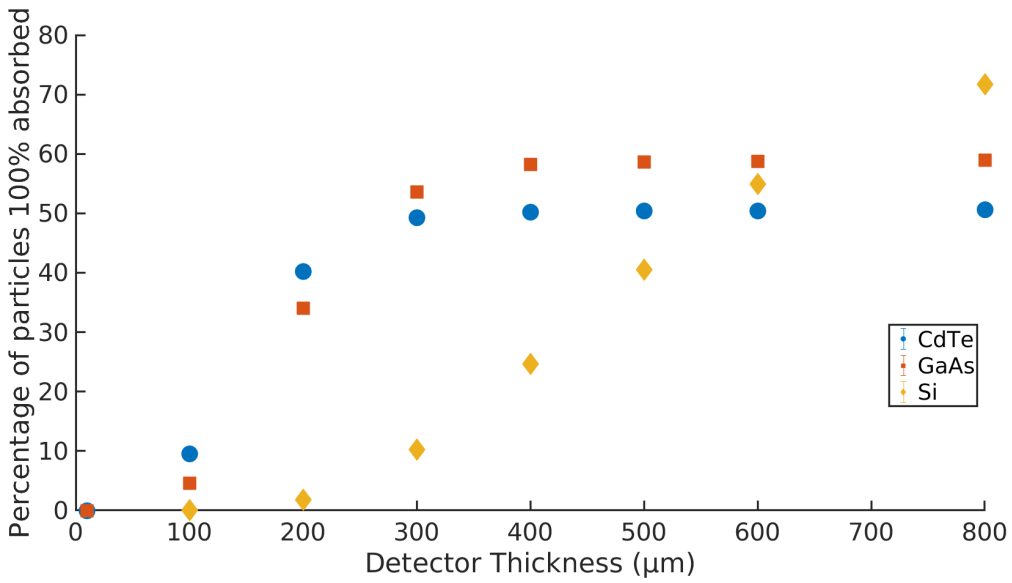

Figure B.1: A comparison of 0.546 MeV beta particle absorption in GaAs (squares), CdTe (circles), and Si (diamonds) detectors of varying thickness. Errors are plotted, but not visible due to marker size.

How effectively detectors will absorbed radiation will be determined in part by their thickness. Detectors of varying thickness were modelled with 100 mm^2 surface areas. A beam of 1×10^7 0.546 MeV electrons was fired into the centre of the detector and the energy de-

position of each particle was recorded. Silicon detectors fully absorbed fewer particles than GaAs and CdTe when the material was thinner, due to its lower atomic number and only began to absorb particles at a thickness above 200 μm. The GaAs detector absorbed fewer particles than CdTe until the thickness reached 300 μm. As the detectors became thicker the increase in particles absorbed in GaAs and CdTe detectors plateaued while Si detectors began to absorb more and more radiation. This is a consequence of differing levels of electron backscattering in each material. As backscattering is less prevalent in Si, it is able to completely absorb a greater proportional of particles when the thickness is sufficient.

A more realistic groundwater borehole scenario was modelled to consider the real world application of such a detector. This was achieved by modelling a 5 cm diameter and 2.5 cm deep cylinder of groundwater, and its contamination with 10 $\times 10^7$ isotropic decaying ^{90}Sr ions and ignored the resulting ^{90}Y . The surface area of the detectors was increased from 1 mm^2 to 100 mm^2 while the thickness was held constant at 400 μm . Figure B.2 displays the results. Only 162 hits were recorded in a detector with a 1 mm^2 surface area, and the maximum energy deposited in the detector with at least 5 counts was 0.103 MeV. As the surface area increased to 100 mm^2 detector counted a total of 13015 particles. As the radiation is emitted from random positions and in random directions, most of the particles will never reach the detector or are attenuated before they reach the sensor.

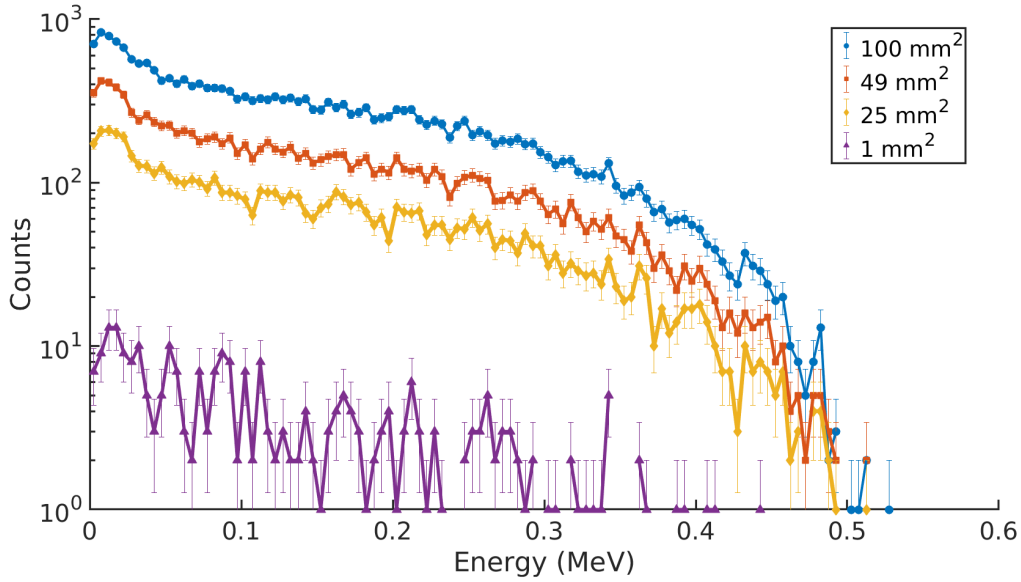

Figure B.2: ^{90}Sr spectra observed in 400 μm thick GaAs detectors with increasing surface surface areas.

B.4 Conclusion

A detector for the direct detection of ^{90}Sr in groundwater must maximise the number of particles incident on and fully absorbed within the detector. This paper has developed a Geant4 simulation code for examining the thickness, surface area and materials which can maximise the absorption of ^{90}Sr and ^{90}Y decay in a photodiode detector. The complete absorption of 0.546 MeV beta particles plateaus for CdTe for approximately 300 μm thick devices with 50.6 % of particles completely absorbed. GaAs completely absorbs a maximum of 58.9 % particles after 400 μm of material. GaAs performs better as an absorber for particles as the effect of backscattering is reduced compared to CdTe. However, CdTe detected more particles at higher energies, 2.28 MeV, where a minimum of 400 μm thick devices was required with 1 mm thick devices offering the greatest absorption. A wide area diode is required to sufficiently capture the fully range of radiation released from ^{90}Sr decay in groundwater. Simulations which modelled a groundwater borehole scenario determined that a 100 mm^2 surface area detector had the greatest detection efficiency. The spectra from 10^8 decaying ^{90}Sr ions, and the resulting ^{90}Y daughters, in 1 mm thick and 100 mm^2 CdTe and GaAs de-

tectors were compared. Each material offered the similar detection efficiency, but the shape of the spectra collected varied slightly. While CdTe offered marginally better absorption in the energy range from 1.725 - 2.3 MeV, the backscattering which resulted upon contact with lower energy particles produced a larger peak at low energies compared to that observed in the GaAs detector.